



**University of  
Zurich**<sup>UZH</sup>

# Enhanced carbon sequestration and soil productivity with land improvement – a case study on orchards and vineyards in Sicily

GEO 511 Master's Thesis

**Author**

Michèle Bösiger  
15-711-328

**Supervised by**

Prof. Dr. Markus Egli  
Prof. Salvatore Raimondi (salvatore.raimondi@unipa.it)

**Faculty representative**

Prof. Dr. Markus Egli

26.01.2021

Department of Geography, University of Zurich

UNIVERSITY OF ZURICH

MASTER THESIS

---

Enhanced carbon sequestration and soil productivity  
with land improvement – a case study on orchards and  
vineyards in Sicily

---

*Author:*

Michèle BÖSIGER

*Supervisor:*

Prof. Dr. Markus EGLI  
Prof. Salvatore RAIMONDI

January 26, 2021



UNIVERSITY OF ZURICH

## *Abstract*

Faculty of Science  
Department of Geography

Master in Geography

### **Enhanced carbon sequestration and soil productivity with land improvement – a case study on orchards and vineyards in Sicily**

by Michèle BÖSIGER

Soil is known to be one of the largest carbon pools on earth, however has not been considered an important part in the short-term sequestration of  $CO_2$  despite its mitigation potential. In this thesis, the carbon sequestration and storage potential of amended soil in a semi-arid region in Sicily is identified. A chronosequence of ten soil profiles, which have undergone a transformation within the last 50 years have been studied. The soil was transformed at different points in the past (17, 27, 35, 45 and 48 years ago). Crushed calcarenite was added on top of the existing soils or was partially mixed with naturally developed vertisol. To explore the most important carbon sequestration mechanisms, the grain size, the soil pore system, the oxalate extractable contents of Al, Fe and Mn, clay minerals, elemental contents and losses and general soil characteristics (bulk density, pH, C/N ratio, soil skeleton and organic matter content) were determined.

The soil indeed sequestered carbon in the past 50 years. A maximum of  $919 \text{ g m}^{-2} CO_2$  was buffered with silicate weathering per year and  $12'317 \text{ g m}^{-2}y^{-1} CO_2$  with carbonate weathering. Furthermore, organic carbon accumulated at a rate of  $0.07$  to  $0.34 \text{ kg m}^{-2}y^{-1}$  in the soil. The storage of organic material was facilitated by clay minerals and oxyhydroxides that contributed to the fixation of carbon in the soil, while silicate and carbonate weathering played a less important part in the stabilisation of carbon.

Transformed soils using unweathered and crushed calcarenite for improving soil quality in Sicily have therefore a large potential of sequestering carbon from the atmosphere. As weathering is progressing, compounds are being continuously produced which are able to bind atmospheric  $CO_2$  and thus helping to mitigate climate change.





## *Acknowledgements*

I wish to thank Markus Egli, who, despite the corona crisis, was tirelessly available to answer my questions and despite having a busy schedule, always accompanied me well in various contexts such as field and laboratory work. I also like to express my thanks to Salvatore Raimondi, who not only introduced me to the soil properties of Sicily, but also to the beauty of the island. I would also like to thank Gabriele Lauria, without whom we would probably have encountered many more problems in Sicily and who welcomed us with open and warm arms. I also thank the whole laboratory team - Tatjana Kraut, Esmail Taghizadeh, Dmitry Tikhomirov, Alessandra Musso and Guido L.B. Wiesenberg - for their time, their incredible knowledge sharing with me and the inspiring conversations we had. For the external laboratory work I would like to thank Michael Plötze from ETH Zurich and Krzysztof Lamorski as well as Shao-Yiu Hsu from the Institute of Agrophysics PAS in Lublin, without whom I would probably still be standing in the laboratory today. Last but not least, I would like to thank my private environment, especially my fellow master students, my boyfriend, my family and friends for their strength of nerves when I had none.



# Contents

<b>Abstract</b>	<b>iii</b>
<b>Acknowledgements</b>	<b>v</b>
<b>1 Introduction</b>	<b>1</b>
1.1 Background information . . . . .	1
1.2 Mechanisms of carbon fixation . . . . .	2
1.2.1 Accumulation of organic carbon through biomass . . . . .	2
1.2.2 Enhanced weathering and its environmental potential . . . . .	3
<b>2 Study area</b>	<b>7</b>
2.1 Canicatti research area . . . . .	9
2.2 Mazara del Vallo research area . . . . .	10
<b>3 Research questions and experimental setting</b>	<b>13</b>
<b>4 Material and Methods</b>	<b>15</b>
4.1 Statistics . . . . .	15
4.2 Sample preparation . . . . .	15
4.3 Physical Analysis . . . . .	16
4.3.1 Bulk density . . . . .	16
4.3.2 X-ray computational tomography . . . . .	16
4.3.3 Grain size analysis . . . . .	16
4.3.4 Clay mineral extraction . . . . .	17
4.3.5 Profile development index (PDI) . . . . .	17
4.4 Chemical analysis . . . . .	18
4.4.1 Total element contents . . . . .	18
4.4.2 pH measurement . . . . .	18
4.4.3 Carbon and nitrogen . . . . .	18
4.4.4 Oxalate-extractable elements . . . . .	19
4.4.5 Carbonates . . . . .	19
4.4.6 Loss on ignition (LOI) . . . . .	19
4.4.7 Chemical weathering indices . . . . .	20
4.4.8 Silicate and carbonate weathering (CO <sub>2</sub> consumption) . . . . .	21

<b>5 Results</b>	<b>23</b>
5.1 General soil characteristics . . . . .	23
5.2 Carbon compounds . . . . .	25
5.2.1 Carbon stocks and sequestration rates . . . . .	26
5.3 Grain size evolution . . . . .	26
5.4 Clay minerals . . . . .	27
5.4.1 Lauria P1a . . . . .	27
5.4.2 C.Fazio . . . . .	28
5.4.3 Cazzola 4 . . . . .	28
5.4.4 Mazara del Vallo P7 . . . . .	28
5.5 Oxalate-extractables (Fe, Al and Mn) and investigated clay fraction . . . . .	29
5.6 Total elemental content and weathering indices . . . . .	30
5.6.1 Chemical drift and weathering indices . . . . .	30
5.6.2 Elemental loss . . . . .	30
5.6.3 PDI . . . . .	31
5.7 Soil pore analysis . . . . .	31
<b>6 Discussion</b>	<b>51</b>
6.1 Carbon isotopes and compounds . . . . .	51
6.2 Chemical weathering and mineral composition of the soil . . . . .	53
6.2.1 Oxalate-extractables and weathering indices . . . . .	54
6.2.2 Clay minerals . . . . .	54
6.3 Physical weathering . . . . .	55
6.3.1 Soil pore analysis . . . . .	55
6.3.2 Grain size and soil structure . . . . .	56
6.4 Synthesis: Factors influencing carbon sequestration . . . . .	57
6.4.1 Organic carbon sequestration and storage . . . . .	58
Agricultural influences on carbon sequestration and storage . . . . .	59
Further influences on soil organic carbon storage . . . . .	60
6.5 Outlook and feasibility of the 4 per 1000 initiative . . . . .	61
<b>7 Conclusion</b>	<b>63</b>
<b>A Supplements</b>	<b>65</b>
<b>Bibliography</b>	<b>79</b>

# List of Figures

1.1	Mineral weathering reaction equation. . . . .	4
1.2	Mineral weathering timescale. . . . .	5
2.1	Soil preparation and rock excavation . . . . .	7
2.2	Sampled profiles with horizon indication. . . . .	11
2.3	Map of sampled profiles in each observed region. . . . .	12
4.1	Illustration of Bragg's law. . . . .	18
5.1	Soil characteristics development. . . . .	24
5.2	Stored and sequestered organic carbon over time. . . . .	26
5.3	Distribution of carbon compounds with soil depth and the development of pedogenic carbonate over time. . . . .	36
5.4	Grain size for each sampling location. . . . .	37
5.5	Smoothed XRD diffractograms. . . . .	38
5.6	Concentration of weathered fraction of oxalate-extractables over soil depth. . . . .	39
5.7	Mass of weathered fraction of oxalate-extractables over time. . . . .	39
5.8	Changes of clay mineral fractions over time. . . . .	40
5.9	The relationship of oxalate extractables with clay minerals. . . . .	41
5.10	Weathering indices as a function of depth. . . . .	42
5.11	Weathering indices as a function of immobile elements. . . . .	43
5.12	Normalised ratio of the trace elements of the primitive mantle. . . . .	44
5.13	Relative mass losses of different compounds. . . . .	44
5.14	Profile development index (PDI) over time. . . . .	45
5.15	Soil pore characteristics ( $> 0.03mm$ ) over time. . . . .	46
5.16	Soil pore characteristics ( $> 0.06mm$ ) over time. . . . .	47
5.17	Soil pore volume frequency distribution (diameter $> 0.03mm$ ). . . . .	48
5.18	Soil pore volume frequency distribution (diameter $> 0.06mm$ ). . . . .	49
5.19	3-Dimensional images of the sampled soil cores. . . . .	50
6.1	Relationship of oxygen and carbon isotopes from the bulk soil and carbonate with the organic and carbonate fraction of the soil. . . . .	52



# List of Tables

2.1	Details of the study areas. . . . .	8
5.1	Mineral composition of the clay fraction. . . . .	33
5.2	Stock/production rate of weathered <i>Al, Fe, Mn</i> . . . . .	34
5.3	Soil profile description with physical and chemical parameters. . . . .	35
A.1	Main chemical parameters of the soil probes in oxide and carbonate form normalised over the total sample. . . . .	65
A.2	XRF data - Part 1. . . . .	66
A.3	XRF data - Part 2. . . . .	67
A.4	Organic matter content (LOI), Carbon fractions, -stocks and -accumulation. . . . .	68
A.5	Weathering indices as a function of immobile elements. . . . .	69
A.6	Tau (open system mass-losses). . . . .	70
A.7	Stocks of the oxalate extractables per horizon. . . . .	71
A.8	Oxalate-extractable concentrations of <i>Al, Fe, Mn</i> . . . . .	72
A.9	Soil pore analysis (pore diameter > 0.03mm) for the sampled horizons. . . . .	73
A.10	Soil pore analysis (pore diameter > 0.06mm) for the sampled horizons. . . . .	74
A.11	Correlation of variables - Part 1. . . . .	75
A.12	Correlation of variables - Part 2. . . . .	76
A.13	Correlation of variables - Part 3. . . . .	77





# List of Abbreviations

<b>C</b>	<b>Carbon</b>
<b>CO<sub>2</sub></b>	<b>Carbon Dioxide</b>
<b>C<sub>inorg</sub></b>	<b>Inorganic Carbon</b>
<b>C<sub>org</sub></b>	<b>Organic Carbon</b>
<b>ETH</b>	<b>Eidgenössische Technische Hochschule</b>
<b>HIS</b>	<b>Hydroxy Interlayered Smectite</b>
<b>HIV</b>	<b>Hydroxy Interlayered Vermiculite</b>
<b>LOI</b>	<b>Loss On Ignition</b>
<b>NGO</b>	<b>Non Governmental Organisation</b>
<b>OE</b>	<b>Oxalate Extractables</b>
<b>PDI</b>	<b>Profile Development Index</b>
<b>SOC</b>	<b>Soil Organic Carbon</b>
<b>SOM</b>	<b>Soil Organic Matter</b>



# 1 Introduction

## 1.1 Background information

The principal idea for this master thesis comes from the 4 per 1000 initiative, that was launched in 2015 at the United Nations Framework Convention on Climate Change. Besides national and regional governments, the parties involved are research facilities, private corporations, trade associations and NGOs (United Nations Framework Convention on Climate Change, 2015). The initiative suggests that an increase of 0.4 % carbon in the topsoil per year could remediate annual anthropogenic  $CO_2$  outputs in the atmosphere (output in 2018:  $37.1 \pm 1.8 \text{ Gt } CO_2$ ) (Global Carbon Project, 2018). The biosphere already stores three times more carbon than the atmosphere with 1580 *Gt* of carbon in soil/detritus alone and additional 610 *GT C* in vegetation (Boardman et al., 2002; Ramaiah, 2014). In comparison, 750 *GT C* are stored in the atmosphere (Boardman et al., 2002; Ramaiah, 2014). In addition, it is believed that carbon sequestration in soil makes up to 89 % of the worldwide technical reduction potential (Aertsens et al., 2013).

However, to increase carbon sequestration and achieve the goal of the initiative, changes in land use must be made. These changes include the restoration of soils and plant nutrition, to stabilize and even increase the carbon sequestration. Furthermore, a steady soil carbon/soil organic matter storage would help to improve soil fertility and agricultural productivity (United Nations Framework Convention on Climate Change, 2015).

To study the influence of time on soil development, it was assumed that the soil-forming factors of Jenny (1941) - topography, climate, organisms and parent material - stay approximately the same, however might be corrected if relevant alterations between the sites occur. The sequestration and storage of carbon is in general faster at the beginning of the soil development (Egli et al., 2001a; Dahms et al., 2012) and soil organic matter accumulation reaches saturation after approximately  $< 5'000$  to  $20'000$  years (Egli et al., 2012). A soil chronosequence over the past 50 years could help to understand the effect of time on soil characteristics at the beginning of soil formation, the non-linear development of soil properties (Dahms et al., 2012) and the increasing impact of climate change on this ecosystem. Changing precipitation patterns and rising global temperatures brought by climate change might disturb the natural weathering process within the soil and thus its carbon sequestration potential (Dahlgren et al., 1997; Dahms et al., 2012).

In comparable studies on an initial ecosystem development in the Chicken Creek Catchment in Germany, three phases of soil evolution have been detected. In the first three years, severe gully and wind erosion took place and little organic carbon could be accumulated (Gerwin et al., 2011). These first years in the catchment development mark the first phase of an ecosystem evolution, in which easily soluble compounds are being washed out due to low organic matter content (Elmer et al., 2013). In the second phase, the vegetation cover increases and erosion (Gerwin et al., 2011) as well as leaching decrease (Elmer et al., 2013). Carbonate weathering increases since bicarbonates are found in runoff water (Elmer et al., 2013). The first couple of years in the soil development is driven mainly by external drivers such as precipitation, while the soil structure lays the path for further development (Schaaf et al., 2011; Elmer et al., 2013). In the third phase, the soil is further weathered, however plant root inputs of different nutrients such as organic carbon and nitrogen become increasingly important (Schaaf et al., 2011; Elmer et al. (2013)).

In comparison, the development of our sites is naturally a little different due to tillage. However, some comparisons can be made to the Chicken Creek Catchment. For example, heavy erosion in fallow fields is often encountered in Sicily (Fantappiè et al., 2015). Therefore, agricultural strategies that rely on continuous cultivation with cover crops (grass land; such as used in some study sites) are a fairly reliable indication that more nutrients are retained in the soil and less are being washed out than in areas with conventional agriculture (Aase and Siddoway, 1976; Garland et al., 2014). Since plants have been cultivated shortly after soil transformation, the leaching of nutrients should not increase and decrease as extremely as in a natural system as in the Chicken Creek Catchment, where the plant colonization is more time consuming. The third phase should be analogical for both systems with the establishment of perennial plants on both the amended study sites and in the Chicken Creek Catchment.

## **1.2 Mechanisms of carbon fixation**

### **1.2.1 Accumulation of organic carbon through biomass**

Soil organic matter constitutes only a minority within the soil but is crucial for the functioning of the soil system because it retains water and nutrients and stabilizes the soil (Weil and Brady, 2017).

Soil organic carbon is mainly stored in soil organic matter. SOM is made of 50 % of carbon and can store four to six times more C than the entire vegetation together which makes it an important tool against climate change. Soil organic matter consists mainly of plant and animal remains, but also of animal waste. The organic material is however unevenly distributed globally, as colder (arctic/boreal) climates promote less microbial activity and degradation of organic material, thus more organic carbon had been accumulating in these regions. The respiration of microbes is however needed for mineralization, a process in

which nutrients are being processed and provided to plants for growth (Weil and Brady, 2017). In addition, even though a large amount of carbon stored within arctic soils, almost nothing is currently sequestered.

In a natural system, the microbial respiration of carbon is balanced with the accumulation of new plant material (Weil and Brady, 2017). However, in a disturbed system (e.g. tillage), more carbon may leave the soil than that is stored and can alter the natural carbon mass balances. Moreover, global warming releases large amounts of stored carbon in colder regions, since the carbon is not as well protected from the environment as before. At the same time, plant growth is promoted in regions which were inhabitable before (e.g. glaciers, arctic areas) and the potential of soil carbon sequestration increases again.

### 1.2.2 Enhanced weathering and its environmental potential

Silicate and carbonate weathering are among the most important soil-forming factors (Velbel, 1988). These types of weathering describe the process of hydrolysis on carbonate and silicate minerals, meaning the reaction of rock with water and  $CO_2$ . Both types are thought to bind atmospheric  $CO_2$  as secondary minerals and thus contribute against climate change (Fig. 1.1). However, carbonate weathering is still a debated topic in terms of its effectiveness in binding atmospheric  $CO_2$  (Liu et al., 2011). The fertilization of nitrate might lead to nitric acid, which can switch the carbonate weathering from a possible sink to a  $CO_2$  source at a pH-value below 5 (Hamilton et al., 2007; Taylor et al., 2017; Francaviglia et al., 2019). Zamanian et al. (2016) further indicated that a low pH-value could release  $CO_2$  from inorganic carbon stocks.

The formation of secondary compounds provides thus only short-term answers about the fate of atmospheric  $CO_2$ . The further leaching of the minerals into the groundwater (Jones et al., 2003) and finally into the oceans is decisive in the long term, whether the  $CO_2$  is stored over a large period of several thousand years (Renforth and Henderson, 2017). This is particularly problematic in the context that the world's oceans are acidifying and therefore no longer have a carbonate buffer, which means that the bound  $CO_2$  can degas again (Romero-Mujalli et al., 2019). Yet, with increasing carbonate input into the soil, soil and water alkalinity will increase and a higher amount of carbon dioxide could be stored within waters (Beerling et al., 2018).

The promoted weathering of the soil by added (silicate/calcareous) rock powder is known as enhanced weathering. Enhanced weathering is achieved by the input of fresh rock material which reacts with its environment and binds atmospheric carbon. As a result, enhanced weathering of silicate and calcareous rock could remove up to 30  $Pg\ C/year$  from the atmosphere (equal to a global temperature decrease of  $0.2^\circ C - 1.6^\circ C$  by the year 2100 (Köhler et al., 2010; Taylor et al., 2017; Andrews and Taylor, 2019). In comparison, untreated ground has often been weathering for many centuries and available reaction partners are already

used up or relocated to deeper soil horizons, where a direct exchange with the atmosphere is no longer possible (Porder, 2019). Besides, enhanced weathering of carbonate is thought to capture  $\text{CO}_2$  as soon as the crushed rock has been applied or can take up several years in case of silicate minerals (Fig. 1.2). The short-term removal of carbon dioxide via enhanced weathering hence lies just within the set target of the Paris Agreement and the 4 per 1000 initiative.

Nevertheless, the weathering of calcareous and siliceous material is not only dependent on the input of water and fresh rock material, but also on mineral grain size, climate, agricultural, biological and microbial activity and pedogenic processes (Strefler et al., 2018; Beerling et al., 2018).

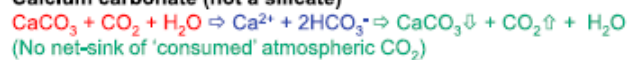
The rock used for the amendments in our study region is limestone. The lime is typically added during the soil transformation and sometimes additionally few years later, depending on the soil properties (e.g. changing porosity (Hamilton et al., 2007)). The addition of lime is a relatively environmentally friendly fertilizer that can be mined locally and slowly releases its nutrients into the soil (Van Straaten, 2007).

Nevertheless, some drawbacks need to be considered: The amount of nutrients within the lime is limited compared to the distributed amount (Chenu et al., 2019) and its price (Van Straaten, 2007). In addition, the rock needs to be extracted and processed which requires a high energy consumption (Van Straaten, 2007). Indeed, further evaluation of the sustainability of this amendment technique needs to be made. Liming can also result in decreasing SOC since mineralization is being promoted by rising soluble C (Ahmad et al., 2013; Zhao et al., 2018).

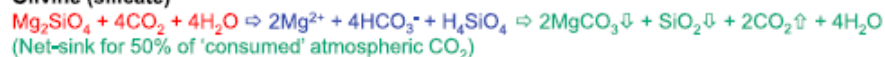
#### Typical mineral reactions

(educts  $\Rightarrow$  ions and silica in solution, secondary minerals  $\Rightarrow$  precipitation reactions in the ocean)

##### Calcium carbonate (not a silicate)



##### Olivine (silicate)



##### Albite (silicate)



FIGURE 1.1: Mineral weathering reactions of carbonates and silicates (Hartmann et al., 2013).

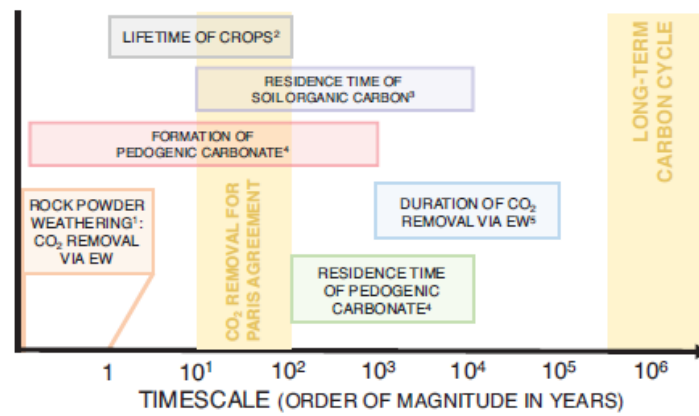


FIGURE 1.2: Mineral weathering timescale (Andrews and Taylor, 2019).





## 2 Study area

In Sicily, where the study area of this thesis lies, a commonly used soil amendment practice is the usage of crushed rocks (often carbonate rich arenites or base limestone), which are distributed over orchards and vineyards. This material is generated by crushing stones which were extracted from the ground (in situ, see Figure 2.1), where farmers are preparing new cropland, or by imported material.



FIGURE 2.1: Soil preparation and rock excavation to produce mineral powder in Sicily (credit: Prof. Dr. Markus Egli).

This soil amendment technique has already been established in the 1970's in this area (Raimondi et al., 2020) and now has been taken up by the 4 per 1000 initiative to create long-term time series on carbon sequestration and soil fertility on agricultural land. Carbon sequestration due to enhanced weathering in Sicily should be even more promoted by the year-round mild temperatures and artificial irrigation. The increased surface area by crushing allows further greater weathering reaction rates (White and Brantley, 2003). The addition of lime to soils has onwards shown to improve soil quality, allowing greater agricultural production (Raimondi et al., 2020). On one hand, the admixture of this rather sandy material allows better aeration of the naturally existing clayey soils (vertisols) in the region. The densely packed clay is loosened up. On the other hand, the soil can be better irrigated, since the sand, in addition to the clay that stores water, allows better filtration through the soil (Riar and Coventry, 2013).

Around the study area of the city of Canicatti (municipal of Agrigento), four locations were sampled and three sites near the city of Mazara del Vallo (see Figure 2.3). Canicatti is located in central, southern Sicily with a mean annual precipitation of 600mm (Arnone et al.,

2013) and mean annual temperature of 16°C (Viola et al., 2014). The Mazara del Vallo region has an annual precipitation of approximately 500mm (Arnone et al., 2013) and 18°C mean annual temperature (Viola et al., 2014) and is situated on the western part of the island. These semi-arid regions were chosen, since the soil is very receptive for storing additional carbon (Francaviglia et al., 2019). Moreover, dryland regions span over 42% of the earth's surface, 55% of the worlds cultivated land, produce 50% of our planets livestock's (Laban et al., 2018) and own 30% of the global SOC stocks (Laban et al., 2018; Manley, 2014). In Sicily, the agricultural focus has been shifted in part in the 1990's from vineyards to olive and almond plantations (Raimondi et al., 2020). Today, the dominant species cultivated in Sicily are legumes such as chickpeas, faba beans and cereal (wheat, barley), as well as forage legumes (Barbera et al., 2012). In the study regions however, especially wine grapes are being cultivated (see Table 2.1).

TABLE 2.1: Details of the study areas.

Profile	Coordinates	Altitude (in m a.s.l.)	MAAT <sup>1</sup> (°C)	MAP <sup>2</sup> (mm)	Slope (%)	Exposure	Parent material	WRB Soil Taxonomy <sup>3</sup>	Land use	Approx. year of transformation
Cazzola 4	37°21'57.7"N/ 13°48'04.7"E	459	16.0	600	3	150°SE	Limestone (Calccare di base)	Anthroposol	Orchard: Table grapes (Uva da tavola)	1985
C.Fazio	37°24'07.5"N/ 13°52'14.0"E	514	16.0	600	5	75°E	Limestone (Calccare di base)	Anthroposol	Orchard: Table grapes (Uva da tavola) and peach	1993
C.Fazio 2	37°24'04.4"N/ 13°52'15.7"E	524	16.0	600	8	335°NW	Limestone (Calccare di base)	Anthroposol	Orchard: Table grapes (Uva da tavola)	1993
Grotta Rossa 2a1	37°24'29.6"N/ 13°53'28.8"E	515	16.0	600	10	150°SE	Limestone (Calccare di base)	Anthroposol	Orchard: Table grapes (Uva da tavola)	1975
Grotta Rossa 2a2	37°24'27.0"N/ 13°53'27.0"E	511	16.0	600	16	150°SE	Limestone (Calccare di base)	Anthroposol	Orchard: Table grapes (Uva da tavola)	1975
Grotta Rossa 4a1	37°24'30.2"N/ 13°53'27.0"E	519	16.0	600	1	150°SE	Limestone base)	Anthroposol	Orchard: Table grapes (Uva da tavola)	1975
Lauria P1	37°19'15.0"N/ 13°54'43.0"E	375	16.0	600	12	10°N	Limestone (Calccare di base)	Anthroposol	-	(2020) (undisturbed)
Lauria P1a	37°19'05.0"N/ 13°54'43.0"E	387	16.0	600	10	10°N	Limestone (Calccare di base)	Anthroposol	Orchard: Table grapes (Uva da tavola)	2003
Mazara del Vallo P4	37°43'10.51" N/ 12°35' 19.43" E	63	18.0	500	-	-	Limestone (Calcarenite)	Anthroposol	Orchard: Citrus plants	1975
Mazara del Vallo P7	37°43'20.73" N/ 12°35' 04.34" E	63	18.0	500	-	-	Limestone (Calcarenite)	Anthroposol	Orchard: Citrus plants	1972
Mazara del Vallo Ferla	-	-	-	-	-	-	Limestone (Calcarenite)	Remains of an Alfisol	-	- (undisturbed)

<sup>1</sup>Viola et al. (2014)

<sup>2</sup>Arnone et al. (2013)

<sup>3</sup>WRB (2015)

The region is under the influence of a Mediterranean climate that is characterised by hot and dry summers, whereas the winters are mild and wet. In Sicily, an all-year cultivation is possible in areas having greenhouses. The research area in Canicatti is characterised by an Oligocene to Pliocene geology (Trumpy et al., 2015), where large amounts of “*calcare di base*” - base limestone can be found (Egli et al., 2020b). In the region of Mazara del Vallo, calcarenite parent material is dominant which originates from Quaternary deposits. The excavated calcareous material in Canicatti and Mazara del Vallo is used for the soil amendments (Raimondi et al., 2020).

The undisturbed soils around Canicatti and Mazara del Vallo show characteristics of vertisols, with alternating wet-dry cycles and shrink-swell clays (WRB, 2015). However, the agricultural amendments transformed original vertisols into anthroposols. The transformed soil contain a higher amount of sand and carbonate buffer and are thus better suited for agricultural purposes. Although the soil transformation is rather invasive (see Fig. 2.1), this method of cultivation is regarded as “reduced tillage” in this thesis, as no chemical fertilisation or ploughing is used after the transformation.

## 2.1 Canicatti research area

The farmers normally start to irrigate the area around Canicatti in April in a cycle of 5-9 days. Approximately  $12 \text{ l/m}^2$  of water are typically used and in total  $400 \text{ m}^3$  of water per year (when ripeness is reached). Up until  $800 - 1000 \text{ m}^3/\text{y}$  is used if harvested in November/December. Today, irrigation is done via pumps or waterlines which are placed within the tree crowns and release water through small openings. Without irrigation, broccoli, fennel and cabbage are being grown through the winter months until March, followed by eggplants, tomatoes and pumpkins. Wine grapes are yearly harvested (Maurici, 1983). The soil is harrowed once a year in March with a motor hoe for smaller parcels of land, while bigger areas are being harrowed via tractor (Lombardo and Raimondi, 1991). Usually, cover crops are being planted between the vine stocks to prevent soil erosion.

The three profiles in Grotta Rossa (see Fig. 2.3; Table 2.1), transformed in 1975, can be seen as a soil sequence along a hill. Grotta Rossa 4a1 is located on top of the hill in a nearly flat slope ( $1^\circ$ ), while Grotta Rossa 2a1 and 2a2 are lying on the hillside with a  $10^\circ$  and  $16^\circ$  slope, respectively (see Fig. 2.2). The yellowish soil colour in the profiles indicate the appearance of oxidized iron. The soil on this site is now being prepared for the plantation of table grapes. In the past, organic fertilizer/material has been used besides liming (Raimondi et al., 2020). Cazzola 4 (Fig. 2.3 and Table 2.1), transformed in 1985, lies in a flat valley and owns a deeply developed, harrowed, organic Ap horizon. The yellowish soil colour reveals the appearance of oxidized iron.

Both C.Fazio sites (see Fig. 2.3), transformed in 1993, lie on a flat orchard hillside and are

harrowed. The profiles are showing an undifferentiated mixture of organic material in the entire soil profile (Ap) (see Fig. 2.2). The pale yellowish-brown soil colour also indicates the appearance of oxidized iron and little organic material.

Lauria P1a (Fig. 2.3; Table 2.1), transformed in 2003, is not well developed, having a small organic layer mixed with base calcite. Lauria P1 has not been cultivated yet and still bares the parent material at the surface (white calcite). The profiles are stony with a slope of 12° in Lauria P1 and 10° in Lauria P1a.

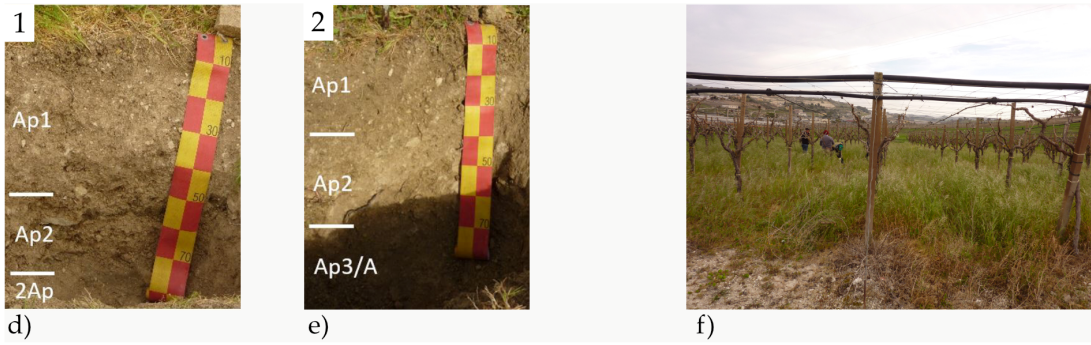
## **2.2 Mazara del Vallo research area**

At present, lemons, strawberries and watermelons are being grown in this region (Raimondi, 2019). The strawberries are sown in September and the watermelons in March, growing under a plastic cover (Raimondi, 2019). The area is being irrigated in the summer in a 15-day cycle, beginning in June until September (Raimondi, 2019). Both artificial profiles in Mazara del Vallo P4 and P7 are deeply developed with well blended A horizon due to harrowing (see Fig. 2.2). The dark soil colour indicates a relatively high organic content and the reddish hue oxidized iron. A natural, undisturbed soil profile (Mazara del Vallo Ferla) in the region consists of a base horizon made of calcarenite with an undisturbed A horizon (remains of an Alfisol).

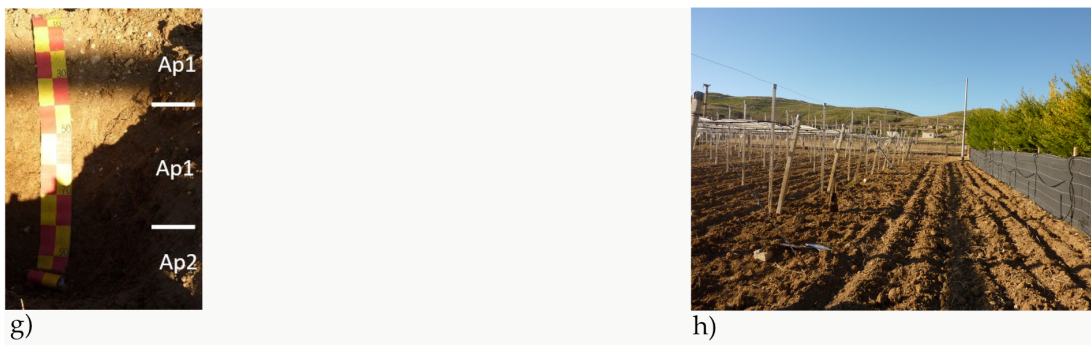
**Lauria**



**C.Fazio**



**Cazzola 4**



**Grotta Rossa**

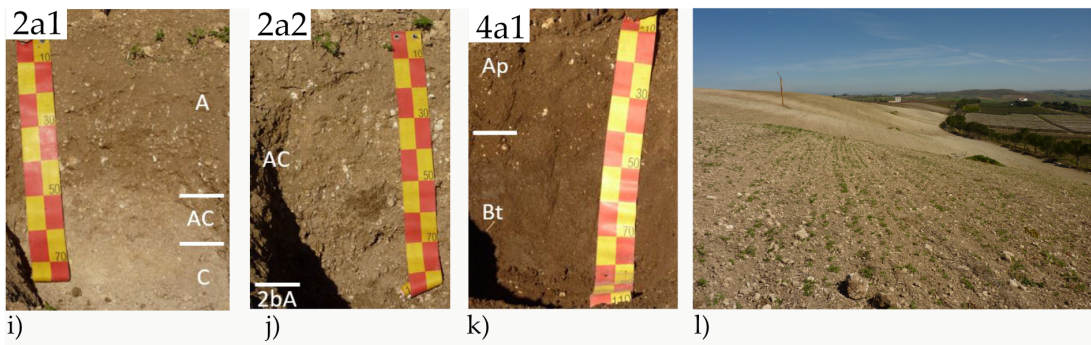


FIGURE 2.2: Sampled profiles with horizon indication.

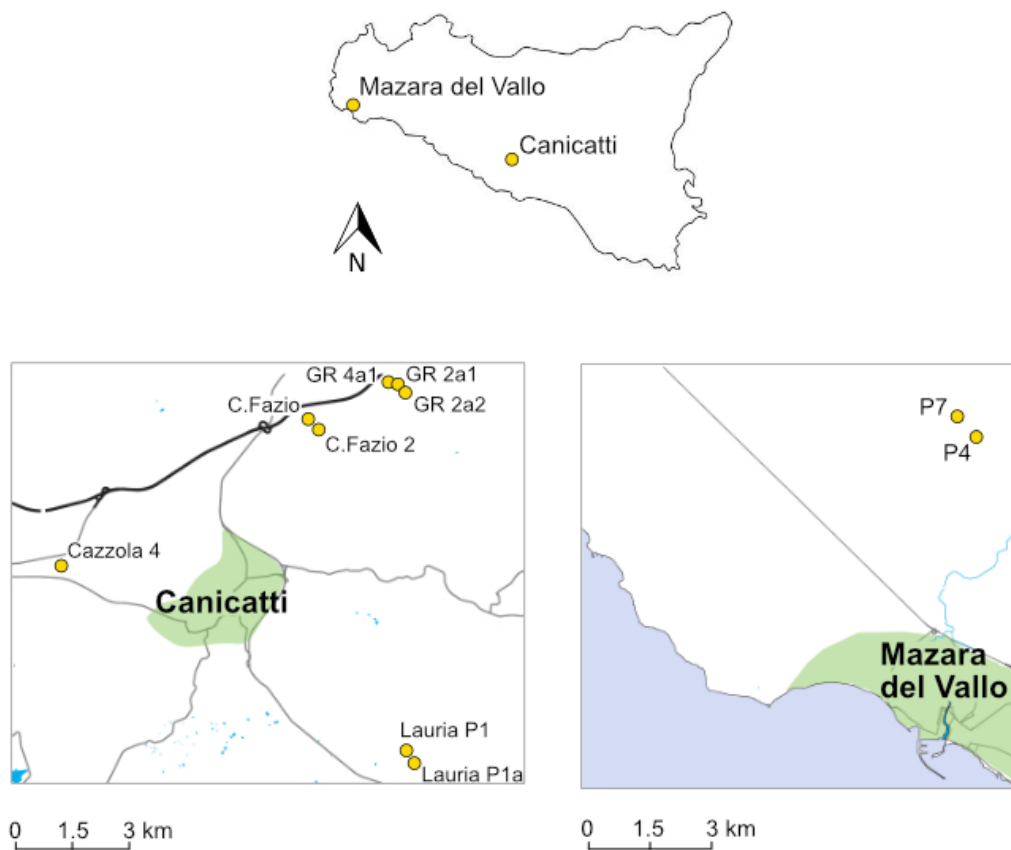


FIGURE 2.3: Map of sampled profiles in each observed region. Green areas indicate city area; black lines designate main streets; GR = Grotta Rossa; overview map by NA (2020); map data: Open street map; Mapping program: OCAD.

### 3 Research questions and experimental setting

The potential of soils in Mediterranean regions to sequester and store carbon will be split into following research questions and hypothesis:

- How effective is the carbon sequestration/storage due to this soil amendment practices?
- How much carbon has been additionally stored (in the topsoil) since the start of the soil amendment in the 1970's?

*Hypothesis: Organic and inorganic carbon has been stored in significant amounts since the start of the land amendments.*

- Which are the sequestration rates and when is a saturation reached?

*Hypothesis: Carbon sequestration will be detectable in the data and a saturation limit will not be reached yet.*

- Has carbonate been leached?

*Hypothesis: Carbonate leaching will be detectable over the observed time period.*

- Is silicate weathering detectable over a time span of a few decades?

*Hypothesis: Silicate weathering has been found in the recent years of land transformation.*

*Additional questions:*

- Did soil (crop) productivity increase since the 1980's?
- What crops could be used to help the additional storage of carbon?

To measure the sequestration rates over time and to estimate the saturation level, a time for space (chronosequence) approach was used. The times were not given in the unit BP (before present) as is it usual in geochronology, but instead in years (a) since transformation. The reference year is 2020, in which this paper is written. This seems to be clearer for the consideration of the short time intervals of the formation of the profiles.



**ATTENTION:** For simplicity, the undisturbed profile of Lauria P1 is shown as the start of the soil development ( $t = 0$  years) in the graphs and Mazara del Vallo Ferla as a possible endpoint of soil development.

## 4 Material and Methods

### 4.1 Statistics

The data was analysed with *R* Studio 1.2.504 and Microsoft Excel. A Shapiro-Wilkinson test was performed, followed by a Kruskal-Wallis test for not normally distributed data (including a pairwise Wilcoxon-test for specification between the groups (Benjamini-Hochberg method)) and an ANOVA (analysis of variance) for normally distributed data (including a ANOVA pre-test: fligner test (homogeneity of the variances)) and a pairwise-t-test (Benjamini-Hochberg method);  $p$ -value = 0.05. For correlation analysis,  $R^2$  was used as well as Spearman's rank and pearson's  $r$  correlation coefficient.

### 4.2 Sample preparation

For sampling, soil pits were dug as deep as possible by hand or excavator and were classified with the WRB soil taxonomy (WRB, 2015). In order to avoid a too large sample size, no replicates were taken. Instead, a sufficiently large amount (several kilos) of material was removed from each horizon to obtain a representable range for the later analysis in the laboratory. To identify the bulk density of each horizon, two smaller probes were taken in a soil corer the size of  $100\text{cm}^3$  (Eijkelkamp). For topsoil and subsoil comparisons, additional soil corer probes were taken for computational tomography (CT) evaluation. The capsules were hammered into the ground by hand.

The sampled material was first dried for 48h at  $70^\circ\text{C}$ . After, it was crushed in a mortar to separate the skeleton ( $> 2\text{mm}$ ) from fine earth ( $< 2\text{mm}$ ). To determine the amount of coarse material, the skeleton was taken as the weight percentage of the total material. During the grinding, the probes were repeatedly sieved through a  $2\text{mm}$ -mesh sieve to extract the fine soil fraction. In a next step, an aliquot of the fine earth was milled in a horizontal mill to reach a sample size of 60 *microns*. The samples were milled in wolfram vessels, containing approximately 16g of material per vessel and sample. The samples were milled at a frequency of 280 Hz for 9min. up to 12min., depending on the original granularity of the probe.

## 4.3 Physical Analysis

### 4.3.1 Bulk density

The bulk density was calculated as follows by an average of two samples per horizon taken in the field. The skeleton content was not subtracted since most samples had a rather large clay content anyway:

$$\rho = \frac{M}{V} \quad (4.1)$$

$\rho$  denotes the bulk density,  $V$  the packing volume in  $cm^3$  and  $M$  the dry mass in gram.

### 4.3.2 X-ray computational tomography

Nine samples were measured via X-ray computational tomography (XRT) at the IA PAS XRT lab (Institute of Agrophysics, Lublin, Poland) with a GE Nanotom 180S tool (GE Sensing & Inspection Technologies GmbH, Wunstorf, Germany). The scan resolution (voxel size) was  $0.029mm$  with an X-ray source voltage of  $130kV$ , a cathode current of  $200A$  and a  $0.2mm$  Cu filter to avoid beam hardening effect. Only pores bigger than  $0.029mm$  have been represented.

The 2D images were averaged from X-ray pictures for noise cancelling. These served as the basis for the 3D images, which were generated in DatosX 2.0 (GE Sensing & Inspection Technologies GmbH, Wunstorf, Germany). The 3D 16-bit grayscale images were thus analysed with VG Studio Max 2.0 and Avizo 9. To find regions of interest, a cylinder with a diameter of  $49.1mm$  and  $46.7mm$  height was taken out of the soil core image (Fiji software (U.S. National Institutes of Health, Bethesda, MA, USA)). To minimize noise, a kernel filter with a size of  $3px$  was used and thresholded with the IsoData algorithm (Ridler and Calvard, 1978) of the Fiji software. After, thresholding (Fiji software) was used to distinguish between soil skeleton and soil pores to extract the pore network skeleton. Individual pores were defined as a group of voxels connected by at least one other voxel. Subpores were constructed by splitting larger pores. Finally, the sum of the external pore surface, the volume of the voxels and their corresponding diameter was measured (Avizo 9 software (FEI, Hillsboro, Oregon, USA)). The pore network was determined with a distance map (central pore areas) and thinning (creating the pore network), again using the Avizo 9 software.

### 4.3.3 Grain size analysis

For the grain size analysis, samples  $< 2mm$  between with  $50 - 75g$  weight were mixed with three percent hydrogen peroxide until no reaction was visible anymore. After, the mixture was wet sieved through  $2000, 1000, 500, 250, 125, 63, 45$  and  $32\mu m$  sieves and the fraction  $< 32\mu m$  was caught into a bucket for sedimentation. To differentiate the fraction  $< 32\mu m$ , an aliquot of  $20 - 40ml$  containing  $3 - 5g$  of of the fraction (depending on the amount of

fraction within the solution) was mixed in a 1:1 solution with hexametaphosphate (1%). After, the prepared sample was measured with the Sedigraph 5100.

#### 4.3.4 Clay mineral extraction

After the removal of organic material with a Na-acetate buffered  $H_2O_2$ -solution (3 %), the soil material (20 – 30g, < 2mm) was then dispersed with Calgon and  $MgCl_2$  for sedimentation in deionized water.

After, the samples were on one hand saturated with potassium and heated to 335°C and 550°C. On the other hand, they were saturated with magnesium and after glycerol. The procedure needed to be repeated, since the glycerol evaporated before the measurement. The magnesium saturated samples were further prepared with ethylene glycol to see if better results could be obtained. The results were finally taken from the ethylene glycol treated samples. The samples were then measured using XRD (X-ray diffraction).

Each mineral type has its own lattice structure and typical distances between the individual molecules. X-ray diffraction makes use of this by causing interferences with the X-rays arriving on the samples, as the wavelengths of the incoming X-rays correspond to the lattice spacing of the minerals. When the X-rays reach the sample at a certain angle, peaks of interfering wavelengths are formed. The results are shown in a diffractogram, each peak corresponding to one type of mineral lattice and thus minerals can now be identified. The diffraction of the incoming radiation follows Bragg's law of reflection (see Fig. 4.1). The data needed to be converted corresponding to the copper block through which the X-ray radiation was generated.

The quantification of the soil minerals in the bulk soil was carried out by Michael Plötze from the ETH. To make the time trend of the mineral content visible, sites with zero kaolinite were excluded since they falsify the regression analysis. Calcite has also been removed (normalisation of each relative mineral content on the sample content excluding calcite), because of its vast amounts in the total mineral fraction and since it overlaid/distorted the trend of the other minerals immensely.

#### 4.3.5 Profile development index (PDI)

The profile development index is a relative dating technique for soil where no exact age is obtained (Harden, 1982). It translates soil properties such as texture, structure and soil colour into numeric values. The properties of each horizon are compared to the original soil material (C-horizon) if existing. In the case of Grotta Rossa 2a2, 4a1 and Cazzola 4, the profiles were compared with the C-horizon of Grotta Rossa 2a1, since they do not own a C-horizon themselves. The profiles of C.Fazio and C.Fazio 2 were compared to the corresponding Ap2 horizon, since the lower most horizon contains a different substrate.

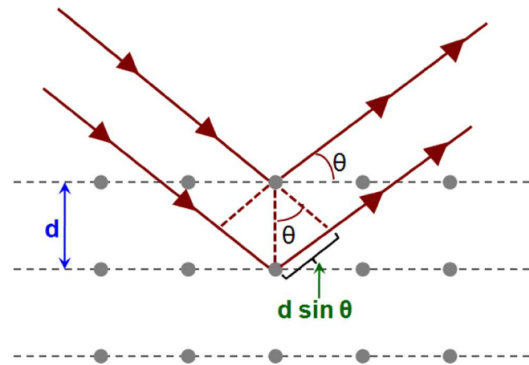


FIGURE 4.1: Illustration of Bragg's law ( $n \cdot \lambda = 2 \cdot d \cdot \sin(\theta)$ ) (Baskaran, 2010) showing incoming X-ray waves on a mineral lattice producing coherent diffraction;  $d$  represents the distance from the lattice planes;  $\theta$  corresponds to the incoming and reflected angle of the wave.

## 4.4 Chemical analysis

### 4.4.1 Total element contents

To measure the total element content of each sample the X-Ray Fluorescence (XRF) was used. A laboratory internal standard NCS DC 73326 (soil with a known elemental content) was used. 5g fine milled sample (approx. 60 *microns*) was filled in a plastic cup, each cup containing one probe. The results were then normalised to oxides.

### 4.4.2 pH measurement

To determine the pH, 5g of each sample (< 2mm) was mixed with 12.5ml 0.01mol/l  $\text{CaCl}_2$  on a magnetic stirrer for 15min. The pH measuring tool was first cleaned with deionized water and then calibrated to pH 7 in standard solution before further use. The accuracy of the pH measurement lies within 0.3 to 0.8 pH units.

### 4.4.3 Carbon and nitrogen

For the total carbon and nitrogen content of each sample the element analysis isotope ratio mass spectrometry (EA-IRMS) was used. 2mg of the milled soil (< 2mm) need to be weighed into zinc capsules. The analysis were made with a Thermo Fisher Scientific Flash HT Plus elemental analyser, in addition with a thermal conductivity detector and a Conflo IV connected to a Delta V Plus isotope ratio mass spectrometer. A Caffeine (IAEA-600) and a Chernozem standard were used for the isotopic data.  $\delta^{18}\text{O}$  and  $\delta^{13}\text{C}$  isotopes were measured, however, N isotopes were not evaluated, since the amount of nitrogen was too small to reach an accurate measurement.

To obtain the organic carbon (OC) stock in any layer, the percentage of organic carbon was multiplied by bulk density ( $\rho_i$ ), layer thickness ( $\Delta z_i$ ) and percentage of fine earth (SS = soil

skeleton). The sequestration rates were then calculated with the stocks over soil age (time since transformation).

$$OC_{stock} = \sum_{a=1}^n OC_i \cdot \Delta z_i \cdot \rho_i \cdot (1 - SS). \quad (4.2)$$

#### 4.4.4 Oxalate-extractable elements

For the measurement, the samples were prepared in an oxalate solution. In the light-protected flasks 16.1g of ammonium oxalate and 10.9g oxalic dihydrate were blended. Droplets of 25 % hydrochloric acid (HCl) were added to reach a pH of 3 and mixed with 900ml deionized water. After, 2g of dried and sieved sample ( $< 2mm$ ) was added and shaken for 2 hours before filtrating (150mm filter). The oxalate suspension was then analysed within an Atomic Absorption Spectrometer (AAS - AAnalyst 700, Perkin Elmer) to measure manganese, iron and aluminium contents in the soil (in comparison to a Sigma-Aldrich standard). The AAS can detect trace quantities and is thus much more accurate than the X-Ray spectroscopy.

To receive the oxalate-extractable (OE) stocks (production rate) in any layer, the concentration of each extractable was multiplied by layer thickness ( $\Delta z_i$ ), bulk density ( $\rho_i$ ) and percentage of fine earth ( $SS =$  soil skeleton):

$$OE_{stock} = \sum_{a=1}^n OE_i \cdot \Delta z_i \cdot \rho_i \cdot (1 - SS). \quad (4.3)$$

#### 4.4.5 Carbonates

The carbonate content was first measured with a Thermo Fisher Scientific GasBench II coupled to a Delta V Plus isotope ratio mass spectrometer. A sample and standard subset with 20 – 100  $\mu g$  Ccarb were automatically drenched with He for 10min. and 25 – 50 $\mu l$  phosphoric acid were then admixed. After the release of the carbonate C, aragonite and dolomite from  $CaCO_3$  (approx. after 60min. (Egli et al., 2020b)), the probes were measured. A Merck standard for  $CaCO_3$  and the isotopic measurements of  $\delta^{13}C$  and  $\delta^{18}O$  was used. The amount of organic carbon was determined by subtracting the amount of inorganic carbon from the total C. Error measurements of the Corg content by the IRMS were reproduced with the Walkley-Black method which is thought to give qualitative similar results as the EA-IRMS (Gessesse and Khamzina, 2018). Pedogenic carbonate was determined with a rule of three of the  $\delta^{13}C_{carb}$  measurements and a corresponding typical  $\delta^{13}C$  value of the region for the biogenic material ( $-24.8 \text{ ‰}$  (Egli et al., 2020b)) and  $-1 \text{ ‰}$  for 100 % carbonate.

#### 4.4.6 Loss on ignition (LOI)

The amount of organic matter and adsorbed water within the soil sample was determined by loss on ignition. 2g of sample was being oven-dried at 550°C for 6 h until all organic

remains are lost. The weight difference before and after drying was then calculated to obtain the organic material from the sample. The combustion temperature was chosen below 600°C to prohibit that carbonates start to decompose. The accuracy of LOI is furthermore largely dependent on the clay content of the samples, the sample mass, duration of ignition and stove type (Hoogsteen et al., 2015).

#### 4.4.7 Chemical weathering indices

The indices show element variations within the soil due to chemical weathering. The WIP is especially suitable to detect weathering of silicate rock (Shao et al., 2012). The CIA is mostly used to see how much feldspar is transformed into clay (Nesbitt and Young, 1989; Fedo et al., 1995; Yang et al., 2004). Due to the carbonate rich soils, a modified version  $(K + Na)/Ti$  of the molar ratio  $(K + Ca)/Ti$  has been used, as it prevents falsification of washed out carbonate (Egli et al., 2020b). The indices are based on rations of basic cations ( $Ca, K, Na, Mg$ ) which are easily soluble to relatively immobile soil elements such as titanium, aluminium and/or silicates (Egli and Fitze, 2000; Egli et al., 2020a).

The following chemical indices were used:

$$WIP^1 = 100 \left[ \frac{2Na_2O}{0.35} + \frac{MgO}{0.9} + \frac{2K_2O}{0.25} + \frac{CaO}{0.7} \right]. \quad (4.4)$$

The  $CaO$  corresponds to the silicate fraction of  $Ca$ .

$$CIA^2 = 100 \left[ \frac{Al_2O_3}{Al_2O_3 + CaO + Na_2O + K_2O} \right]. \quad (4.5)$$

$$\text{Molar ratio}^3 = \frac{K + Na}{Ti}. \quad (4.6)$$

The open-system mass transport Tau was also calculated. Tau provides results on the relative transport of elements including silicates and carbonates (Chadwick et al., 1990; Egli and Fitze, 2000). Tau is based on the variable Epsilon:

$$\epsilon_{i,w} = \left( \frac{\rho_p \cdot C_{i,p}}{\rho_w \cdot C_{i,w}} \right) - 1. \quad (4.7)$$

for which applies  $C_{i,p}$  as the concentration of the immobile element  $Ti$  in the non-weathered parent material;  $C_{i,w}$  as the concentration of the immobile element  $Ti$  in the weathered material;  $\rho$  denoting the bulk density of the parent ( $p$ ) and the weathered ( $w$ ) material, respectively.

$$\tau_{j,w}^4 = \frac{C_{j,w} \cdot C_{i,p}}{C_{i,w} \cdot C_{j,p}} - 1. \quad (4.8)$$

Relative mass loss ( $\tau_{j,w}$ ) in %, for which applies  $C_{j,p}$  as the concentration of the element  $j$  in the non-weathered parent material;  $C_{i,w}$  as the concentration of the immobile element (non-carbonate fraction of the soil (Egli et al., 2001b)) in the weathered material.

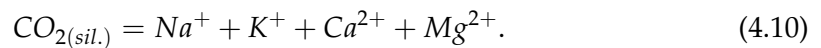
$$\bar{m}_{j,flux(z_w)} = \sum_{a=1}^n C_{j,p} \cdot \rho_p \cdot \left( \frac{1}{\epsilon_{i,w} + 1} \right) \cdot \tau_{j,w} \cdot \delta z_w. \quad (4.9)$$

Absolute mass loss ( $\bar{m}_{j,flux(z_w)}$ ) in  $kg/m^2$ , for which applies  $C_{j,p}$  as the mean total content of the element  $j$  in the parent material;  $\rho_p$  denotes the bulk density of the parent material;  $\epsilon_{i,w}$  as the concentration of the immobile element (non-carbonate fraction of the soil (Egli et al., 2001b)) in the weathered material;  $\tau_{j,w}$  as the relative mass of the weathered element  $j$  and  $\delta z_w$  as the horizon thickness of the weathered material.  $CaO$  represents the silicate fraction of  $Ca$ , and in the silicate weathering flux  $CaO$ ,  $Na_2O$ ,  $K_2O$  and  $MgO$  were included.

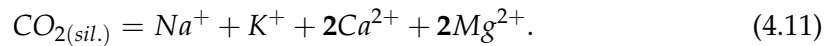
#### 4.4.8 Silicate and carbonate weathering ( $CO_2$ consumption)

##### Silicate weathering

- 1:1 ratio of silicates and  $CO_2$  (Hilley and Porder, 2008):

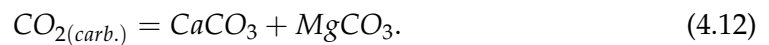


- 2:1 ratio silicates and  $CO_2$  (Hartmann et al., 2013):



##### Carbonate weathering

- 1:1 ratio of carbonates and  $CO_2$  (Hartmann et al., 2013):




---

<sup>1</sup>Parker (1970)

<sup>2</sup>Nesbitt and Young (1982)

<sup>3</sup>Harrington and Whitney (1987)

<sup>4</sup>Egli et al. (2020b)





## 5 Results

### 5.1 General soil characteristics

The soil thickness increases up to 110 *cm* in the deepest developed soil profile Mazara del Vallo P7 from the 1970s. While Mazara del Vallo P7 evolved an Ap1-Ap2-C profile structure, the other profiles from this location are slightly shallower and developed an Ap-C profile. The profiles of Grotta Rossa, which were also transformed in the 1970s show a similar depth development with over 85 *cm* (see Fig. 2.2). While Grotta Rossa 2a1 has an organic layer A and mixed layer AC, Grotta Rossa 2a2 shows a mixture of the A horizon with the parent material C at the surface and a mineral base layer B. Grotta Rossa 4a1 possesses a ploughed surface and a washed-in clayey Bt horizon with a high organic material content.

As we continue further towards the 1980s (Cazzola 4) and 1990s (C. Fazio), the soil thickness does not change remarkably while the mineral surface horizon A gains substantial thickness (see Fig. 2.2).

The newly transformed profiles from the Lauria location are still only shallowly developed with a C-horizon still appearing at the surface. Beside the amended locations, two undisturbed sites were additionally observed: *Lauria P1*, a location where no real soil development processes have yet started and *Mazara del Vallo Ferla*, where a full soil development is visible.

The bulk density is generally decreasing with increasing soil age (from 1.57 down to 1.26  $g/cm^3$  (Fig. 5.1a)) which is a normal process in soil (Osunbitan et al., 2005). However, the undisturbed site of Lauria P1 has a comparably lower bulk density than the amended Lauria P1a. This contradicts the fact that Lauria P1 is formed from solid bedrock. A possible source of error for this result could be during sieving, where too much rock material was identified as fine soil ( $< 2mm$ ). The bulk densities are mostly  $< 1.6 g/cm_3$  which leaves enough space for root growth (Brown and Wherrett, 2020).

In contrast, the untreated Mazara del Vallo Ferla site retains a rather high density in respect to the other amended profiles of that location. A possible reason could be the amendment of sandy calcarenite on the amended sites which may have increased the pore space. It lowers the bulk density and corresponds with observations of agricultural practices that leave internal soil structure intact and therefore do not lead to soil compaction (Carter and Gregorich, 2006).

With the increasing weathering of the inorganic carbon of the calcareous parent material, the pH value decreases slightly with soil age, but remains in a neutral to alkaline range (7.8 – 7.2) (see Fig. 5.3; 5.1b), indicating the presence of large amounts of carbonate (see

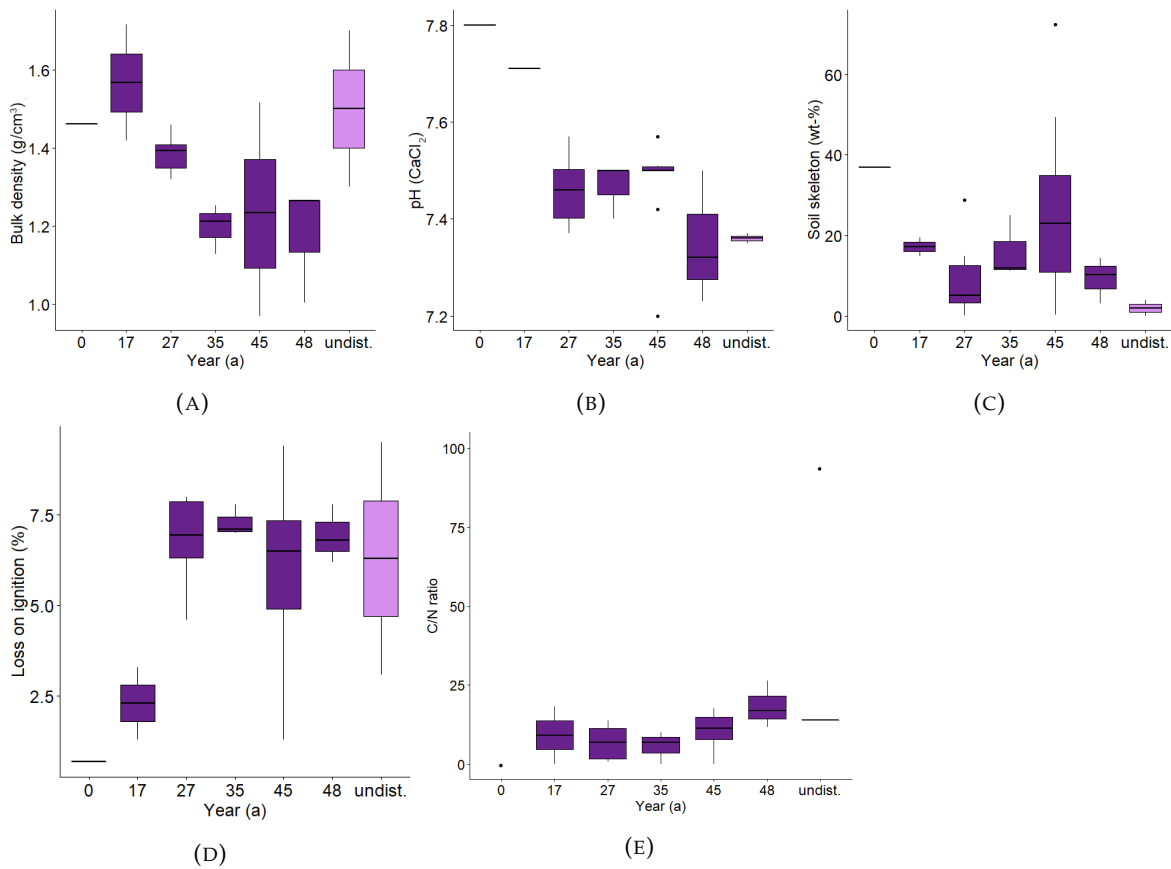


FIGURE 5.1: Soil characteristics development over time of general parameters summarised over each transformation year; pink stands for the undisturbed profile (undist.).

Table 5.3).

Soil skeleton decreases from 2020 until the 1990s and grows again slowly until 1975. It then decreases in the undisturbed soil profile of Mazara del Vallo Ferla (1970), declining from 72 *weight* – % in Grotta Rossa 2a1 to almost zero *weight* – %. The range appears to be quite large, however most values lie in a spectrum of 0 – 40 *weight* – % (see Fig. 5.1c). While most variability is found in the transformed profiles of 1975, no statistically proven difference over soil age was found.

The LOI, an indication for the organic matter content within the soil (Hoogsteen et al., 2018), remains throughout the past 50 years around a median of 6.7 (see Fig. 5.1d), except from the newest transformed soil profile of 2003, in which the organic matter content is low (around 1 %), which can be explained by the little soil development so far. A strong negative relationship between LOI and pH was found ( $\rho = 0.615$ ,  $p < 0.05$ ), which is most likely due to the  $H^+$  dissociating from the organic matter and hence decreasing pH (Weil and Brady, 2017). Yet it is questionable if this large effect has been achieved in these few years since the soil transformations.

The C/N ratio increases from Cazzola 4 up to Lauria and with the highest *Corg* content

and thus widest ratio in the oldest transformed soil profiles of Mazara del Vallo and Grotta Rossa. The C/N ratio has a median of 10.1, a usual value for agricultural soil in middle Europe (Blume et al., 2010) and decreases with increasing depth which is typical for arable land (Weil and Brady, 2017). Otherwise the C/N ratio does not change much, except for Mazara del Vallo Ferla C with a value of 92.4. However, this outlier is caused by the nitrogen measurement being close to 0, which overestimates the ratio (see Table 5.3 and Fig. 5.1e). Other samples with various soil ages did not contain any nitrogen (see Table 5.3), thus the C/N ratio is zero (see for example year 0). The decreasing ratio over time furthermore shows that an advanced degradation of biological material has occurred (Weil and Brady, 2017).

## 5.2 Carbon compounds

The newly transformed Lauria P1 and P1a contain the largest percentage of total carbon (bound in carbonates) besides Mazara del Vallo P4, while the oldest transformed (Mazara del Vallo P7 and Grotta Rossa 4a1) exhibit the least total C (see Fig. 5.3 a).

The carbonate content is quite high throughout all soil profiles due to the carbonate rich parent material (see Table 5.3). The C horizons typically contain the highest carbonate concentrations, however, also some horizons near the surface (C. Fazio Ap1) contain up to 57 % of  $CaCO_3$ . The quite homogeneous carbonate depth distribution can be explained by the mixing of the soil material by ploughing and other human contributions (Egli et al., 2020b). The total inorganic carbon is the highest in the profiles with an identified C horizon, however Mazara del Vallo P7 has a comparably small amount in the topsoil to Mazara del Vallo P4 (see Fig. 5.3 c).

A diffuse distribution and a slight decrease of organic carbon is observable with depth since most organic matter and therefore soil organic carbon are found on the soil surface (see Fig. 5.3 b). The C horizons do not even contain any organic carbon in some cases (Lauria P1 and Mazara del Vallo P4, see Table 5.3) (Weil and Brady, 2017). Grotta Rossa 4a1 and the Mazara sites contain the highest *C<sub>org</sub>* fraction (see Fig. 5.3 b). The undisturbed profile of Mazara del Vallo Ferla lost the most *C<sub>org</sub>* with depth and Mazara del Vallo P7 owns a comparably high amount of organic carbon to the other sites from that location. A possible reason might be the allocation of organic carbon/matter by plant roots, corresponding to the augmented LOI values for that horizon.

Looking at the time span in which the soils have been amended, the pedogenic carbonate slightly increases with soil age (see Fig. 5.3 e). The profile of 1975 (Grotta Rossa 4a1) shows the most prominent increase of pedogenic carbonate. Yet, only one profile was sampled from 1985 in relation to the 6 sampled sites from the 1970's, which might bias the result.

### 5.2.1 Carbon stocks and sequestration rates

The organic carbon stocks grow ( $R^2 = 0.5436$ ) with time (see Fig. 5.2 a). The maximum *Corg* stock is reached at  $15.1 \text{ kg/m}^2$  for the oldest transformed locations (Grotta Rossa 4a1). Interestingly, this is followed by the undisturbed profile Mazara del Vallo Ferla with  $13.3 \text{ kg/m}^2$ . These values are higher than other soils of a Mediterranean climate in Andalusia ( $1.59 - 10.76 \text{ kg/m}^2$ , Munoz-Rojas et al., 2012). However, it must be considered that the organic carbon probably already has been stored before the soil was transformed.

The storage of organic carbon is still intensely discussed and is thought to depend on many factors such as air and soil temperature, moisture, texture and soil depth (Weil and Brady, 2017). Organic carbon stocks are believed to increase with increasing moisture and temperature and a finer soil texture (Weil and Brady, 2017). Thus the artificial irrigation on the observed profiles might help to store extra carbon in the soil. Nevertheless, the high amount of organic carbon stored within the undisturbed profile of Mazara del Vallo also could indicate that agricultural activity indeed increases the loss of soil carbon.

The sequestration rate furthermore does not remarkably increase with soil age and the beginning of the soil transformations ( $R^2 = 0.3654$ ) (see Fig. 5.2 b).

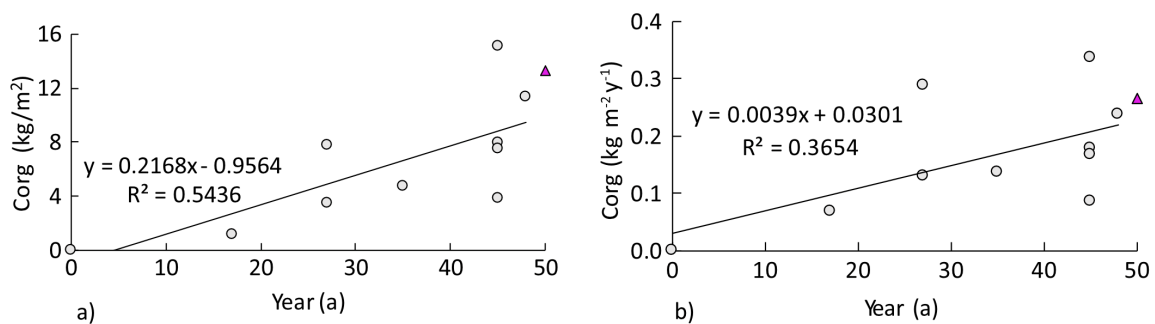


FIGURE 5.2: Stored a) and sequestered b) organic carbon over the last 48 years with trendline; undisturbed profile is designated as pink triangle.

### 5.3 Grain size evolution

The Lauria profiles contain the highest amount of sand (coming from the sandy limestone of the parent material) and the lowest amount of clay, besides the locations at Mazara del Vallo (see Fig. 5.4). The clay content in the Lauria profiles reaches a minimum of 2.7 %. Towards 1993, the amount of clay increases and reaches an overall maximum in C.Fazio, C.Fazio 2 (see Fig. 5.4). The profiles of Cazzola 4, C.Fazio and C.Fazio 2 appear to have probably already been deeply developed before the soil transformation (no parent rock found at a depth of  $1 \text{ m}$ ), inheriting more properties of the previous vertisol. The high clay content in these profiles is matched by an equally high silt content (around 40 %), except from C.Fazio 2 Ap1 in which a decreasing clay content is compensated by a rising sand fraction. This

outlier might be caused by the extra added calcareous arenite from land amendments. In Cazzola 4, the sand content increases somewhat, however the silt and clay content still are in the range of 35 – 40 %. The oldest transformed profiles of Mazara del Vallo and Grotta Rossa are mostly made up of silt (up to 50 %), declining in sand and clay. The two aberrations in Mazara del Vallo with a high sand content both belong to a C horizon (see Fig. 5.4).

According to the previously mentioned grainsizes the Lauria locations can be classified as sandy loam/loam. C.Fazio and C.Fazio 2 already belong to silty clay/clay since they have the highest clay content of all profiles. Cazzola 4, on the other hand, increases in silt and sand (silty clay loam), and the Grotta Rossa and Mazara del Vallo sites follow this trend further (clay to sandy loam). Out of the observed grain sizes, only clay shows a statistically significant change over the observed time period.

The overall amount of clay is of similar magnitude comparing a study of Egli et al. (2020b), yet in most C horizons we have remarkably less clay. An explanation for this could be that we often meet consolidated solid limestone in the C horizon.

## 5.4 Clay minerals

### 5.4.1 Lauria P1a

The Mg-saturated sample enhances peaks at 0.72, 1.00 and 1.42nm. Mica (muscovite, illite and/or biotite) is visible throughout the samples at 1.00nm and increased remarkably after potassium treatment (Fig. 5.5).

Kaolinite is furthermore visible in the samples as the peak lies at 0.72 throughout all samples except for the heated sample (550 °C) where kaolinite becomes amorphous and disappears in the diffractogram. Vermiculite was identified at the peak position 1.42nm because with the potassium saturation, the peak collapses to 1.00nm.

The ethylene glycol treated sample increases the layer spacing to 1.67nm, indicating smectite. However, the K-saturated sample does not show a peak shift to 1.25nm, which would also be typical for smectite. However, a smectite peak is reflected at 0.84 and 0.89nm in the ethylene glycol treated sample.

In the C horizon, the same peaks as within the AC horizon of kaolinite (0.72nm), reflected smectite (0.79 and 0.89nm), mica (1.00nm), vermiculite (1.43nm) and smectite (1.67nm) are observable. However, mica seems to decrease with depth. The peak of 1.19nm in the K-saturated sample shifts with ethylene glycol to the left towards 1.51nm. It shows that a mixed layered clay mineral of smectite/vermiculite with mica or hydroxy-interlayered smectite (HIS) or hydroxy-interlayered vermiculite (HIV) is thus found at 1.19nm and 1.51nm. Besides, vermiculite might also be a reason for the elevated K-saturated line in the diffractogram at 1.19nm.

### 5.4.2 C.Fazio

In the magnesium saturated sample, peaks were identified at 0.72, 0.99, 1.06 and 1.39nm. No shift of the 0.99nm peak with ethylene glycol or potassium treatment was found, therefore indicating mica (Fig. 5.5). The peak at 1.06nm probably designates a mixed-layered clay mineral of mica and vermiculite or smectite and the peak at 1.39nm designates vermiculite. Kaolinite is again present in the samples as the peak lies at 0.72 throughout all samples except for the heated sample (550 °C) where kaolinite becomes amorphous and disappears in the diffractogram. Since no peak shift towards 1.4nm in the heated sample (550 °C) can be seen, chlorite can be excluded.

The ethylene glycol treated sample displays a peak at 1.66, indicating smectite. Smectite is reflected at 0.86nm in the ethylene glycol treated sample.

Unfortunately, the sample from the underlying horizon 2 Ap was accidentally spilt and could no longer be used.

### 5.4.3 Cazzola 4

After measuring the magnesium saturated sample, peaks were found at 0.72, 1.00 and 1.40nm. The peak at 1.00nm peak is identified as mica (Fig. 5.5).

It can also be seen that kaolinite is present in the samples as the peak is continuously at 0.72nm throughout the treatments except for the heated potassium sample (550 °C) where kaolinite becomes amorphous and disappears in the diffractogram. The peak at 1.40nm can again be attributed to vermiculite. Chlorite does not exist in this profile because no peak shift in the heated sample (550 °C) towards 1.40nm is assignable.

The peak at 1.64 in the ethylene glycol treated sample can be attributed to smectite, since the replacement of water by ethylene glycol increases the layer spacing. The peak at 0.88nm represents a reflection of the smectite peak (ethylene glycol).

In the underlying Ap<sub>2</sub> horizon, the peak at 1.45nm represents a mixed-layered clay mineral of mica and smectite or vermiculite or HIV/HIS. Otherwise no big alteration can be seen within the profile.

### 5.4.4 Mazara del Vallo P7

In the magnesium saturated sample, peaks were observed at 0.72 and 1.00nm. Mica is visible throughout the samples at 1.00nm since no shift of peak with ethylene glycol or potassium treatment was found (see Fig. 5.5).

Kaolinite is again visible at 0.72nm throughout all samples except for the heated sample (550 °C) where kaolinite becomes amorphous and disappears. In addition, the K-saturated sample does show a hardly visible peak shift to 1.24nm, indicating smectite/vermiculite interlayered with mica.

In the C horizon, the same peaks as within the Ap<sub>1</sub> horizon of kaolinite (0.72nm) and mica

(1.00nm) are observable. However, mica seems to decrease with depth. At 1.40nm, vermiculite appears in the profile. At 1.11nm, a mixed-mineral layer is observable which shows a left-skewed slope in the K-saturated sample (position 1.00nm) and thus probably represents a HIV.

In general, the profiles do not vary notably in their mineral composition. All profiles contain smectite, vermiculite, mica and kaolinite. This might be due to the short time span in which the soil have developed yet or/and due to the agricultural activity among the soil which homogenises the material with depth. In all profiles except in C.Fazio (no C horizon measured), mixed-layered minerals of mica and smectite/vermiculite or HIV/HIS have been found in the C horizons.

Lauria P1a C contains distinctively less kaolinite and mica than the other investigated profiles (Table 5.1) and smectite and kaolinite increase remarkably with depth in C.Fazio (see Ap1 and 2Ap, Table 5.1).

The total mineral fraction revealed that calcite is the most abundant mineral within the measured profiles (3 – 98 %) followed by smectite and quartz (Table 5.1). Mica can be found in all horizons except some C horizons. The kaolinite content varies from 0 (Mazara del Vallo P4 C) to 10.8 % (C.Fazio 2Ap). The highest smectite content by far was measured in Grotta Rossa 4a1 (43 – 45 %).

## 5.5 Oxalate-extractables (Fe, Al and Mn) and investigated clay fraction

The weakly and poor-crystalline phases of *Fe*, *Al* and *Mn* have been measured via an oxalate extraction since at the beginning of soil formation specifically mineral phases are present in poor- to weakly crystalline forms (Dahms et al., 2012). The amount of weathered *Al*, *Fe* and *Mn* generally increases over time (Fig. 5.7).

C.Fazio, Mazara del Vallo P7 and Grotta Rossa 4a1 have the largest amount of oxalate-extractables, indicating active weathering (Fig. 5.9a), whereas Mazara del Vallo P4 and Lauria P1a own the least extractables (Fig. 5.9a). The unamended profiles of Mazara del Vallo Ferla and Lauria P1 have interestingly a similar amount of weathered oxalate-extractables as their amended counterparts.

The maximum of weathered aluminium is reached in the 45 year old soil (Profile Grotta Rossa 4a1) with 1048  $g/m^2$ . The same location also had the highest amount of weathered manganese (247  $g/m^2$ ) and second highest value of degraded Fe (473  $g/m^2$ ). The highest stock of iron was found in Mazara del Vallo P7, a profile which also shows mostly high weathering of oxalate-extractables (Table 5.2). The lowest amount of weathered *Al* is found in C.Fazio 2 with 15  $g/m^2$ . Lauria P1 C owns the least weathered quantity of *Fe* (12  $g/m^2$ ) and Mazara del Vallo P7 the minimum value of 0  $g/m^2$  manganese. The mass of weathered *Al* is generally the highest of the oxalate-extractables over time, followed by *Fe* and *Mn* (Fig.



5.7). However, in 2003 the amount of weathered *Fe* surpasses aluminium.

With depth, the concentrations of *Al*, *Fe* and *Mn* show a diffuse trend of increasing/decreasing in the majority of cases (see Figure 5.6). Nevertheless, some profiles should be pointed out: Mazara del Vallo Ferla shows the strongest decrease of the observed elements with depth. C.Fazio has in contrast the strongest increase of extractables with depth.

Overall, the statistics could not show a significant increase in stocks/production rate during the observed time period of the extractables. The stocks are generally smaller than the concentration of the extractables which is consistent with other studies (Dahms et al., 2012).

## 5.6 Total elemental content and weathering indices

### 5.6.1 Chemical drift and weathering indices

The elements of the normalised ratio of the primitive mantle vary only little between and within the different soil profiles (see Fig. 5.12). *Rb*, *Ba*, *Th* and *U*, as well as *Sr* show a contradictory trend between the profiles of Lauria P1 and P1a and Grotta Rossa 2a1 and C.Fazio (2). The elements *Rb*, *Th*, *U*, *Pr* and *Sm* are enriched while *Nb*, *Ce*, *Zr* and *Ti* are rather depleted. Lauria P1 and P1a are the profiles with the highest accumulation of *Rb*, *Th*, *U*, *Pr* and *Sm* (Fig. 5.12). Simultaneously, Lauria P1 is the site with the highest depletion in *Zr*.

The most depleted element in total is titanium. Uranium is the most enriched element of all, found in Lauria P1 and P1a. The concurrent trend of the primitive mantle elements indicates that most of the material has the same origin, however the contradictory values of Lauria P1 and Lauria P1a regarding elements *Rb*, *Th*, *Ba* and *Sr* mirror that Lauria P1 has not been cultivated yet and Lauria P1a has only been recently started to be amended and still are largely composed of calcareous bedrock.

### 5.6.2 Elemental loss

The relative loss of elements over time was described by Tau. Tau was calculated using the non-carbonate fraction and the immobile element *Ti*. The non-carbonate fraction of the soil can be regarded as an immobile element in calcareous rich soils (Egli et al., 2001b). Despite these corrections, the variability of the data is still relatively high, so no definite statement can be made about the element losses in the last decades. With time, only a slight weathering of silicates (including *CaO*) is visible. Approx.  $0.96 \text{ kg m}^{-2}\text{y}^{-1}$  of silicates were lost (looking at the profile which lost most silicates - Mazara del Vallo P4) (see Fig. 5.13).

In comparison, the silicate weathering ( $\text{Ca}^{2+}$ ,  $\text{Mg}^{2+}$ ,  $\text{K}^+$  and  $\text{NO}_3^-$ ) of the Ohio river basin from 1979 to 2009 has a yearly silicate discharge of  $2.5e^9 \text{ kg/m}^2$  (Fortner et al., 2012) which

exceed our calculations. However, the river basin is much bigger than our study area. In addition, the numbers were calculated as a river discharge, while ours are just measured within the soil in a much smaller study area. Fortner et al. (2012) suggested that weathering started as the alkalinity was used up via nitrogen fertilization. In contrast, the carbonate weathering with values of  $28 \text{ kg m}^{-2}\text{y}^{-1}$  (for the same profile as above) is much higher than silicate weathering, but still not in the order of Fortner's (Fortner et al., 2012) figures.

### 5.6.3 PDI

The PDI delivers an overview over the relative weathering degree of the soil profiles. Factors such as rubification, melanization, texture and pH were considered. Our analysis revealed that the PDI gave a correct relative age determination. With progressive weathering and increasing soil age the PDI increases (see 5.14). An inconsistency was found in Cazzola 4 which seems to have experienced the greatest weathering, despite not being the oldest transformed soil profile. A relatively strong rubification and melanization in comparison to the newer soils might be an explanation for these results.

## 5.7 Soil pore analysis

Generally, we see a similar frequency distribution of pores throughout all soil profiles (Fig. 5.17). Up until the newest transformed soil profiles, a monomodal distribution is dominant, turning into a bimodal distribution. The pore volumes lie between approx.  $1 \text{ mm}^3$  and  $10^{-4} / 10^{-5} \text{ mm}^3$ . The frequency of the large and small pore volumes do not show a trend with depth (Fig. 5.17) and the highest frequency of large pores can be seen in Grotta Rossa 2a1 and Lauria P1 (see Fig. 5.17). Over time, no change of the frequency in large pores can be seen (see 5.17), while the smaller pores tend to decrease over time.

In comparison, the frequency of macropores (diameter  $> 0.06 \text{ mm}$ ) shows a throughout monomodal distribution (see Fig. 5.18). Most pores have a volume of  $10^{-4}$  to  $10^{-1} \text{ mm}^3$ , while almost no pores larger than  $1 \text{ mm}^3$  exist.

Macroporosity was calculated with the formula  $M_p = V_{mp} / V_{total}$  where  $M_p$  is the macroporosity (-),  $V_{mp}$  denotes the volume of macropores ( $\text{mm}^3$ ) and  $V_{total}$  is the total volume of the sample core ( $100 \text{ cm}^3$ ). The macroporosity ranges from 0.016 to 0.13 %. These values are much lower than values from undisturbed sites (Amer et al., 2009; Musso et al., 2019) and could be caused by the overall rather clayey soil. However, other studies indicate that macropores often make up less than one percent of the soil volume (Hirmas et al., 2018; Musso et al., 2019). The macropores further decrease very slightly with time, if equal soil horizons are compared.

The maximum graph (pore) length lies between  $1'365 \text{ mm}$  and  $222'319 \text{ mm}$  (Fig. 5.15 b). The longest graph length belongs to the profile Lauria P1a from 2003 which is of sandy composition. The profiles which were transformed prior to 2003 show a stable trend around

80'000mm. However C.Fazio (1993) displays a sudden drop to the minimum of 9'677mm length probably due to large clay fraction. The graph length altogether increases hardly with depth but decreases significantly with time (35 to 17 years soil age;  $p < 0.05$ ).

The pore network length does not correspond with the network number (Fig. 5.15 f), indicating that the more networks appear, the shorter the network is. Especially in the upper most soil horizon this trend is visible. Over time, no major changes in the graph number are found.

If only macropores are considered, the network reaches a length of 4'137mm to 176'475mm (Fig. 5.16 b), whereas the longest network again belongs to Lauria P1a and has a minimum at C.Fazio. Moreover, the network length does not correspond with the network number (Fig. 5.16 f), just as the pores with a diameter of  $> 0.03mm$ . With time however, a slight increase of the pore length is visible.

The total pore volume ranges from 1'365 mm<sup>3</sup> up to 10'870mm<sup>3</sup> (Fig. 5.15 a) and the total pore surface area (mm<sup>2</sup>) has a minimum of 8'916mm<sup>2</sup> at C.Fazio 2Ap and a maximum of 130'528mm<sup>2</sup> at Lauria P1 C. The total surface area does not show a clear depth or time trend. The mean tortuosity decreases from a maximum at Grotta Rossa 2a1 A (1.16) towards a minimum of 1.12 at Cazzola 4 and does not change in particular with time.

The total pore volume of the macropores is very similar to the volume of the smaller pores, with a minimum at 1'387 mm<sup>3</sup> and a maximum of 9'785 mm<sup>3</sup> (Fig. 5.16 a), whereas the pore surface area is also in the same range as the smaller pores ( $> 0.03mm$ ) (7'964 mm<sup>2</sup> - 118'565 mm<sup>2</sup>). Again the pore surface area and the pore volume do not seem to change with time, while the pore network tortuosity reaches a peak in the C.Fazio profile (see Fig. 5.16 e).

TABLE 5.1: Mineral composition and standard error of the clay fraction of chosen samples.

Site	Horizon	Quartz %	K-Feldspar %	Na-Plagioclase %	Aragonite %	Calcite %	Dolomite/Ankerite %	Vaterit %	Goethite %	Rutile %	Anatase %	Kaolinite %	Muscovite/Illite %	Smectite %	Chlorite %
Mazara del Vallo	A	32.1 ± 0.04	5.1 ± 0.05	2.3 ± 0.02	0.8 ± 0.01	17.5 ± 0.02	0.2 ± 0.01		1.3 ± 0.02	0.4 ± 0.01	0.8 ± 0.01	7.4 ± 0.05	5.4 ± 0.05	24.2 ± 0.11	2.5 ± 0.02
Ferla															
Mazara del Vallo	C	0.9 ± 0.02		4.0 ± 0.02		90.4 ± 0.06						1.2 ± 0.05		1.9 ± 0.09	1.6 ± 0.02
Ferla															
Mazara del Vallo	Ap1	28.7 ± 0.03	4.0 ± 0.05	1.8 ± 0.02	0.5 ± 0.02	22.0 ± 0.02			1.0 ± 0.02	0.5 ± 0.01	0.9 ± 0.01	6.9 ± 0.05	5.3 ± 0.05	26.7 ± 0.09	1.7 ± 0.02
P7															
Mazara del Vallo	C	21.1 ± 0.03	2.3 ± 0.05	2.0 ± 0.02	0.9 ± 0.02	33.6 ± 0.04			1.5 ± 0.02	0.3 ± 0.02	0.8 ± 0.01	7.0 ± 0.05	5.3 ± 0.07	23.2 ± 0.13	2.0 ± 0.02
P7															
Mazara del Vallo	Ap	8.7 ± 0.02	0.5 ± 0.02		1.4 ± 0.02	80.7 ± 0.07			0.6 ± 0.02		0.4 ± 0.01	1.6 ± 0.05	1.5 ± 0.05	2.6 ± 0.11	2.0 ± 0.02
P4															
Mazara del Vallo	C	1.3 ± 0.02				98.0 ± 0.02			0.4 ± 0.02						0.3 ± 0.01
P4															
Grotta Rossa 2a2	AC	6.8 ± 0.02	2.1 ± 0.04	1.5 ± 0.01	1.0 ± 0.02	62.1 ± 0.04			0.4 ± 0.01		0.4 ± 0.01	2.0 ± 0.03	4.8 ± 0.04	17.9 ± 0.07	1.0 ± 0.02
Grotta Rossa 2a2	2bA	9.0 ± 0.02	2.1 ± 0.03	1.9 ± 0.01	1.1 ± 0.02	53.3 ± 0.04			0.5 ± 0.01		0.3 ± 0.01	2.9 ± 0.05	4.4 ± 0.05	23.4 ± 0.09	1.1 ± 0.02
Grotta Rossa 4a1	Ap	19.3 ± 0.02	3.9 ± 0.03	3.7 ± 0.01		12.1 ± 0.02			0.7 ± 0.02	0.5 ± 0.01	0.7 ± 0.01	6.6 ± 0.05	8.0 ± 0.04	43.0 ± 0.08	1.5 ± 0.02
Grotta Rossa 4a1	Bt	21.0 ± 0.02	5.5 ± 0.03	3.6 ± 0.01		3.4 ± 0.02		1.2 ± 0.02	0.8 ± 0.02	0.5 ± 0.01	0.6 ± 0.01	6.8 ± 0.05	9.2 ± 0.04	44.9 ± 0.09	1.6 ± 0.02
Cazzola 4	Ap1	13.4 ± 0.02	3.3 ± 0.03	2.3 ± 0.01	0.7 ± 0.02	35.5 ± 0.02			0.4 ± 0.02	0.1 ± 0.01	0.5 ± 0.01	4.7 ± 0.05	6.8 ± 0.04	30.2 ± 0.09	2.1 ± 0.02
Cazzola 4	Ap2	16.0 ± 0.03	2.7 ± 0.03	2.9 ± 0.01	0.2 ± 0.01	33.9 ± 0.02	0.4 ± 0.01		0.1 ± 0.01	0.3 ± 0.01	0.6 ± 0.01	5.0 ± 0.04	6.8 ± 0.05	29.4 ± 0.08	1.6 ± 0.02
C.Fazio	Ap1	6.4 ± 0.02	1.8 ± 0.03	1.0 ± 0.02	0.6 ± 0.02	69.7 ± 0.04			0.3 ± 0.01		0.4 ± 0.01	3.0 ± 0.03	4.8 ± 0.04	11.2 ± 0.06	0.9 ± 0.02
C.Fazio	2Ap	23.9 ± 0.03	3.5 ± 0.04	3.5 ± 0.02		10.0 ± 0.02			1.2 ± 0.02	0.4 ± 0.01	0.7 ± 0.01	10.8 ± 0.05	9.4 ± 0.05	33.9 ± 0.09	2.7 ± 0.02
C.Fazio 2	Ap1	12.1 ± 0.02	1.8 ± 0.03	1.5 ± 0.02		55.4 ± 0.05			0.5 ± 0.01		0.6 ± 0.01	4.8 ± 0.05	6.4 ± 0.05	15.7 ± 0.09	1.2 ± 0.02
C.Fazio 2	Ap3/A	14.6 ± 0.02	2.0 ± 0.03	1.6 ± 0.01		44.5 ± 0.03			0.6 ± 0.02		0.6 ± 0.01	7.7 ± 0.05	7.0 ± 0.05	20 ± 0.09	1.4 ± 0.02
Lauria Pla	AC	2.0 ± 0.01	0.5 ± 0.01	0.4 ± 0.01		89.2 ± 0.05						1.1 ± 0.04	1.5 ± 0.02	5.3 ± 0.05	
Lauria Pla	C	0.7 ± 0.01				96.8 ± 0.02						0.2 ± 0.01		2.3 ± 0.03	

TABLE 5.2: Sum of the mass (stock/production rate) of *Al*, *Fe*, *Mn* in each profile (regarding weathered horizons) per area unit.

Site	Al g/m <sup>2</sup>	Fe g/m <sup>2</sup>	Mn g/m <sup>2</sup>
Cazzola 4	673	489	374
C. Fazio	277	705	187
C. Fazio 2	141	628	167
Grotta R 2a1	337	285	102
Grotta R 2a2	332	286	93
Grotta R 4a1	1565	800	404
Lauria P1	-	-	-
Lauria P1a	100	74	60
Mazara del Vallo Ferla	643	293	102
Mazara del Vallo P4	173	126	158
Mazara del Vallo P7	1270	977	196

TABLE 5.3: Soil profile description with physical and chemical parameters with its standard deviation of the isotopic and total fraction of inorganic carbon and from the bulk soil.

Site	Horizon	Depth cm	Munsell colour moist	Skeleton wt%	Bulk density g/cm <sup>3</sup>	Sand %	Silt %	Clay %	pH	C <sub>org</sub> %	CaCO <sub>3</sub> %	C <sub>secondary</sub> %	N %	$\delta^{13}\text{C}^5$ (bulk soil) ‰	$\delta^{13}\text{C}$ (CaCO <sub>3</sub> ) ‰	C/N <sup>6</sup> ratio	$\delta^{18}\text{O}$ (CaCO <sub>3</sub> ) ‰
Cazzola 4	Ap1	0-40	7.5 YR 4/4	11.9	1.13	16.8	48.1	35.0	7.50	0.48 ± 0.19	35.10	35.9 ± 0.22	0.05	-12.75	-9.54 ± 0.22	10	-4.24 ± 0.06
	Ap1	40-80	7.5 YR 4/4	11.2	1.26	16.1	48.9	35.0	7.40	0.64 ± 1.94	33.79	37.3 ± 0.08	0.09	-12.38	-9.87 ± 0.08	7	-4.35 ± 0.13
	Ap2	80-	7.5 YR 5/6	25.0	1.21	23.3	41.0	35.8	7.50	0.00 ± 0.21	34.54	36.7 ± 0.16	0.02	-12.29	-9.72 ± 0.16	0	-4.22 ± 0.05
C.Fazio	Ap1	0-50	10 YR 6/3	5.4	1.32	11.0	43.7	45.4	7.48	0.89 ± 0.33	57.42	0.8 ± 0.02	0.06	4.81	-1.18 ± 0.02	14	-0.79 ± 0.09
	Ap2	50-75	2.5 Y 5/3	14.9	1.38	10.4	37.9	51.7	7.39	0.76 ± 0.09	25.04	7.5 ± 0.26	0.06	7.66	-2.80 ± 0.26	12	-1.83 ± 0.28
	2Ap	75-	2.5 Y 5/4	0.0	1.46	17.2	31.3	51.5	7.37	0.68 ± 0.04	11.94	21.5 ± 0.27	0.07	-15.79	-6.11 ± 0.27	9	-3.45 ± 0.20
C.Fazio 2	Ap1	0-40	2.5 Y 5/4	4.8	1.40	77.3	8.8	13.9	7.44	0.63 <sup>7</sup>	51.99	0 ± 0.03	0.15	-5.64	-0.62 ± 0.03	1 <sup>7</sup>	-0.16 ± 0.05
	Ap2	40-70	2.5 Y 7/3	2.8	1.41	11.7	44.9	43.4	7.51	0.02 <sup>7</sup>	71.48	0 ± 0.10	0.04	-0.93	-0.20 ± 0.10	1 <sup>7</sup>	0.15 ± 0.14
	Ap3/A	70-80	2.5 Y 7/4	28.8	1.34	7.7	42.3	50.0	7.57	0.02 <sup>7</sup>	42.12	0 ± 0.07	0.04	-2.80	-0.77 ± 0.07	1 <sup>7</sup>	-0.43 ± 0.06
Grotta Rossa 2a1	A	0-50	7.5 YR 3/4	49.3	1.41	28.1	48.7	23.1	7.50	0.83 ± 0.16	63.13	12.3 ± 0.09	0.08	-7.18	-3.92 ± 0.09	10	-3.54 ± 0.16
	AC	50-65	10 YR 4/4	72.3	1.52	38.7	42.6	18.8	7.50	0.34 ± 0.34	72.59	10.2 ± 0.15	0.04	-5.27	-3.44 ± 0.15	8	-3.54 ± 0.16
Grotta Rossa 2a2	C	65-	2.5 Y 8/2	25.5	1.15	29.1	58.3	12.7	7.51	0.21 ± 0.80	82.67	16.6 ± 0.07	0.00	-5.12	-4.94 ± 0.07	0	-4.04 ± 0.08
	AC	0-30	10 YR 4/4	35.5	1.39	23.4	50.0	26.5	7.50	0.97 ± 0.28	60.52	13.5 ± 0.07	0.13	-7.01	-4.20 ± 0.07	8	-3.29 ± 0.12
Grotta Rossa 4a1	AC	30-85	10 YR 4/4	32.7	1.31	25.9	49.3	24.8	7.51	1.14 ± 0.35	57.15	15.4 ± 0.12	0.07	-7.55	-4.67 ± 0.12	18	-3.39 ± 0.05
	2bA	85-	10 YR 4/4	19.2	1.28	22.5	50.8	26.7	7.50	1.15 ± 0.29	47.29	19.3 ± 0.08	0.09	-8.98	-5.59 ± 0.08	13	-3.61 ± 0.04
Lauria P1 (undist.)	Ap	0-40	7.5 YR 2/3	7.2	1.13	17.0	53.5	29.5	7.50	2.03 ± 0.14	12.63	25.3 ± 0.13	0.17	-19.19	-7.01 ± 0.13	12	-4.25 ± 0.10
	Bt	40-80	7.5 YR 2/3	0.2	1.03	26.3	41.0	32.7	7.42	1.60 ± 0.04	4.86	50.4 ± 0.15	0.11	-23.11	-13.00 ± 0.15	15	-5.69 ± 0.07
Lauria P1a	C	0-	2.5 Y 8/2	36.8	1.46	62.2	35.1	2.7	7.80	0.00 ± 0.45	96.62	8.1 ± 0.04	0.01	-3.16	-2.92 ± 0.04	0	-1.74 ± 0.03
	AC	0-30	2.5 Y 5/3	19.6	1.42	47.6	37.7	14.7	7.71	0.34 ± 0.25	82.40	8.8 ± 0.10	0.02	-4.32	-3.10 ± 0.10	18	-3.35 ± 0.13
Mazara del Vallo	C	30-	2.5 Y 8/3	14.9	1.72	54.9	38.2	6.9	7.71	0.00 ± 0.42	92.18	2.2 ± 0.03	0.00	-1.99	-1.51 ± 0.03	0	-3.45 ± 0.12
	Ap	0-50	5 YR 3/6	20.5	1.26	44.6	35.6	19.9	7.20	1.74 ± 0.45	69.09	13.2 ± 0.07	0.11	-7.97	-4.15 ± 0.07	16	-3.03 ± 0.07
P4	C	50-90	10 YR 8/6	8.1	1.27	81.3	14.2	4.4	7.57	0.00 ± 0.31	91.22	12.1 ± 0.34	0.00	4.10	-3.88 ± 0.34	0	-2.83 ± 0.24
Mazara del Vallo	Ap1	0-20	5 YR 2/4	10.3	1.00	28.4	41.8	29.7	7.32	1.59 ± 0.11	22.48	13.1 ± 0.50	0.09	-11.71	-4.1 ± 0.50	17	-2.69 ± 0.33
	Ap2	20-75	5 YR 2/4	3.0	1.26	30.8	43.9	25.3	7.23	0.79 ± 0.20	24.22	13.0 ± 0.54	0.07	-11.08	-4.08 ± 0.54	12	-2.56 ± 0.40
Mazara del Vallo	C	75-110	5 YR 3/4	14.4	1.21	34.3	36.1	29.6	7.50	0.81 ± 0.39	34.57	13.4 ± 0.25	0.03	-8.19	-4.19 ± 0.25	26	-2.45 ± 0.08
	A	0-20	5 YR 2/4	3.9	1.30 <sup>8</sup>	37.5	49.0	13.5	7.35	2.80 ± 0.28	22.61	5.6 ± 0.49	0.20	-13.92	-2.33 ± 0.49	14	-3.35 ± 0.38
Ferla (undist.)	C	20-	7.5 YR 5/8	0.0	1.70 <sup>8</sup>	63.5	26.1	10.4	7.37	0.46 ± 0.91	83.14	15.0 ± 0.14	0.01	-5.40	-4.57 ± 0.14	92	-2.43 ± 0.04

<sup>5</sup> no standard deviation given

<sup>6</sup> calculated with *Corq*

<sup>7</sup> no standard deviation - direct measurement with Walkley-Black

<sup>8</sup> assumed value; no bulk density available

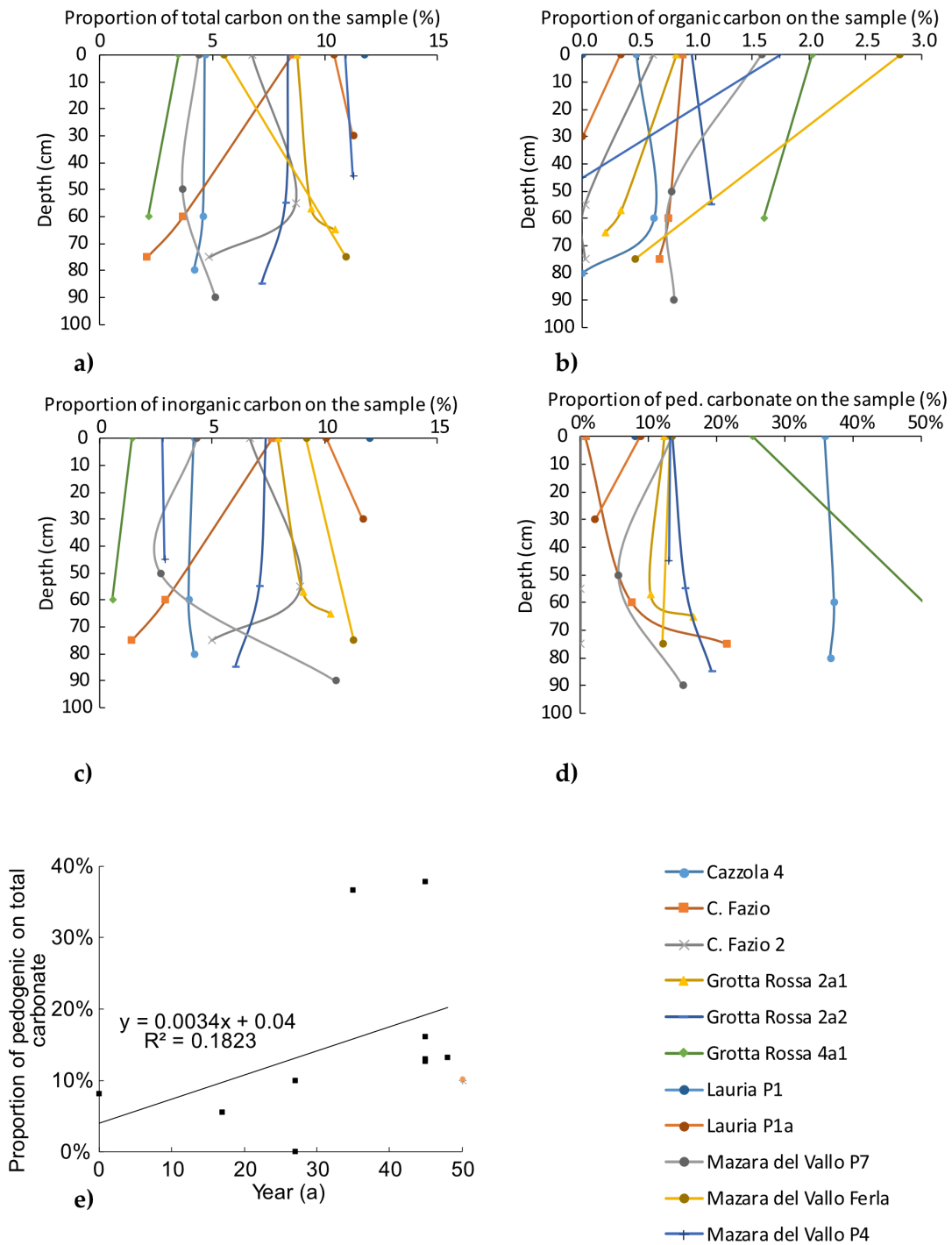


FIGURE 5.3: Distribution of carbon compounds with soil depth (a-d)) as an average of each location; Development of pedogenic carbonate over time illustrated in e); undisturbed site indicated as an orange point.

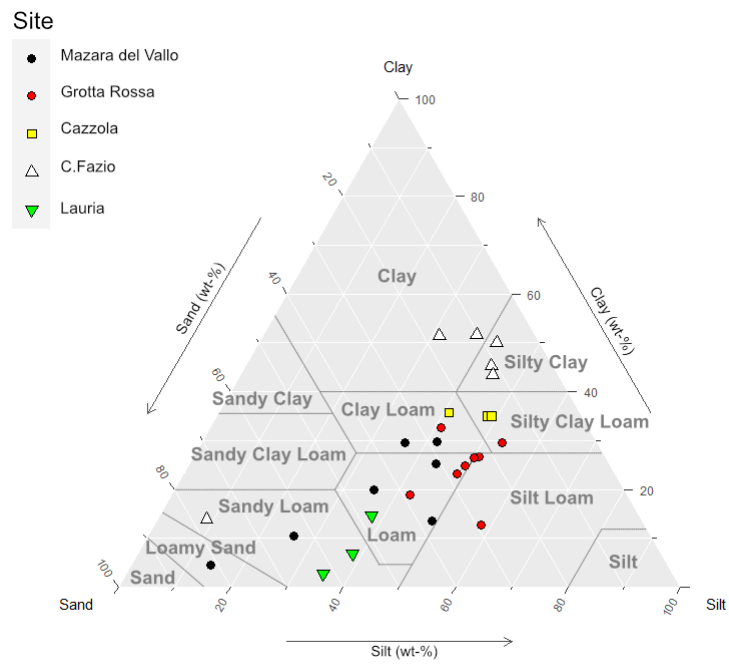


FIGURE 5.4: Grain size for each sampling location with USDA soil textural classes (USDA, 1987)



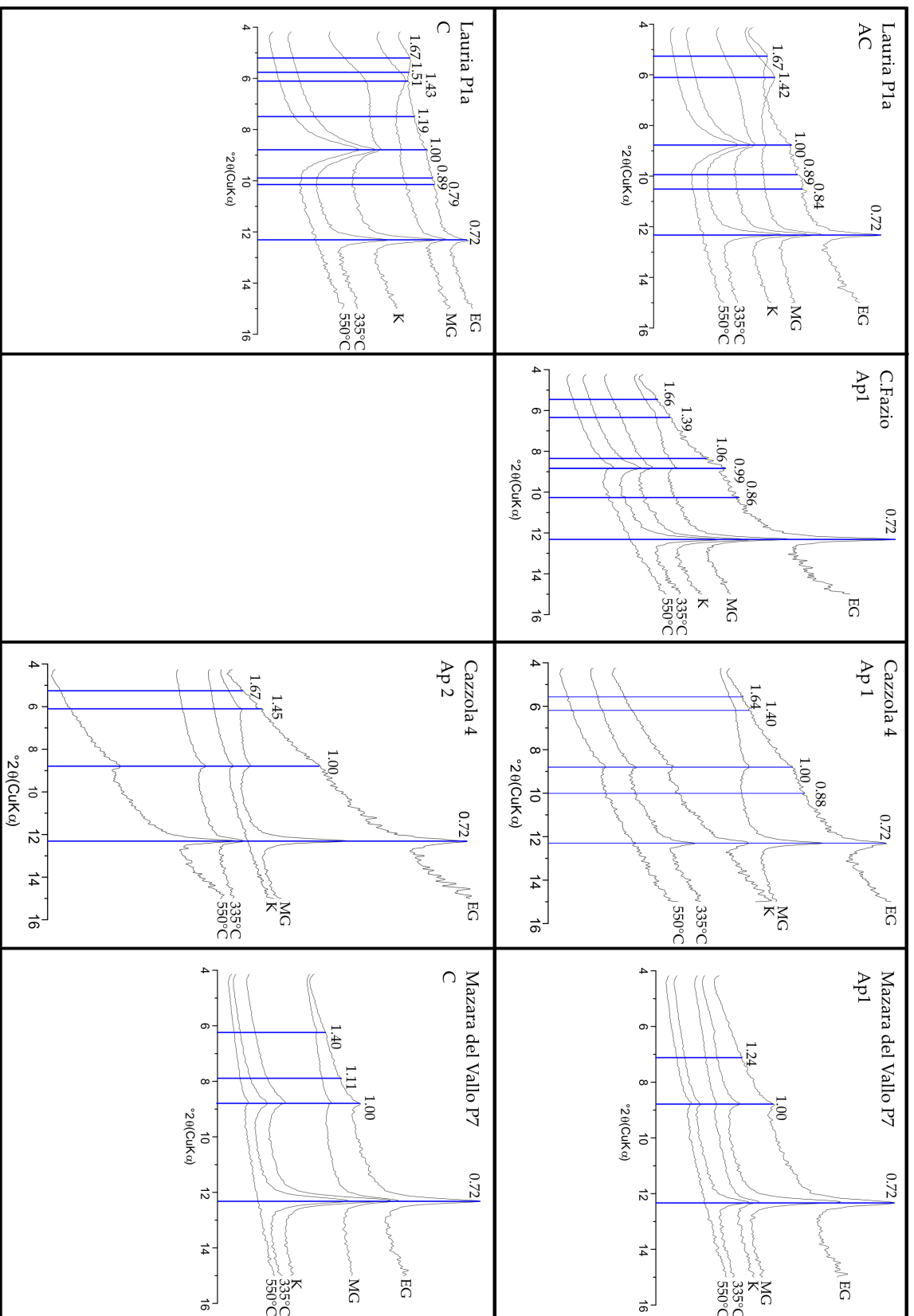


FIGURE 5.5: Smoothed XRD diffractogram after Lorentz polarization and polarization correction over time (left to right) and depth (top to bottom); Peaks are denoted with d-spacings in  $\text{\AA}$ . EG = ethylene glycol solvation, MG = Mg-saturation, K = K-saturation, 335°C = heated K-saturation and 550°C = heated K-saturation.

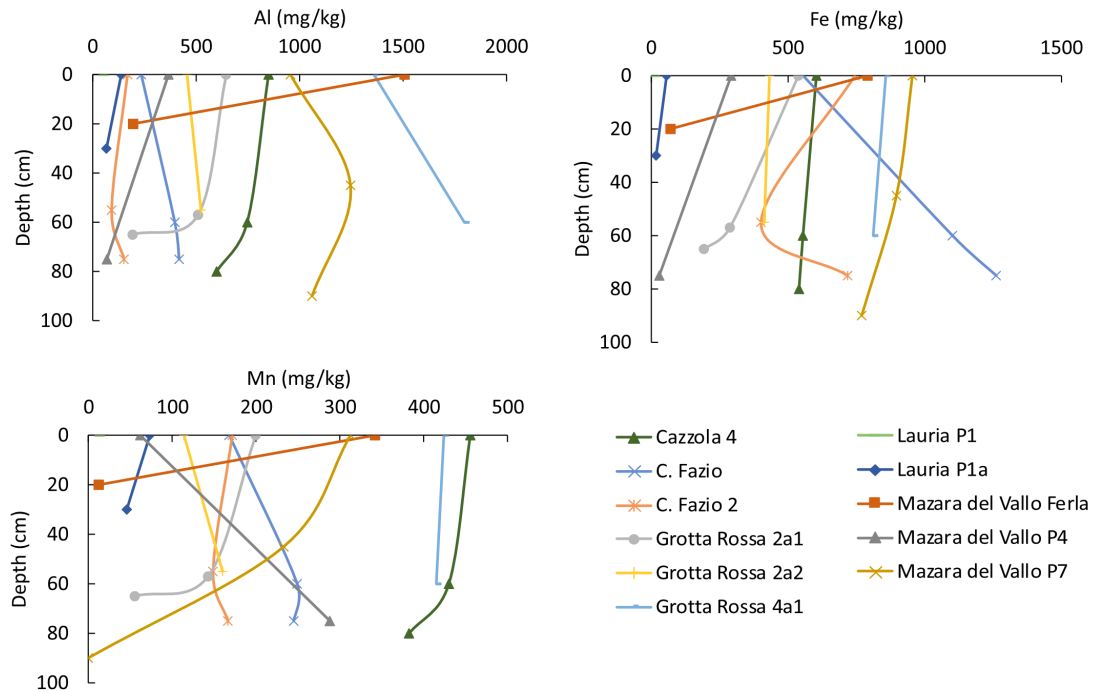


FIGURE 5.6: Concentration of weathered oxalate extractables (aluminium, iron and manganese) over soil depth. Lauria P1 is not visible since the profile is still too shallow.

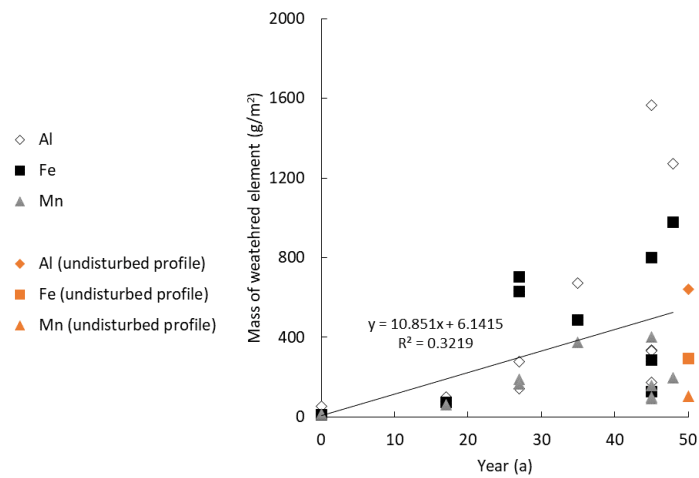


FIGURE 5.7: Mass of weathered fraction of oxalate-extractables calculated with the mean of each transformation year.

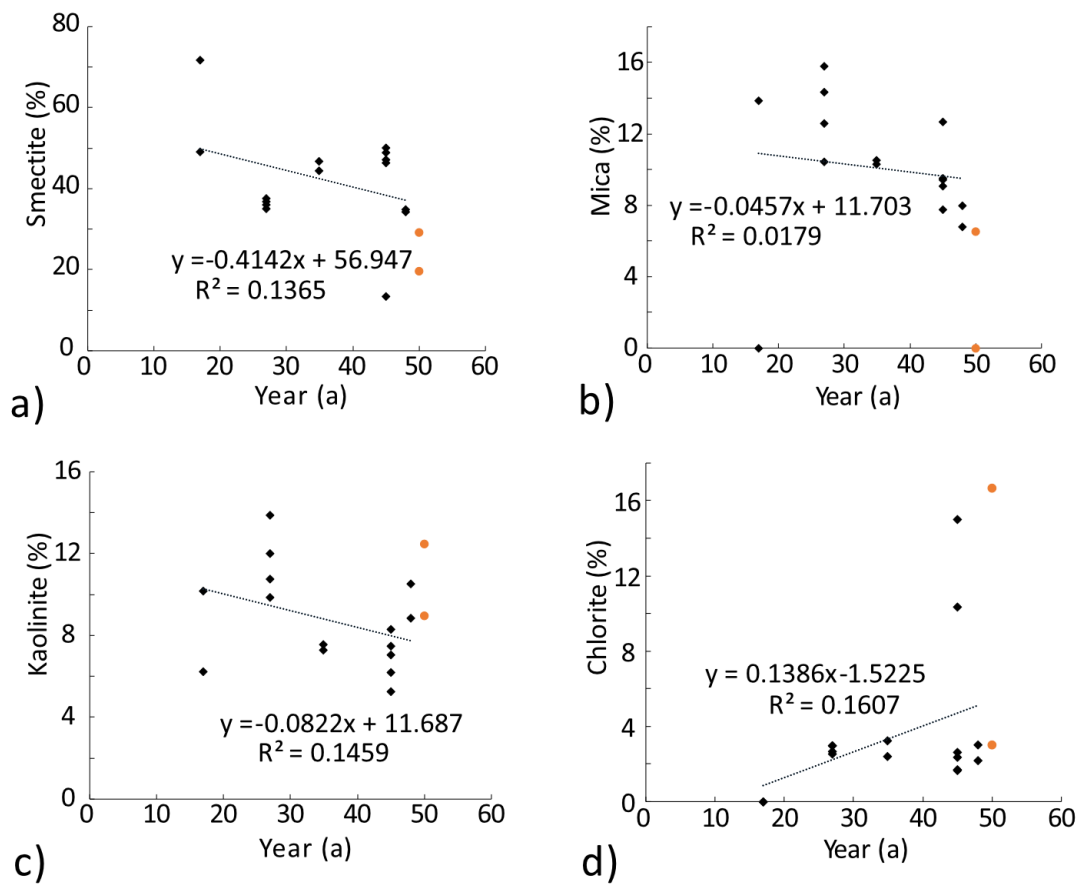


FIGURE 5.8: Changes of clay mineral fractions over time for a) smectite, b) mica, c) kaolinite and d) chlorite of the sampled soil profiles.

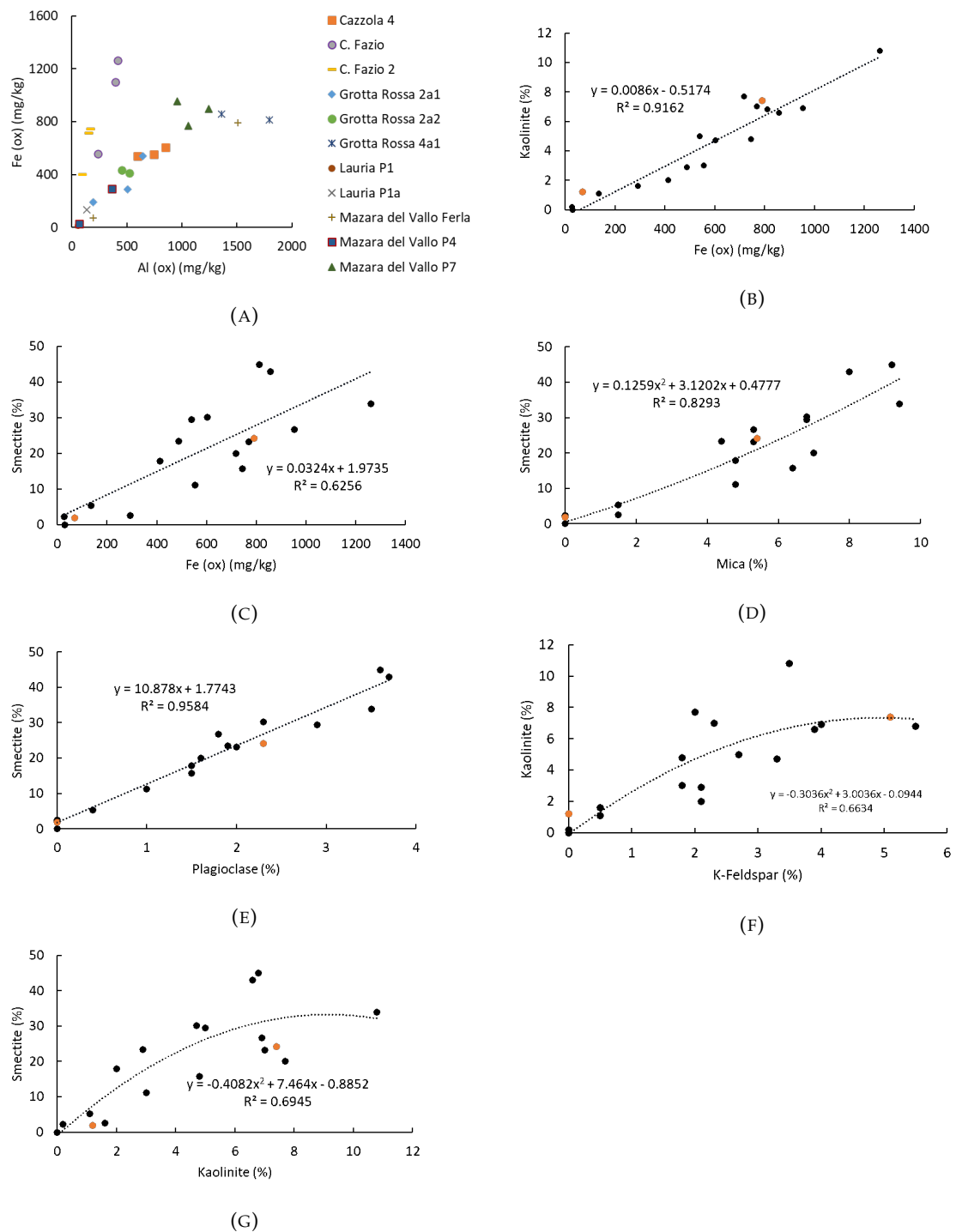


FIGURE 5.9: The relationship of oxalate extractables with different clay minerals; A) shows the extracted iron concentration over the aluminium concentration; B) Kaolinite and C) Smectite over iron; D) Smectite over Mica E) Smectite over Plagioclase; F) Kaolinite over K-Feldspar; G) Smectite over Kaolinite; Orange data points indicate the undisturbed profile. All the clay minerals were from the clay fraction illustrated as the total percentage of the < 2mm soil fraction.

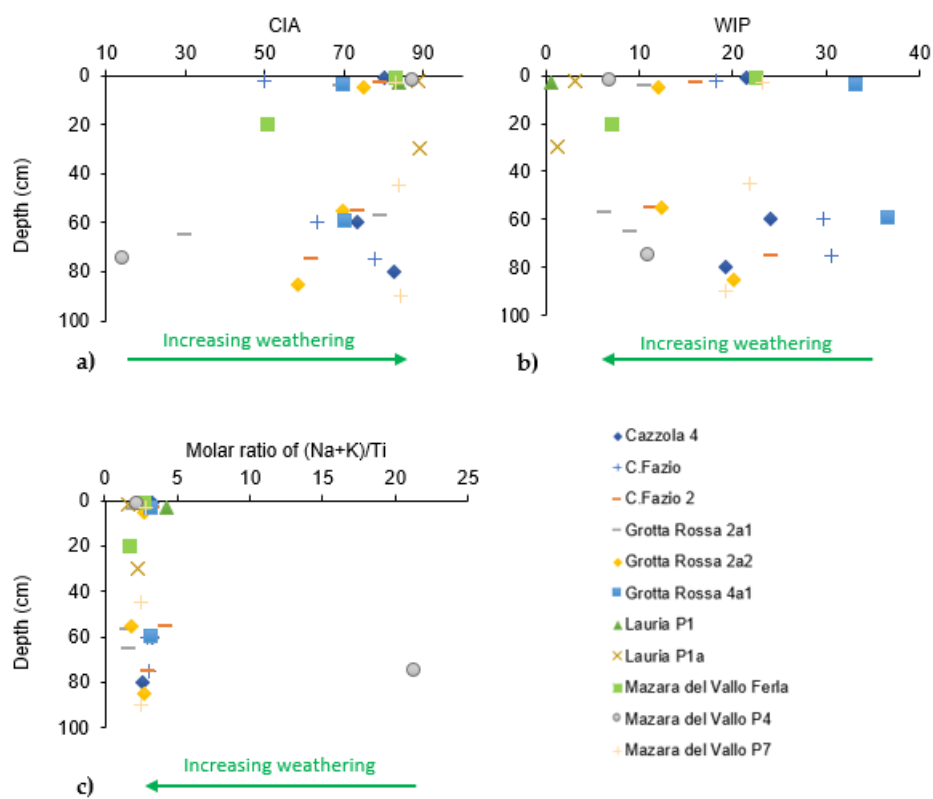


FIGURE 5.10: Weathering indices a) *CIA*, b) *WIP* and c)  $(Na + K)/Ti$  as a function of depth.

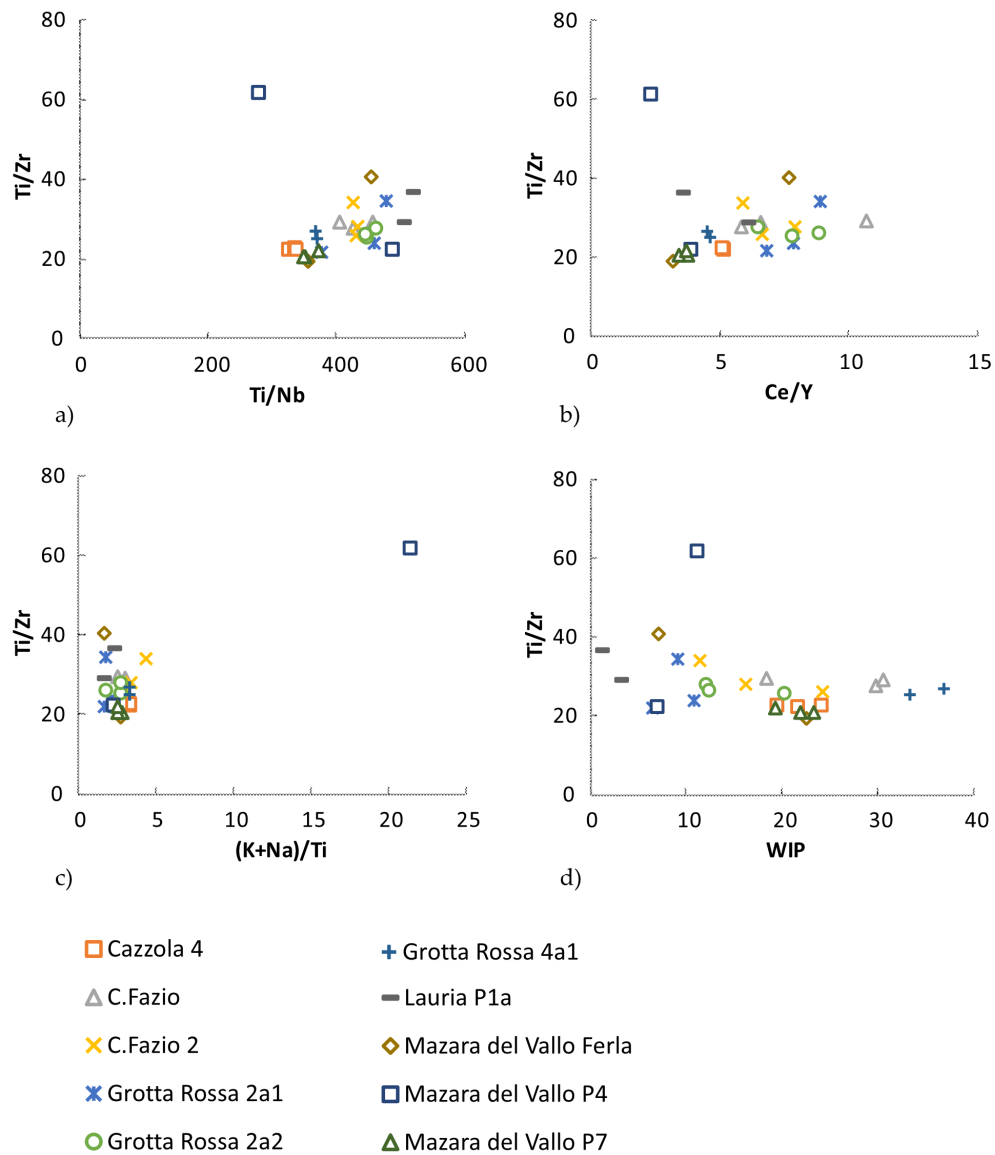


FIGURE 5.11: Weathering indices as a function of immobile element ratios (concentrations) summarised over each soil profile corresponding to the a)  $Ti/Nb$  ratio, b)  $Ce/Y$  ratio, c)  $(Na + K)/Ti$  ratio and d)  $WIP$ ; Lauria P1 was omitted, since the initial content of  $Zr$  is too low to be detectable.

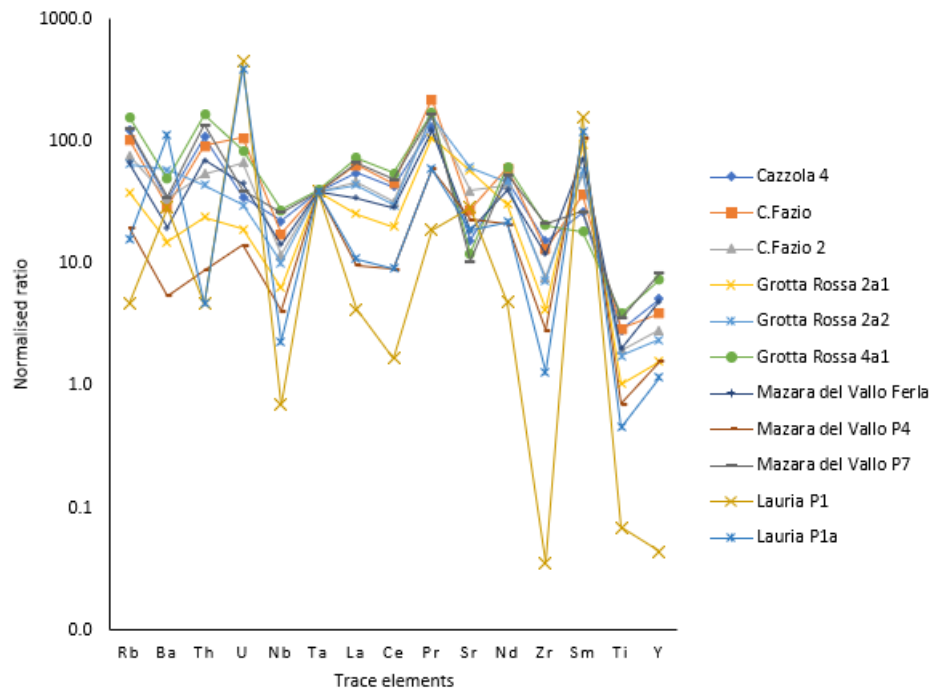


FIGURE 5.12: Normalised ratio of the trace elements of the primitive mantle with averaged values per soil profile.

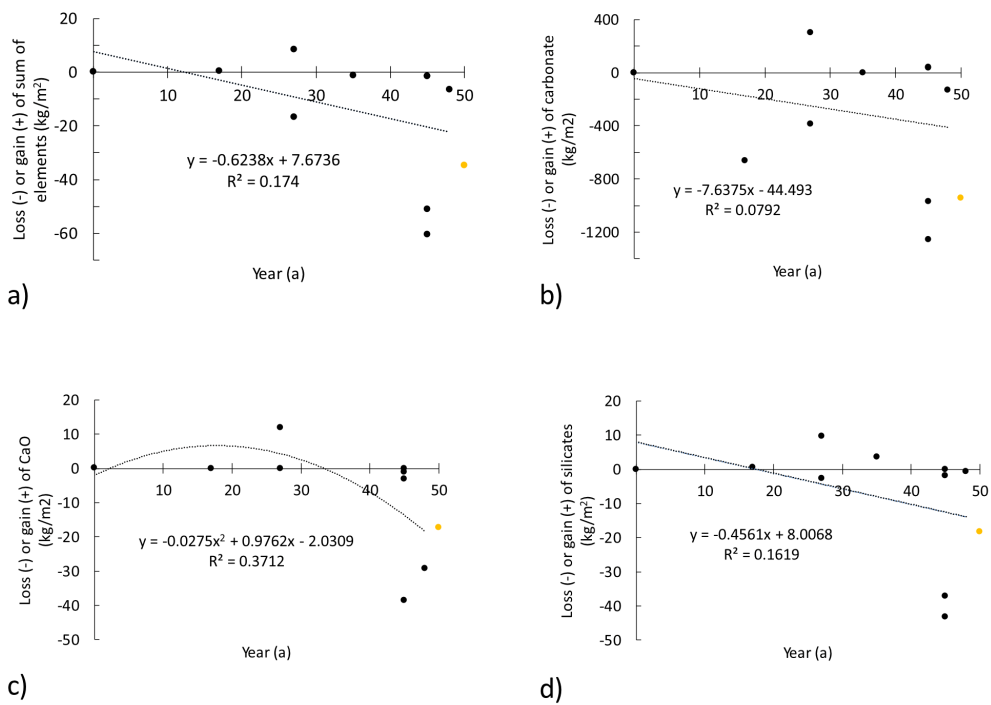


FIGURE 5.13: Relative mass losses of a) all elements (cations), b) carbonates, c)  $CaO$  and d) silicates as a function of time in an open system ( $\tau$ ); The undisturbed profile is indicated in orange.

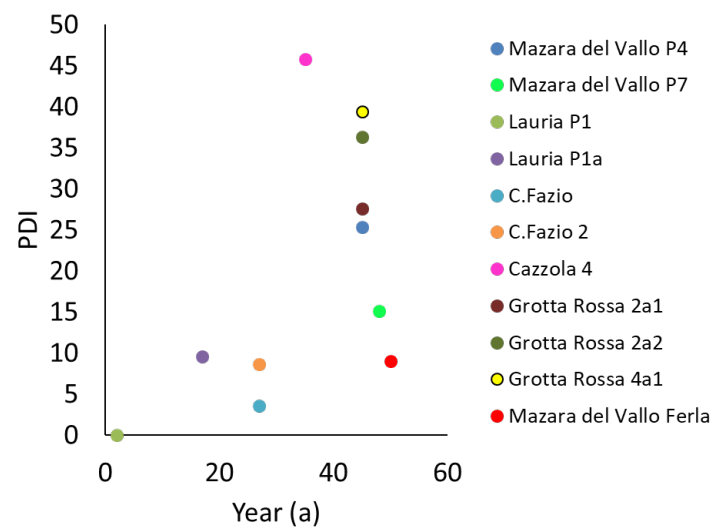


FIGURE 5.14: Profile development index (PDI) over time.



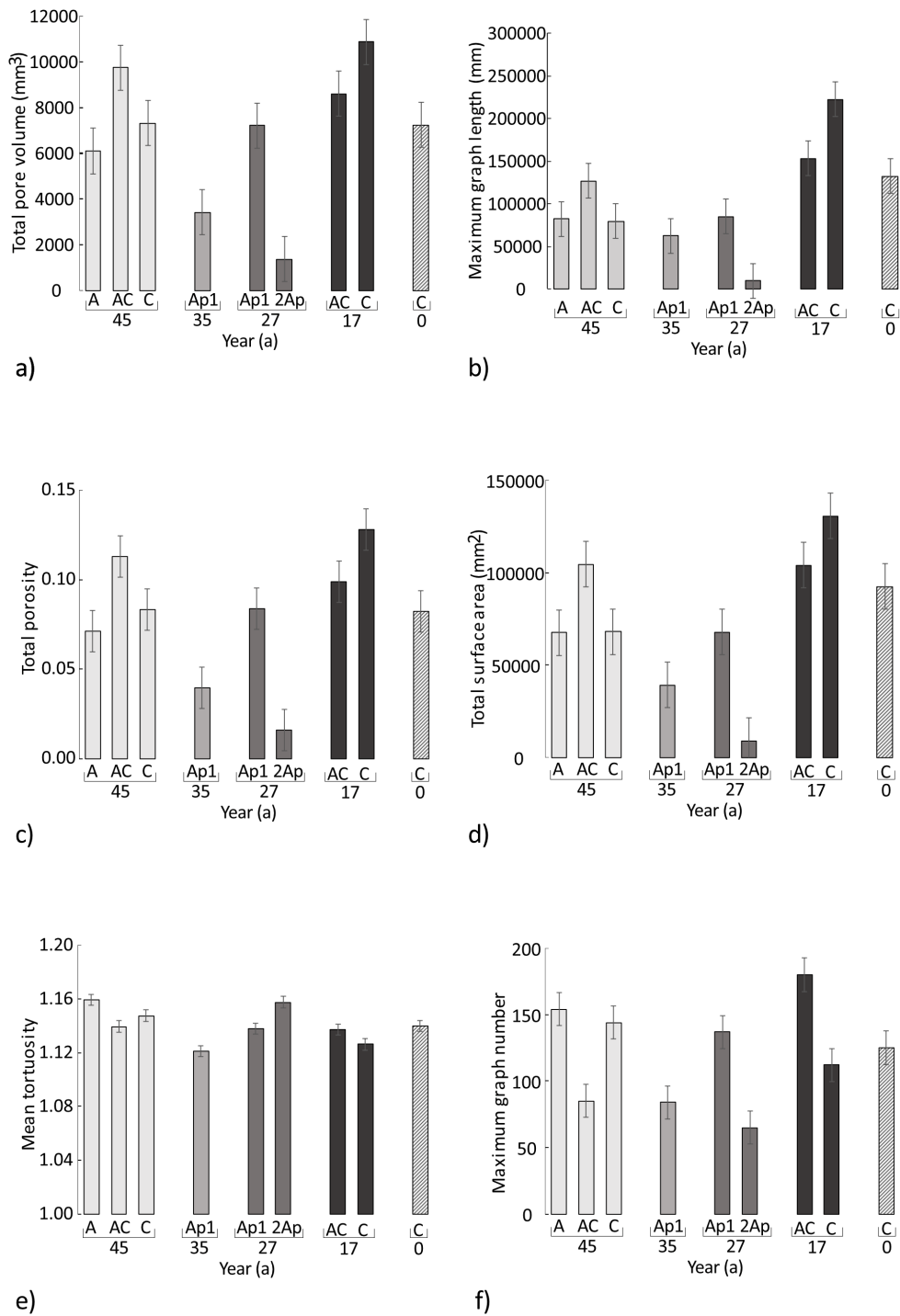


FIGURE 5.15: Soil pore characteristics ( $> 0.03mm$ ) over time with error margin; Letters indicate soil horizons; a) denotes the soil pore volume; b) the maximum length of a specific pore network ; c) the total porosity (total pore volume divided by the sample volume); d) total pore surface area; e) the mean tortuosity of each horizon and f) the maximum number of networks (graphs) in the sampled core.

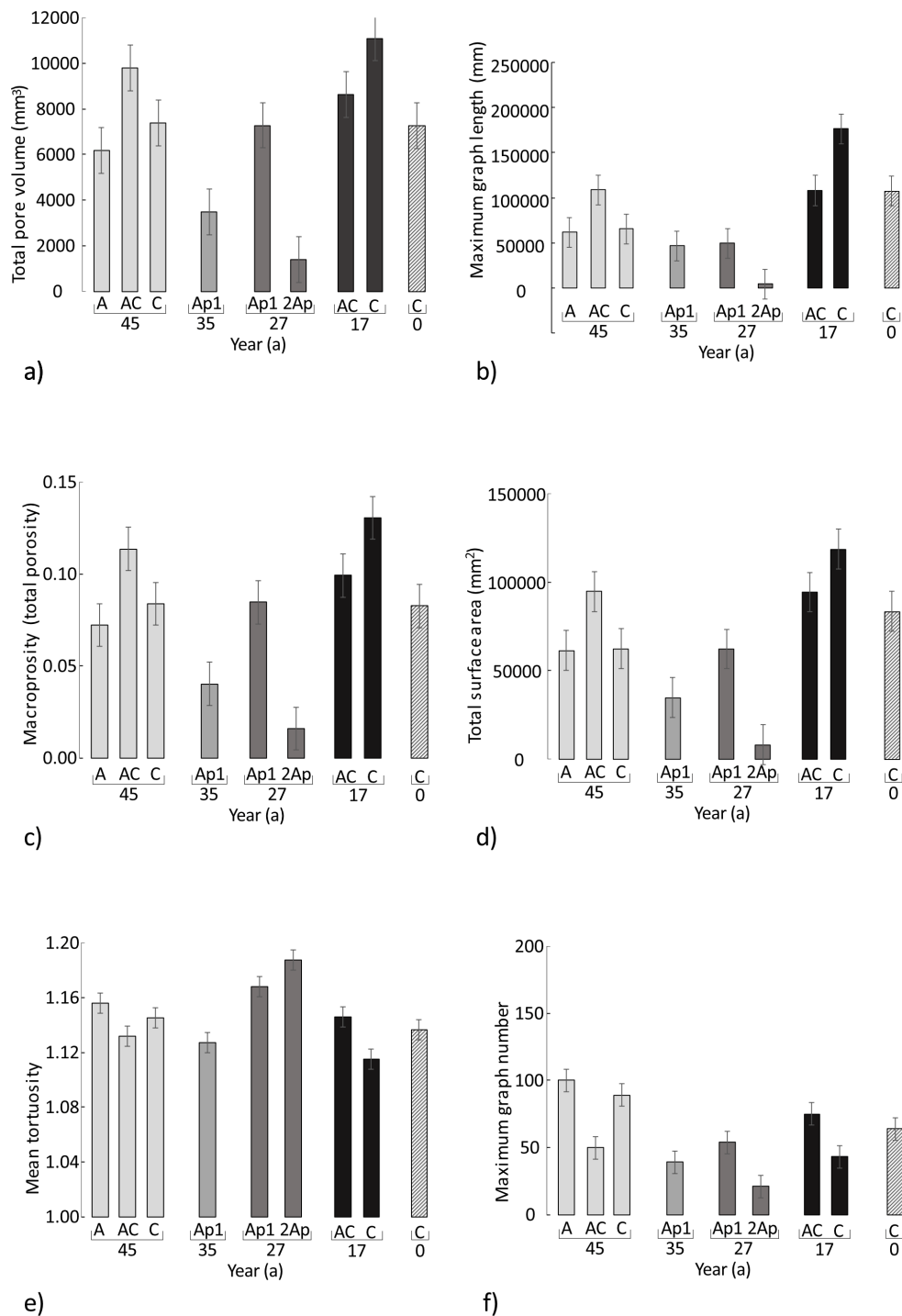


FIGURE 5.16: Soil pore characteristics ( $> 0.06mm$ ) over time with error margin; Letters indicate soil horizons; a) denotes the soil pore volume; b) the maximum length of a specific pore network ; c) the total porosity (= macroporosity); d) total pore surface area; e) the mean tortuosity of each horizon and f) the maximum number of networks (graphs) in the sampled core.

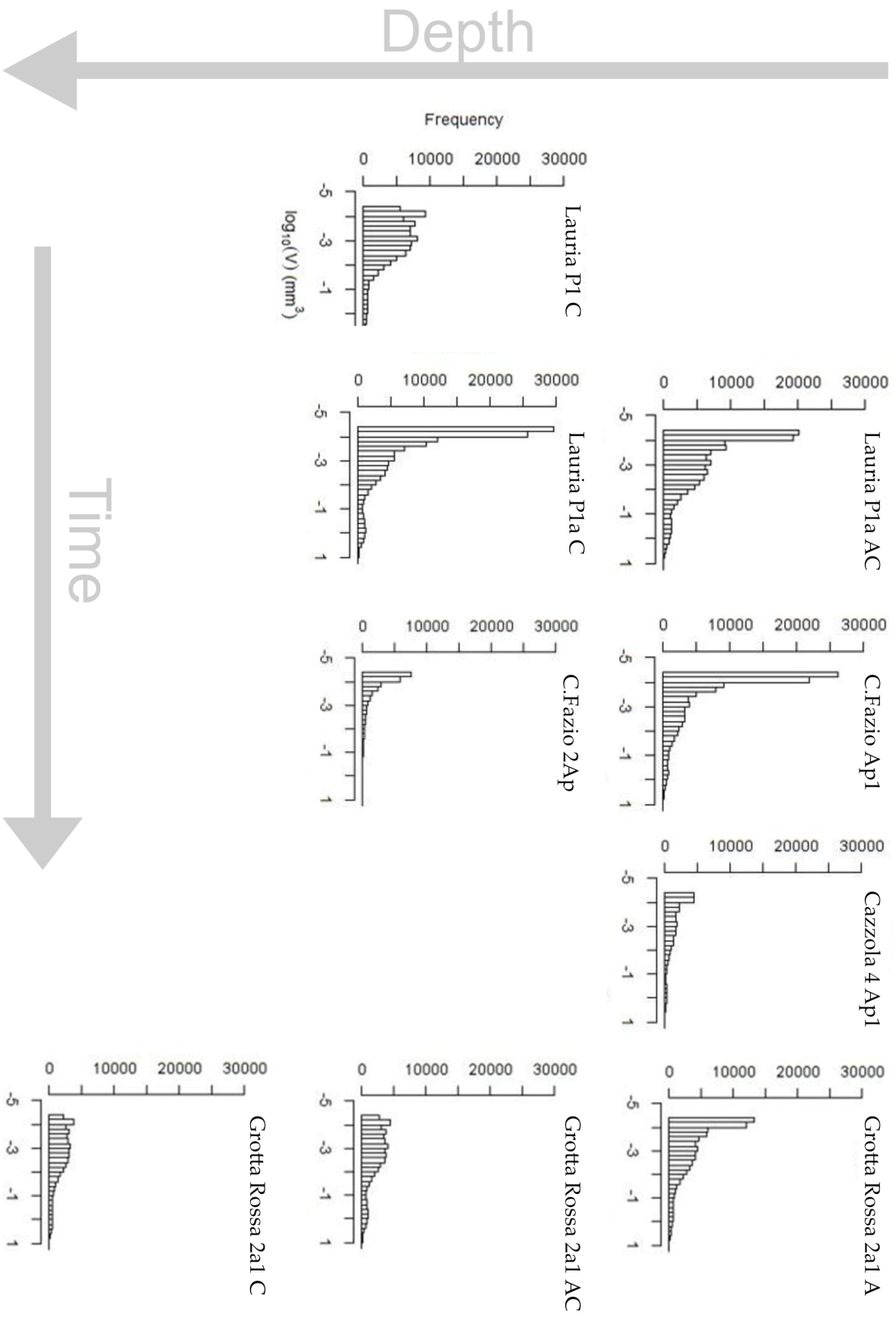


FIGURE 5.17 : Soil pore volume frequency distribution (pores with a diameter  $> 0.03mm$ ) as a function of depth and time.

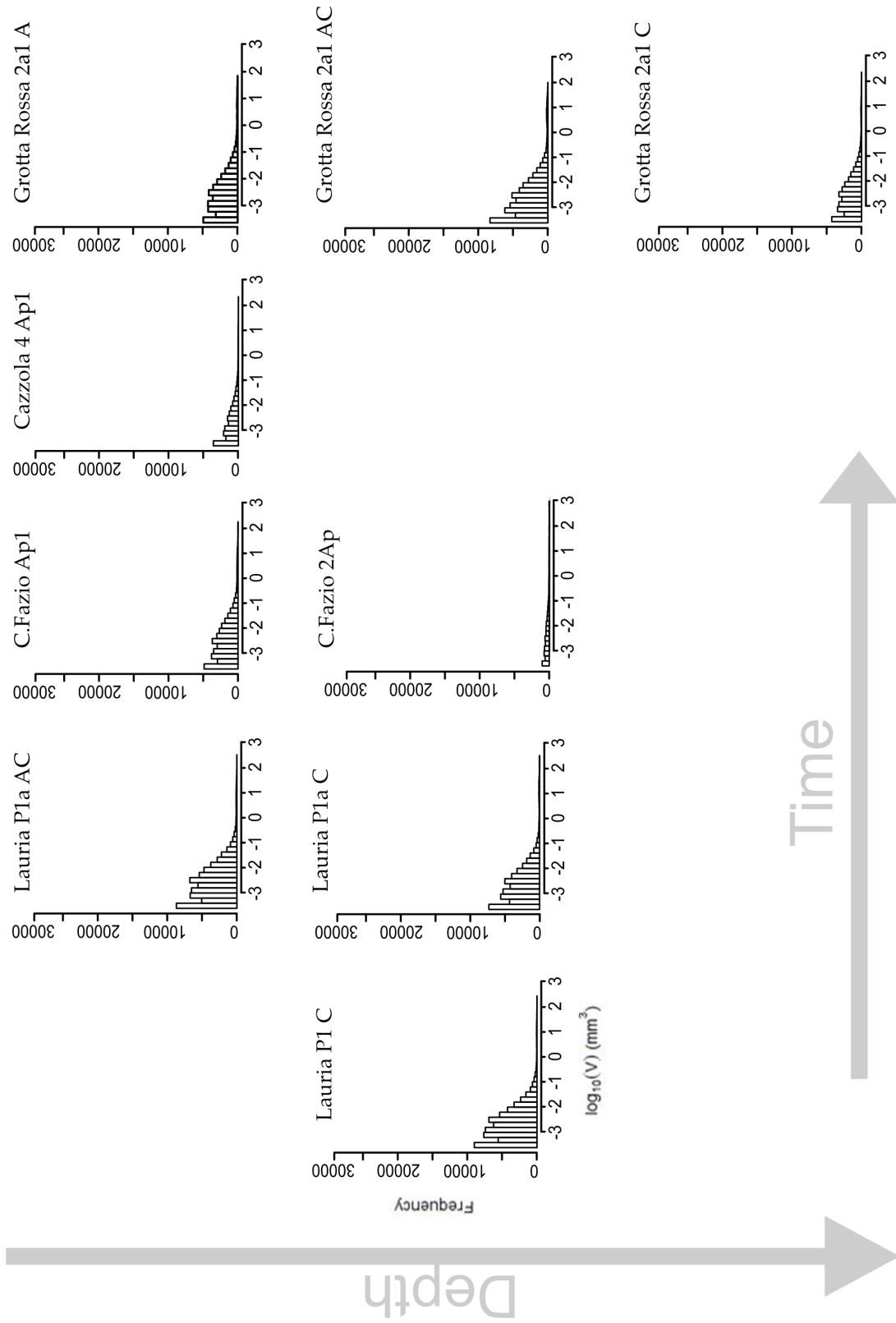


FIGURE 5.18: Soil pore volume frequency distribution (pores with a diameter  $> 0.06mm$ ) as a function of depth and time.

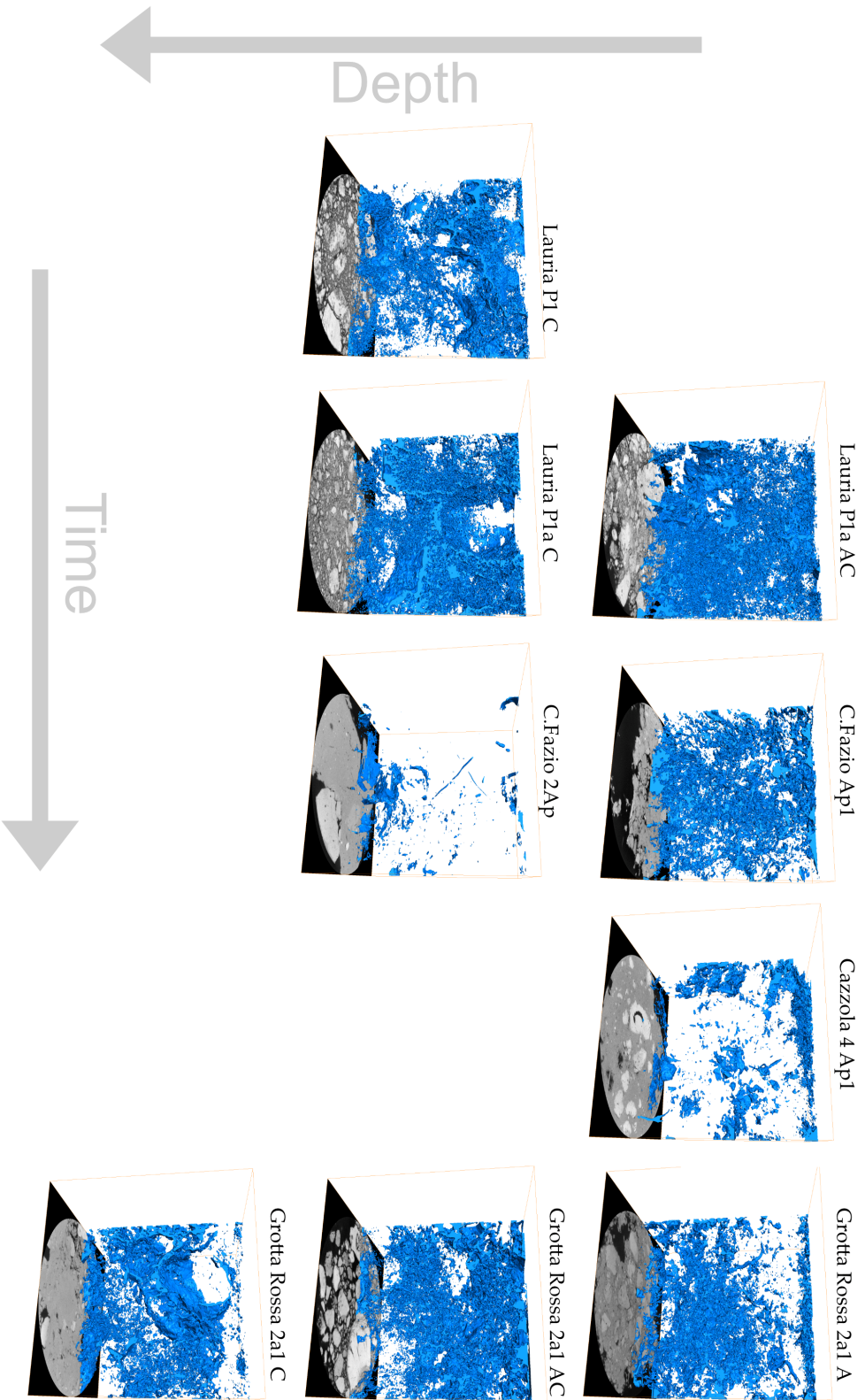


FIGURE 5.19: 3-Dimensional images of the sampled soil cores; blue enhances the macro- and mesopores.

## 6 Discussion

### 6.1 Carbon isotopes and compounds

The carbonate reaches  $\delta^{18}\text{O}$  values between  $-5.8$  and  $+0.2$  ‰ (Fig. 6.1 e). These values suggest that the carbonate has either been formed in a mixed-water environment between saline and fresh water (Di Bella et al., 2020) or an ocean regularly influenced by freshwater (Oehlert and Swart, 2014; Caruso et al., 2015; Egli et al., 2020b). During weathering, rainwater additionally might have an impact of the  $\delta^{18}\text{O}$  composition of the carbonates (Egli et al., 2020b).

The  $\delta^{13}\text{C}$  value of carbonate should be typically around zero. As the amount of carbonate in the soil increases, so do the isotopic values (Fig. 6.1 b and d). This is reflected in the positive relationship of total inorganic carbon and  $\delta^{13}\text{C}_{\text{Carb}}$  with  $\rho = 0.53$  ( $p < 0.05$ ) and  $\text{CaCO}_3$  with  $\delta^{13}\text{C}_{\text{Carb}}$  ( $\rho = 0.43$  ( $p < 0.05$ )). The correlation is especially visible in the more recently transformed profiles such as Lauria P1a, which have a relatively high carbonate content. However, even older transformed sites have  $\delta^{13}\text{C}$  bulk soil values close to zero, as they have a distinct C horizon and the isotopic value of the bulk soil is still influenced to a large part by carbonates.

Meanwhile,  $\delta^{13}\text{C}$  of the bulk soil ranges between  $-5$  and  $-20$  ‰ due to increasing organic carbon (see Fig. 6.1 a and c, Egli et al., 2020b) and thus corresponds to typical values in regions with Mediterranean climate (Tabor et al., 2013; Egli et al., 2020b).

Furthermore, the formation of secondary carbonate on one hand lowered the  $\delta^{13}\text{C}$  values of the carbonate ( $\rho = -0.98$ ;  $p < 0.05$ ) which was also observed by Gocke et al. (2011) and Egli et al. (2020b) and decreases also the  $\delta^{13}\text{C}$  of the bulk soil ( $\rho = -0.84$ ;  $p < 0.05$ ).

Secondary carbonate was identified in almost all soil profiles with the smallest amount in the C horizons and up to 50 % in Grotta Rossa 4a1 Bt (see Fig. 5.3 d). Apart from Grotta Rossa 4a1, Cazzola 4 contains also a relatively large amount of secondary carbonate while most profiles range between 5 – 10 % pedogenically produced carbonate. The only site not containing any secondary carbonate is C.Fazio 2. The high isotopic values of  $\delta^{13}\text{C}$  and  $\delta^{18}\text{O}$  of C.Fazio 2 reveal a low reaction of the rock with water thus explaining the absent of secondary carbonate within this profile (Martín-Martín et al., 2015; Egli et al., 2020b). Overall, the pedogenic carbonate increases slightly with soil depth. A possible reason might be either the leaching from upper horizons (Gocke et al., 2012), the direct recrystallization of pedogenic carbonate (Gocke et al., 2012) or the dissolution of carbonate from the C horizons to secondary carbonate (Zamanian et al., 2016), which would need further investigation.

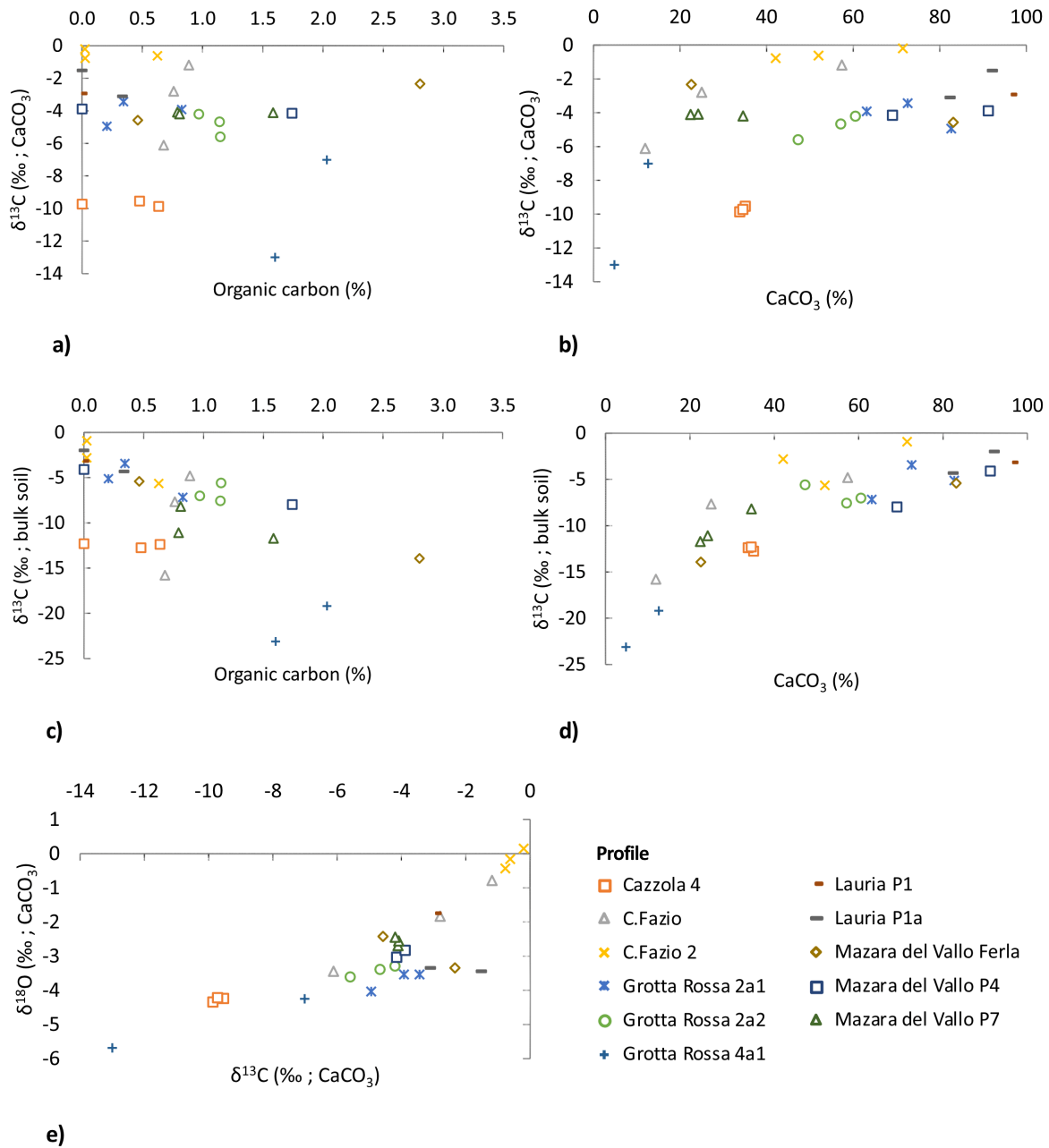


FIGURE 6.1: Relationship of oxygen and carbon isotopes from the bulk soil and carbonate with the organic and carbonate fraction of the soil.

The slight increase of pedogenic carbonate albeit shows that the inorganic carbon stocks are still being fed by the formation of secondary carbonate.

## 6.2 Chemical weathering and mineral composition of the soil

Looking at the summarised elemental losses/gains (see Fig. 5.13), almost no loss of carbonates and silicates is visible with time. The apparently highest silicate weathering rate is measured at Mazara del Vallo P4 (amended 45 years ago) which lost  $20.88 \text{ mol/m}^2$  per year of silicates. If a ratio of 1 : 1 between the consumption of  $\text{CO}_2$  and weathered silicates is assumed (1 *mol Ca* or *Mg* with 1 *mol CO*<sub>2</sub> (Hilley and Porder, 2008)),  $919 \text{ g/m}^2 \text{ CO}_2$  could be sequestered per year for this profile. Other authors suggest a silicate- $\text{CO}_2$  ratio of 1:2 (see Fig. 1.1) which would be  $1'605 \text{ g/m}^2$  of sequestered  $\text{CO}_2$  per year for the same profile as mentioned above. In addition, carbonate weathering could additionally sequester  $12'317 \text{ g/m}^2 \text{ CO}_2$  per year in Mazara del Vallo P4. Nevertheless, the high values calculated for the 2:1 ratio for the silicate weathering and the carbonate weathering do not consider that the  $\text{CO}_2$  is partially stored in  $\text{HCO}_3^-$  which could degas again. Thus, the 1:1 ratio of silicate weathering seems to give the most realistic results.

These findings correspond with the results of the weathering indices where the weathering degree was identified as rather large. Meanwhile matched the undisturbed soil profiles the trend of the cultivated profiles which implies that agriculture neither positively nor negatively influences the sequestration rates.

Nevertheless, according to Hilley and Porder (2008), only numbers close to *zero mol/ha/y* of silicate weathering can be expected for our study site since it does not belong to a large river catchment or tectonic active area or has a granitic bedrock composition thus our results should be treated with caution.

In contrast, carbonate weathering reached much higher values than silicate weathering. Liu et al. (2011) stated that carbonate weathering rates are typically  $10^2 - 10^8$  higher than silicate weathering rates. The release of carbon due to carbonate weathering is large regarding the stored C within calcareous rock. Hence carbonate weathering should also be considered an influential factor in carbon budgets (Gaillardet et al., 2019).

External factors such as aeolian contributions which might alter the sequestration rates can be mostly excluded. The immobile elements *Ti*, *Nb*, *Y*, *Ce* and *Zr* (Muhs and Benedict, 2006) reveal that the material is mostly autochthonic and has a small chemical discordance (see Fig. 5.11).

Regarding the CIA (see Fig. 5.10 a), the WIP (see Fig. 5.10 b) and  $(K + Na)/Ti$  (see Fig. 5.10 c) weathering index, it is believed that Mazara del Vallo P4 C is a rather weakly weathered horizon while the A horizon from the same profile is rather strongly weathered horizon (see Fig. 5.11). The relatively large ratios of *Ti/Zr* as well as  $(Na + K)/Ti$  in the C horizon are due to low *Ti* and *K* values. Nevertheless, it also needs to be considered that the



$(Na + K)/Ti$  ratio describes the weathering progress in the top soil (Dahms et al., 2012). The Lauria profiles seem further among the most exposed to weathering. However, in Lauria P1 a  $Ti$  and  $Zr$  depletion is visible indicating that these profiles already contained a small initial amount of immobile elements (which are thus susceptible to inaccuracies) and were not weathered as strong as suspected. The other profiles are between those two extremes and do not show a clear relationship between weathering degree and time. Adding the PDI (see 5.14), however, a fairly clear increase of the weathering degree with time is revealed. The unamended profiles of Mazara del Vallo Ferla and Lauria P1 are further showing relatively little weathering, pointing out that the weathering indices need to be considered over a longer time period than the last 50 years.

### 6.2.1 Oxalate-extractables and weathering indices

In respect to the oxalate-extractables, Mazara del Vallo P4 and the Lauria profiles belong to the weakly weathered profiles with a small amount of extractables being found. This finding is rather surprising, since the more weathering occurs, the more extractables should be released. Yet taking a closer look at the profile of Mazara del Vallo P4 shows that only the C horizon is depleted in the extractables, thus lowering the average of the entire profile. In addition, the weathering indices do not consider an initial lack of cations or immobile elements within the soil (see Section 6.2). Moreover, the loss of the cations observed in the weathering indices might have resulted in the passive accumulation of the oxalate-extractables and a translocation of the oxalate extractables from the parent material to the remaining horizons (Cortizas et al., 2003; Dahms et al., 2012).

Even though both the concentration (see Table A.8) and the stocks (see Table 5.2) of extracted  $Al$  and  $Fe$  correlated positively with organic carbon, the extracted  $Mn$  indicated no relation with  $C_{org}$ . Manganese often appears in separate enrichment within the soil, independent of the other oxalate-extractables (Blume et al., 2010). In spite of that, the manganese concentration showed a significant increase over a certain time period (0 to 35 years back) as well as iron (0 to 27 and 5 years). The stocks of the same compounds did however not show any statistically significant increase over time.

The observed oxides are important because they can bind material and stabilize it (Wiesmeier et al., 2019). The reactive surface of the compound is particularly important as they are attracted by clay and silty particles which also have a large reaction surface. The resulting clay minerals with expandable surfaces such as vermiculite and smectite form very stable compounds with organic material.

### 6.2.2 Clay minerals

The oxalate-extracted iron further follows a positive trend with kaolinite ( $R^2 = 0.9162$ ) and suggests current weathering (see Fig. 5.9b) since with an increasing amount of weathered iron also kaolinite is inherited from parent material (Scalenghe et al., 2016; Egli et al., 2020b).

Smectite corresponds to iron also quite strongly (see Fig. 5.9c). However, *Fe* stocks do not only depend on pedogenic formation rates, but also on the initial amount in the parent rock (Egli et al., 2020b). In semi-arid climates the C horizons are considered a significant origin for clay minerals (Omdi et al., 2018; Egli et al., 2020b). The strong positive correlation of plagioclase with smectite ( $R^2 = 0.9584$ ) (see Fig. 5.9e) and similarly strong relationship of smectite and mica (see Fig. 5.9d) and a rather strong positive trend of smectite with kaolinite (see Fig. 5.9g) indicate that no new smectite nor kaolinite has been formed in the recent years but originates from the previous vertisol or parent material (Mavris et al., 2011; Egli et al., 2020b). Furthermore, the positive correlation of kaolinite and K-feldspar (see Fig. 5.9f) points out that the kaolinite has not been recently formed but relocated within the soil. Since neither mica nor feldspar is decreasing with the appearance of secondary formed clay minerals (smectite, kaolinite), the clay minerals overall seem to originate from the parent material (Barbera et al., 2008; Scalenghe et al., 2016; Egli et al., 2020b).

In summary, mica, chlorite, kaolinite and smectite show a rather diffuse trend and not seem to change much over the observed time period (see Fig. 5.8) because the duration of the observed soil development has probably not been long enough. However, some mixed layered clay minerals were found with interlayered mica and vermiculite/smectite. This indicates that the weathering of the clay minerals has at least begun. The appearance of goethite in the total fraction of the soil supports this assumption because  $Fe^{2+}$  is being released through weathering and oxidizes to goethite (Blume et al., 2010). Goethite is one of the most common pedogenic iron oxides (Fink et al., 2016) causing a yellow-brownish colour of the soil.

Chlorite was also found in the total fraction of the soil. In pedogenic processes mainly dioctahedral chlorite is formed, whereas trioctahedral chlorite often originates from the parent rock (Weaver and Pollard, 1973). Since we found mainly trioctahedral chlorite, we can conclude that the chlorite behaved similar as the other clay minerals and hardly underwent any weathering process.

## 6.3 Physical weathering

### 6.3.1 Soil pore analysis

Soil pores are effecting the soil organic carbon cycle by changing numbers and sizes of pores which ultimately alter soil texture and the accumulation of organic matter (Singh et al., 2018). Likewise, as particles shrink further as they dissolve during weathering reactions (Taylor et al., 2017), the fine fraction of the soil can lead to changes in soil permeability and pore size (Andrews and Taylor, 2019).

The rather sandy soil (high carbonate content) at the start of the soil evolution suggests that the soil pores have a comparably large soil pore volume (macroporosity) (Singh et al., 2018). Sandy soils have only a small relevance in protecting SOC from mineralization because of

the lack of smaller pore sizes stabilizing organic material (Chivenge et al., 2007). Beyond that, the pore volume does not show a remarkable trend over time, despite a drop at C. Fazio 2Ap to a minimum of  $1'365\text{mm}^3$  which might be due to the relatively large clay content in the C.Fazio samples. This suggestion is also supported when we look at other sites such as Cazzola 4, where the soil pore volume is low and the clay content high. Yet, the pore volume was defined as the diameter of at least one connecting voxel, thus undermining the appearance of pores smaller than the size of the voxel ( $0.029\text{mm}$ ). Since the porosity only changes little over time (see Fig. 5.15 c), the overall connectivity within the soil therefore stays more or less the same (Vervoort and Cattle, 2003). In places where many network numbers were found, the tortuosity is rather high and the network length small. Musso et al. (2019) explained these parameters with the appearance of soil organic matter which changes the overall structure of the soil. Since no change in soil pore characteristics could be statistically proven with our samples, the development of organic matter must have left the overall soil structure intact.

However, the pore volume overall increases slightly with depth which could be caused by increasing root growth which generates pore space (Musso et al., 2019). Besides, few macropores have been developing in the soil (see Table A.9) with an albeit overall decreasing porosity (if comparing equivalent soil horizons with each other, see Fig. 5.19). The formation time of macropores is not known, however is estimated to be as fast as 15 years (Hirmas et al., 2018) which could explain why still not many macropores have been established within the sampled sites. Even though the macroporosity was quite small in the samples, macropores still are thought to infiltrate 70 % of the total soil water (Hirmas et al., 2018; Musso et al., 2019). The development of macropores is dependent on factors such as SOC percentage, grain size distribution (Nemes et al., 2005), agricultural techniques and soil biology (Jarvis, 2007). Macroporosity and the max. graph length indeed correlate ( $r = 0.89$ ), indicating that macropores tend to extend the soil pore network. Harrowed soils do generally contain more macropores, yet this could not be proven with our samples (Larsbo et al., 2014).

The pore system has overall not changed exceptionally. The establishment of macropores may still improve the water infiltration through the soil. The mix of sandy limestone material and the original clayey soil had already shown a positive influence on the grape quality in the area (see chapter 2).

### **6.3.2 Grain size and soil structure**

The preferential flow of infiltrating water was identified to use 50 % of the macropore space in sandy loam (Mooney, 2002). The Lauria sites (composed of sandy loam/loam) thus seem to have a comparably low fraction of active macropores. The remaining sampled sites are a mixture of clay/silt with a relatively little sand (see Section 5.3). Clayey and silty soil compositions have a used macropore space of up to 90 % (Mooney, 2002).

Especially the deeply developed sites contained remarkably high clay contents (independent of time), besides that the clay percentage overall significantly ( $p < 0.05$ ) increased with time. In contrast, the unamended site of Lauria P1 which still largely consists of parent material has a comparable low clay fraction. Even though clay and silt are considered an important stabilizer for organic carbon, no correlation has been found between organic carbon and the grain sizes.

Nevertheless, different studies indicated enrichment in soil organic carbon in various grain sizes, depending on the formation of small ( $< 25\mu\text{m}$  (Gerzabek et al., 2001) and large ( $75 - 250\mu\text{m}$ ) microaggregates (Barbera et al., 2012). In addition, Barbera et al. (2012) recommended to use agricultural practices on vertisols which promote the formation of macroaggregates, rather than microaggregates, since SOC is more likely to be accumulated in coarser aggregates. The decomposition of soil organic carbon however seem to be higher in coarse fragmented soil (Hassink, 1992; Singh et al., 2018).

Apart from the clay and silt content, oxalate-extractables (*Al* and *Fe*), pH and exchangeable  $\text{Ca}^{2+}$  ions are relevant influences for SOC in arid regions (Rasmussen et al., 2018).  $\text{Ca}^{2+}$  ions form soil aggregates which bind soil organic carbon (Zhao et al., 2018). Clay minerals own a surface- and pH dependent surface charge (Rasmussen et al., 2018) and hence clay minerals are thought to be the controlling factor for mineralogical interactions with water, minerals, metals and organic compounds (Sposito et al., 1999; Rasmussen et al., 2018). Indeed, organic carbon is less likely to be mineralized within clayey soils than sandy soil because carbon is more likely to be occluded and adsorbed at the clay surface (Sissoko and Kpombrekou-A, 2010). The resulting stabilized soil structure again serves through SOC preservation in aggregates (Elliott, 1986; Singh et al., 2018).

## 6.4 Synthesis: Factors influencing carbon sequestration

The binding of  $\text{CO}_2$  from the atmosphere with silicate weathering did not seem to be the most important capturing mechanism for atmospheric C, but the building of organic matter and compounds of metal-, mineral- and organo-organic compounds. Both the concentrations (e.g. aluminium ( $\rho = 0.671$ )) and the stocks (e.g. aluminium ( $\rho = 0.736$ )) of the oxyhydroxides have a strong relation with organic carbon and seem to form compounds with the organic material. A positive correlation of kaolinite and mica with organic carbon suggests further that the clay minerals are related with the appearance of oxyhydroxides. Clay absorbs organic molecules and serves as a protection against microbial decomposition (Ladd et al., 1996; Bai et al., 2019) and representing a physical barrier between the carbon molecule and the environment (Singh et al., 2018).

The weathering indices, the oxalate-extractables, the PDI, as well as grain size were concise in terms of the weathering degree. Since the weathering indices and the silicate weathering both consider the same chemical compounds, it is not surprising that Mazara del Vallo P4 shows the highest silicate weathering ( $\tau$  - Tau) and weathering degree using the indices. These results do however not correspond with the accumulation of organic carbon. The biggest organic carbon stock was found in Grotta Rossa 4a1, followed by the undisturbed site of Mazara del Vallo Ferla. This could indicate that the soil transformations did not automatically lead to a great organic carbon loss or that the undisturbed site did not receive as much organic matter input by plant material. In addition, the sequestration rates of Mazara del Vallo Ferla were in the same range as the amended profiles which leads to the assumption that tillage does not negatively effect carbon sequestration.

It appears that the input of organic material is either higher at Grotta Rossa 4a1 and/or the carbon pools are more stable than in Mazara del Vallo P4. Moreover, the little weathering occurring in the C horizon of Mazara del Vallo P4 has probably released only a small amount of clay minerals and oxyhydroxides, limiting the carbon sequestration potential of this profile. In comparison, Cazzola 4 does not have a large *Corg* stock, nor a high sequestration rate, although the clay and silt content is high. Cazzola 4 however contains only a small oxalate-extractables concentration and stock, which therefore again prohibit higher sequestration and storage of organic carbon.

#### 6.4.1 Organic carbon sequestration and storage

The *Corg* sequestration is within a good range compared to a study by Aguilera et al. (2013) in Spain under agriculture. Our values lie between  $0.07$  and  $0.34 \text{ kg m}^{-2}\text{y}^{-1}$  and are higher than farmland with only organic amendments ( $0.134 \text{ kg m}^{-2}\text{y}^{-1}$ ) or cover crops ( $0.027 \text{ kg m}^{-2}\text{y}^{-1}$ ) (Aguilera et al., 2013).

Other studies from the Mediterranean region sequestered far less carbon with  $0.046 \text{ kg m}^{-2}\text{y}^{-1}$  to  $-0.0004 \text{ kg m}^{-2}\text{y}^{-1}$  (Álvaro-Fuentes et al., 2009). Our values are rather high, since we have not only looked at the carbon accumulation in the topsoil, but in the whole profile. This can be confirmed by a study of López-Bellido et al. (2010), where within the years 1986 - 2006, only  $0.07 \text{ kg m}^{-2}\text{y}^{-1}$  and  $0.11 \text{ kg m}^{-2}\text{y}^{-1}$  was stored in the topsoil under conventional tillage, respectively no tillage. We also found out that the application of organic fertilizers might have contributed to the fact that higher stock levels were achieved (Luo et al., 2011).

In the study sites, most of the measured organic carbon has been stored at the soil surface, hence probably belonging to a rather labile pool which is frequently replaced by new organic matter or is being respired (Jackson et al., 2017). In fruit orchards with cover crops especially the labile carbon pools and soil organic matter are being fed (Sanz-Cobena et al., 2017). Organic C should however be especially stored in the subsoil (Angst et al., 2018), changing *Corg* stocks in a soil depth of  $40\text{cm}$  and more (Luo et al., 2010; Aguilera et al., 2013) to be

stable over a longer time period. While the deeper allocation of organic carbon influences the long-term sequestration of SOC (Laban et al., 2018), the labile carbon pool is important for the carbon sequestration and soil health. Yet, both the subsoil and topsoil SOC pools are reacting to increasing temperature, stressing the importance of soil compounds which stabilize organic carbon independent of its location within the soil (Hicks Pries et al., 2018). Nevertheless, carbon release is also influenced by the size of the stock (Crowther et al., 2016; Jackson et al., 2017) while stock variations can be explained by up to 90 % by clay fraction differences and organic matter input by roots (Angst et al., 2018).

### **Agricultural influences on carbon sequestration and storage**

Grass was often planted as a cover crop between the rows of table grapes (see Fig. 2.2). Grass is known to store the most carbon in comparison to other plant types (Soussana et al., 2004; McNally et al., 2017; Chen et al., 2019). Cover crops are particularly helpful to prevent soil erosion and with it the loss of soil carbon (Novara et al., 2019). Nevertheless, it needs to be considered that the crops are often selected to achieve the maximum yield possible which means a trade off to belowground growth and thus carbon allocation in depth (Jackson et al., 2017). The deep allocation of SOC is yet not a warrant for stabilizing carbon and would need to be explored in more detail by future studies (Hicks Pries et al., 2018). Besides, it is well reviewed that plants strongly increase chemical weathering reactions by (1) the input of acids (Porder, 2019) and (2) the much greater  $CO_2$  concentration in the rhizosphere than in the atmosphere (Zamanian et al., 2016). Carbonate weathering for example is augmented 5 – 10 times with the appearance of plants.

While the observed time span seems to be too little to see the effect of a higher weathering at beginning of soil formation, the carbon sequestration is already considered to be high (Vicente-Vicente et al., 2016), as the C sequestration rates tend to be the fastest during these first years after the change of the management and progressively slow down. This finding corresponds to the soil evolution from the Chicken Creek Catchment (see Chapter 1 1), where easily soluble compounds such as carbonate are being leached extensively at the beginning of soil formation. With plant growth however, the translocation of soil minerals and nutrients to the subsoil is not prominent. Mazara del Vallo Ferla contains however remains of an Alfisol, a soil type which is known for its leaching of cations and clay (WRB, 2015).

It is also interesting that the unamended site of Mazara del Vallo Ferla does not contain a larger carbon storage than the other sites, verifying that without additional amendment the soils in Sicily are not able to store exceptionally more carbon than without amendments. It was proven that liming and harrowing did not have a negative effect on the production of the table grapes, nor on the carbon sequestration. The soil pore analysis has shown that the soil system was not compacted over the years and that the amount of added organic

matter is stored within the pre-existing soil structures. Again, this observation agreed with the Chicken Creek Catchment, that the existing soil structures remain intact the first years of development.

The strong positive influence of additional C input on agricultural areas indicates that the sequestration potential in Mediterranean regions is far from being exhausted and from saturation (West and Six, 2007; Aguilera et al., 2013). Another reason for the measured SOC sequestration rates might be that fruit orchards can sequester more carbon within organs since they can grow over multiple decades (Vicente-Vicente et al., 2016) and that the sampled soil in Sicily is still developing and clay minerals are still being produced which means that carbon saturation has probably not been reached yet. In summary, organic carbon and organic matter has been accumulating within the soil, and it has been proven that the lime amendments, the tillage methods and the soil characteristics help to stabilize the organic carbon and prevent excessive leaching.

### **Further influences on soil organic carbon storage**

#### **Climate**

In dry Mediterranean climates the most limiting factor for mineral weathering and SOC sequestration is precipitation (MAP) (Hobley et al., 2016; Wiesmeier et al., 2019). Without water, a crucial reaction partner in weathering reactions (see Fig. 1.1) is missing, while plant growth is only possible to a certain extent and thus the production of organic mass. The accumulation of SOC is hence originally lower than in moister climates (Hobley et al., 2016; Wiesmeier et al., 2019). Artificial irrigation may compensate seasonal dryness regardless, while uncontrolled, heavy rainfall events which are typical for the area increase soil erosion and thus carbon loss (Vicente-Vicente et al., 2016). Yet, a study by Hobley et al. (2016) showed that arid areas own more resistant organic carbon pools than locations with a higher amount of rain while other authors suggest that precipitation does not have a clear impact on soil organic carbon fluctuations (Luo et al., 2011).

Relatively high temperatures (MAT) in southern Sicily are responsible for a higher SOC decomposition (Aguilera et al., 2013; Singh et al., 2018). Meanwhile the lack of SOC in the region may offset carbon loss due to warming, since plant growth is initially pushed before C is released back to the atmosphere (Crowther et al., 2016; Lal, 2018). Yet, increasing plant litter must not automatically lead to carbon sequestration, if signs of saturation or priming are involved (Jackson et al., 2017).

#### **Other biogeochemical factors affecting organic carbon storage and sequestration**

Other factors such as litter and substrate quality, soil structures, microbial behaviour and enzymatic processes need also to be considered to have an influence on soil organic carbon storage (Lal, 2018). Furthermore, soil organic matter consumes more nitrogen for storing

additional carbon than plants do (Cotrufo et al., 2019). Thus soils which naturally have a higher C/N ratio (for example forests) tend to store more carbon than agriculturally used soil (Cotrufo et al., 2019).

The C/N ratio in the study sites shows that the soil is fertile with available carbon and nitrogen for plant growth (see Fig. 5.1e). The C horizons have unsurprisingly either a very low or high ratio since nitrogen is adsorbed to the mineral matrix. The higher the adsorption, the lower the ratio since less free nitrogen is available (Egli et al., 2010). Furthermore, the ratio indicates that the soil fauna is mineralizing organic matter which sets the ratio around 10. Besides the building of these resilient organo-mineral compounds, humification prohibits the degradation of organic matter (Blume et al., 2010). The determination of these components in the samples would require further investigation.

Since the parent material cannot provide nitrogen, the natural supply of nitrogen might therefore become limited in Sicily. N-fixing legumes such as faba beans could partially remediate the missing nitrogen. Faba beans are already popular crops in Sicily (see Chapter 2) and would serve well as a nitrogen reservoir. These legumes often however only provide a small fraction of the nitrogen which other crop types require.

Even though nitrogen is crucial for plant growth and thus binding carbon from the atmosphere in organic matter, it also stimulates microbial activity and C respiration (López-Bellido et al., 2010). The amended soils of our study were not treated with additional nitrogen, but with organic material which could also lead to priming (Lal, 2018). In semi-arid regions, it has been reported that despite these drawbacks, additional nitrogen fertilization has a positive effect on C sequestration due to ameliorated vegetation growth (Álvarez-Fuentes et al., 2009) and soil biota activity, which contributes to the building of stable soil compounds (Jackson et al., 2017).

## 6.5 Outlook and feasibility of the 4 per 1000 initiative

The 4 per 1000 initiative's goal to store 0.4 % additional carbon per year in the topsoil are equivalent to 2 – 3 Gt of carbon (Minasny et al., 2017). Other authors (Amelung et al., 2020) mentioned that more realistic sequestration rates lie only between 0.79 – 1.54 Gt C/year including drawbacks such as deforestation and mineral mining. We calculated that 0.07 and 0.34 kg m<sup>-2</sup>y<sup>-1</sup> organic carbon could be sequestered in the soils (considering topsoil and subsoil) in Sicily, which is upscaled to the entire island (25'426 km<sup>2</sup> area) approx. between 0.000177 Gt and 0.000864 Gt of sequestered organic carbon per year. This reaches approx. 0.006 % of the targeted amount of sequestered carbon each year by the initiative. In addition, the calculated amount of inorganic carbon fixed by silicate weathering is equivalent to 9,19 · 10<sup>-13</sup> Gt of carbon per year.

If the sequestration was further upscaled to arid and semi-arid regions, which make up 40%



of the global land mass (Lal, 2018), the impact on global carbon budgets could be immense. Nevertheless, as correctly stated by Luo et al. (2010) the upscaling of carbon storage and sequestration is far from trivial and many new factors which are not covered in this thesis would need to be applied.

In the carbon budget, it needs to be considered that the mining and preparation of the lime can offset the sequestered carbon by 10 – 30 % according to Beerling et al. (2018). Carbon release is further rising with increasing temperature over the next decade (Bradford et al., 2016).

The results of this master thesis should thus be complemented with further research on  $Ca^{2+}$ -ions, as they are thought to be good for predicting SOC accumulation (Wiesmeier et al., 2019). Pedogenic carbonate could furthermore be an additional source of  $Ca^{2+}$ -ions besides carbonate (Dietrich et al., 2017). Moreover, soil organic matter may be analysed and its degree of humification since it can provide information about how stable the SOM is. In addition, carbon pools and soil aggregates are useful to examine carbon storage stability. One could also invest in the development of plant species that have a greater primary production and increase the chance of storing organic C in the soil (Minasny et al., 2017).

Furthermore, social aspects should also be considered in the overall feasibility of the initiative. The primary goal of the initiative was in any case never to achieve a numerical target, but is seen as a means of achieving the goals of the Paris Agreement with as many global parties as possible in a sustainable manner (Paris Agreement, 2015). The aim of the initiative is therefore that by 2050 (when the Paris Agreement should really take effect) as many soils as possible should be sustainably managed and the soil organic carbon reservoirs worldwide should have been increased accordingly (Connors et al., 2020). Anyhow, farmers must have an incentive to earn money from the improved quality of their soils. This would have to be rewarded much better than is currently the case, at least to justify the effort that farmers have to make to use cover crops and additional amendments.

In Sicily, where it has been proven that liming improves and increases the quality and production of crops (Raimondi et al., 2020) in addition to stabilizing carbon storage, the extension of the guidelines of the 4 per 1000 initiative could actually bear fruit and be implemented by farmers. Nevertheless, the initiative seems far from being feasible for farmers worldwide, as the necessary funds and inducement are lacking.

## 7 Conclusion

The goal of this thesis is to explore the carbon sequestration potential of amended soils in Sicily, which went through a transformation to a more organic and productive tillage technique. With the addition of lime, it was hoped that inorganic carbon is increasingly sequestered through weathering reactions of silicates and carbonates. Besides, with the growing productivity of the crops, organic carbon was expected to be stored and stabilized as well. In this context, four main hypothesis and two additional questions have been proposed:

- Organic and inorganic carbon has been stored in significant amounts since the start of the land amendments.
- Carbon sequestration will be detectable in the data and a saturation limit will not be reached yet.
- Carbonate leaching will be detectable over the observed time period.
- Silicate weathering has been found in the recent years of land transformation.

*Additional questions:*

- Did soil (crop) productivity increase since the 1970's?
- What crops could be used to help the additional storage of carbon?

The storage of organic carbon has been proven to have been stabilized over the last 50 years. Organic carbon has been especially accumulated in the topsoil, where fresh organic material is frequently deposited from the crops. The sequestration rates were in the upper range in comparison to other authors which carried out their research under similar conditions in the Mediterranean region.

Carbonate and silicate weathering stayed within the expected frame as proposed by other studies, even though the calculated weathering rates are probably too high, since the study area is not part of a tectonically active area. Nevertheless, the storage of both the organic and inorganic carbon seem to have increased over time without reaching a saturation limit yet.

As expected, carbonate leaching from the top soil towards the parent material was detectable, while the translocation of silicates was not clearly visible, thus resulting in rather

low silicate weathering rates. It is further not known for how long inorganic and organic carbon compounds are finally stored within the soil since leaching would need to be further investigated within soil water.

Regarding the additional questions, soil (crop) productivity did indeed increase within the last 50 years, as well as the crop quality. As previously mentioned, especially crops which are able to store nitrogen and other soil nutrients should be used in the future to further enable weathering processes and the production of organic matter.

Since the study area of this thesis was rather small, it is difficult to consult if the carbon sequestration through liming and organic farming is just as large in other climates. It needs to be considered that the soil is an open system with many influential factors which again interact with each other. The collection of studies across the globe by the 4 per 1000 initiative is thus an important step to bring the knowledge of small scale studies in a larger context.

# A Supplements

TABLE A.1: Main chemical parameters of the soil probes in oxide and carbonate form normalised over the total sample.

Sample ID	Site	Horizon	Na <sub>2</sub> O %	MgO %	Al <sub>2</sub> O <sub>3</sub> %	SiO <sub>2</sub> %	P <sub>2</sub> O <sub>5</sub> %	SO <sub>3</sub> %	K <sub>2</sub> O %	CaCO <sub>3</sub> %	CaO %	TiO <sub>2</sub> %	MnO %	Fe <sub>2</sub> O <sub>3</sub> %	ZrO <sub>2</sub> %	LOI %
100	Cazzola 4	Ap1	0.64	1.20	10.63	36.72	0.19	0.12	1.46	35.10	0.00	0.63	0.14	4.95	0.02	8.10
102		Ap1	0.67	1.24	10.97	37.38	0.18	0.13	1.50	33.79	0.67	0.64	0.14	5.10	0.02	7.46
105		Ap2	0.40	1.10	10.76	38.14	0.13	0.11	1.49	34.54	0.00	0.66	0.15	5.17	0.02	7.22
106	C.Fazio	Ap1	<0.01	0.92	6.52	21.61	0.31	0.14	0.94	57.42	3.02	0.32	0.09	2.63	0.01	5.92
107		Ap2	0.66	1.64	12.03	41.92	0.16	0.14	1.56	25.04	2.29	0.74	0.08	5.67	0.02	7.97
108		2Ap	0.87	1.93	14.54	52.10	0.13	0.26	1.92	11.94	0.35	0.91	0.06	6.41	0.03	8.50
109	C.Fazio 2	Ap1	0.45	0.89	7.55	25.53	0.29	0.14	1.13	51.99	0.00	0.45	0.09	3.60	0.01	7.73
110		Ap2	0.41	0.52	4.62	14.35	0.21	0.10	0.70	71.48	0.13	0.26	0.11	2.35	0.01	4.58
111		Ap3/A	0.55	1.27	9.30	30.81	0.12	0.43	1.28	42.12	1.88	0.59	0.09	4.76	0.02	6.67
129	Grotta	A	<0.01	0.76	5.74	18.61	0.25	0.17	0.72	63.13	0.95	0.31	0.09	2.81	0.01	6.26
130	Rossa 2a1	AC	<0.01	0.49	4.37	14.08	0.19	0.15	0.49	72.59	0.31	0.26	0.07	2.31	0.01	4.48
131		C	<0.01	0.40	2.02	7.54	0.27	0.10	0.20	82.67	2.43	0.11	0.06	1.57	0.00	2.41
132	Grotta	2bA	0.37	1.37	7.64	28.31	0.20	0.19	0.89	47.29	2.10	0.45	0.10	3.78	0.01	7.18
133	Rossa 2a2	AC	0.21	1.02	5.58	20.16	0.22	0.18	0.74	60.52	0.39	0.33	0.08	3.09	0.01	7.31
134		AC	<0.01	1.15	6.41	22.59	0.17	0.18	0.74	57.15	1.07	0.36	0.09	3.24	0.01	6.67
135	Grotta	Ap	0.86	1.63	14.29	48.69	0.22	0.21	2.05	12.63	1.33	0.86	0.17	6.68	0.03	10.27
136	Rossa 4a1	Bt	1.03	1.73	16.10	54.03	0.09	0.17	2.23	4.86	1.44	0.98	0.18	7.34	0.04	9.76
137	Lauria	C	<0.03	0.03	0.43	1.29	0.24	0.14	0.03	96.62	0.00	0.02	0.01	0.17	0.00	0.74
		P1 (undist.)														
138	Lauria P1a	AC	<0.01	0.25	2.56	9.05	0.20	0.19	0.28	82.40	0.00	0.15	0.06	1.32	0.00	3.31
139		C	<0.01	0.07	1.15	3.99	0.22	0.18	0.11	92.18	0.00	0.05	0.04	0.52	0.00	1.24
140	Mazara del	A	0.69	1.21	13.65	42.28	0.19	0.33	1.52	22.61	0.00	0.79	0.10	6.66	0.04	9.88
141	Vallo Ferla	C	<0.01	0.61	2.94	6.60	0.24	0.14	0.20	83.14	1.43	0.11	0.01	1.28	0.00	3.08
		(undist.)														
142	Mazara del	Ap	0.10	0.56	5.21	15.23	0.42	0.20	0.53	69.09	0.00	0.26	0.03	2.45	0.01	5.73
143	Vallo P4	C	0.51	0.57	0.66	2.47	0.31	0.10	0.05	91.22	1.68	0.03	0.01	0.81	0.00	1.32
144	Mazara del	Ap1	0.70	1.16	14.35	44.14	0.16	0.18	1.60	22.48	0.00	0.80	0.09	6.46	0.03	7.78
145	Vallo P7	Ap2	0.59	1.11	14.22	42.92	0.15	0.16	1.58	24.22	0.00	0.84	0.10	6.94	0.04	7.08
146		C	0.52	1.04	12.61	36.23	0.15	0.15	1.36	34.57	0.00	0.73	0.08	6.24	0.03	6.19

TABLE A.2: Raw XRF data of the used elements in the thesis - Part 1.

Sample ID	Site	Horizon	Na (%)	Mg (%)	Al (%)	Si (%)	P (%)	S (%)	K (%)	Ca (%)	Ti (%)	Mn (%)	Fe (%)
100	Cazzola 4	Ap1	0.453	0.990	5.401	16.480	0.080	0.048	1.163	12.560	0.360	0.103	3.325
102		Ap1	0.470	0.981	5.458	16.420	0.075	0.047	1.169	12.540	0.363	0.103	3.352
105		Ap2	0.289	0.945	5.570	17.440	0.057	0.045	1.209	12.640	0.389	0.117	3.536
106	C. Fazio	Ap1	0.010	1.136	3.704	10.840	0.144	0.059	0.833	25.710	0.208	0.072	1.977
107		Ap2	0.462	1.133	5.970	18.380	0.067	0.051	1.216	10.420	0.418	0.055	3.723
108		2Ap	0.609	1.192	7.240	22.920	0.055	0.096	1.499	4.510	0.516	0.047	4.218
109	C. Fazio 2	Ap1	0.345	1.023	4.120	12.300	0.132	0.057	0.963	19.430	0.276	0.071	2.597
110		Ap2	0.303	0.944	2.453	6.725	0.090	0.042	0.580	27.410	0.155	0.087	1.646
111		Ap3/A	0.387	1.078	4.665	13.650	0.049	0.165	1.005	16.440	0.333	0.063	3.154
129	Grotta Rossa	A	0.010	1.027	3.067	8.788	0.112	0.070	0.603	24.970	0.187	0.070	1.986
130		AC	0.010	0.936	2.311	6.581	0.083	0.062	0.404	27.900	0.153	0.057	1.616
131		C	0.010	0.964	1.063	3.512	0.118	0.040	0.169	33.060	0.064	0.049	1.093
132	Grotta Rossa	2bA	0.279	1.272	4.144	13.560	0.088	0.079	0.761	19.950	0.274	0.079	2.706
133		AC	0.151	1.130	2.901	9.263	0.096	0.072	0.607	22.950	0.194	0.059	2.121
134		AC	0.010	1.196	3.391	10.560	0.073	0.073	0.618	22.530	0.216	0.067	2.270
135	Grotta Rossa	Ap	0.589	1.006	6.951	20.910	0.090	0.077	1.565	5.260	0.476	0.122	4.296
136		Bt	0.697	0.993	7.806	23.130	0.034	0.063	1.696	2.592	0.537	0.130	4.702
137	Lauria P1	C	0.022	0.869	0.229	0.601	0.104	0.055	0.025	36.480	0.009	0.011	0.117
138	Lauria P1a	AC	0.010	0.858	1.331	4.153	0.085	0.076	0.226	30.240	0.089	0.045	0.905
139		C	0.010	0.872	0.623	1.903	0.097	0.075	0.093	35.720	0.029	0.031	0.370
140	Mazara del Vallo Ferla	A	0.492	0.891	6.951	19.020	0.078	0.125	1.212	6.523	0.458	0.075	4.481
141		C	0.010	1.115	1.579	3.127	0.105	0.056	0.168	33.140	0.067	0.009	0.907
142	Mazara del Vallo P4	Ap	0.078	1.013	2.941	7.600	0.194	0.086	0.469	26.720	0.164	0.028	1.830
143		C	0.379	1.143	0.349	1.148	0.136	0.040	0.041	35.720	0.020	0.007	0.567
144	Mazara del Vallo P7	Ap1	0.519	0.896	7.584	20.610	0.071	0.071	1.328	7.840	0.478	0.073	4.511
145		Ap2	0.424	0.847	7.230	19.280	0.061	0.060	1.257	7.467	0.484	0.073	4.662
146	C1	0.386	0.937	6.704	17.010	0.068	0.061	1.138	12.400	0.441	0.064	4.383	

TABLE A.3: Raw XRF data of the used elements in the thesis - Part 2.

Y (%)	Zr (%)	Nb (%)	Ce (%)	Cs (%)	Rb (%)	Ba (%)	Th (%)	U (%)	Ta (%)	La (%)	Pr (%)	Sr (%)	Nd (%)	Sm (%)
0.002	0.017	0.002	0.007	0.001	0.008	0.023	0.001	0.000	0.000	0.003	0.004	0.039	0.006	0.001
0.002	0.017	0.002	0.007	0.001	0.008	0.023	0.001	0.000	0.000	0.004	0.004	0.032	0.007	0.001
0.002	0.018	0.002	0.008	0.001	0.008	0.024	0.001	0.000	0.000	0.004	0.003	0.028	0.006	0.001
0.001	0.006	0.001	0.007	0.001	0.004	0.014	0.000	0.000	0.000	0.004	0.008	0.092	0.009	0.003
0.002	0.017	0.001	0.007	0.001	0.007	0.021	0.001	0.000	0.000	0.004	0.004	0.049	0.005	0.001
0.002	0.021	0.002	0.010	0.001	0.009	0.026	0.001	0.000	0.000	0.005	0.007	0.031	0.010	0.001
0.001	0.009	0.001	0.007	0.001	0.005	0.016	0.000	0.000	0.000	0.004	0.006	0.082	0.007	0.002
0.001	0.004	0.001	0.004	0.000	0.003	0.010	0.000	0.000	0.000	0.002	0.003	0.104	0.004	0.003
0.002	0.013	0.001	0.007	0.001	0.006	0.046	0.001	0.000	0.000	0.004	0.005	0.064	0.007	0.002
0.001	0.007	0.001	0.004	0.000	0.003	0.016	0.000	0.000	0.000	0.002	0.004	0.157	0.005	0.004
0.001	0.006	0.001	0.003	0.000	0.003	0.012	0.000	0.000	0.000	0.001	0.002	0.118	0.004	0.003
0.001	0.001	0.000	0.003	0.000	0.001	0.005	0.000	0.000	0.000	0.002	0.003	0.087	0.004	0.005
0.001	0.010	0.001	0.006	0.001	0.005	0.033	0.000	0.000	0.000	0.004	0.005	0.074	0.008	0.002
0.001	0.006	0.001	0.004	0.000	0.004	0.053	0.000	0.000	0.000	0.002	0.002	0.173	0.004	0.003
0.001	0.008	0.001	0.006	0.001	0.004	0.037	0.000	0.000	0.000	0.004	0.006	0.140	0.007	0.003
0.003	0.022	0.002	0.009	0.001	0.010	0.034	0.001	0.000	0.000	0.005	0.004	0.029	0.008	0.001
0.004	0.024	0.002	0.010	0.001	0.011	0.036	0.002	0.000	0.000	0.005	0.005	0.022	0.009	0.001
0.000	0.000	0.000	0.000	0.000	0.000	0.020	0.000	0.001	0.000	0.000	0.001	0.060	0.001	0.007
0.000	0.002	0.000	0.002	0.000	0.001	0.101	0.000	0.001	0.000	0.001	0.002	0.037	0.004	0.005
0.001	0.001	0.000	0.001	0.000	0.001	0.056	0.000	0.001	0.000	0.000	0.001	0.042	0.002	0.006
0.004	0.026	0.002	0.008	0.000	0.007	0.024	0.001	0.000	0.000	0.004	0.004	0.017	0.007	0.001
0.000	0.001	0.000	0.002	0.000	0.001	0.003	0.000	0.000	0.000	0.001	0.003	0.062	0.004	0.006
0.001	0.006	0.000	0.003	0.000	0.002	0.006	0.000	0.000	0.000	0.001	0.002	0.045	0.004	0.003
0.000	0.000	0.000	0.000	0.000	0.000	0.001	0.000	0.000	0.000	0.000	0.001	0.053	0.002	0.007
0.004	0.026	0.002	0.009	0.001	0.008	0.025	0.001	0.000	0.000	0.005	0.005	0.020	0.008	0.001
0.004	0.025	0.002	0.009	0.000	0.008	0.026	0.001	0.000	0.000	0.005	0.004	0.019	0.007	0.001
0.003	0.021	0.002	0.008	0.001	0.007	0.022	0.001	0.000	0.000	0.004	0.005	0.027	0.007	0.002

TABLE A.4: Organic matter content (LOI), Carbon fractions, -stocks and -accumulation.

Sample ID	Site	Horizon	LOI	C <sub>total</sub> (%)	C <sub>inorg</sub> (%)	C <sub>total</sub> stock (kg/m <sup>2</sup> )	C <sub>inorg</sub> stock (kg/m <sup>2</sup> )	CaCO <sub>3</sub> stock (kg/m <sup>2</sup> )	C <sub>org</sub> stock (kg/m <sup>2</sup> )	C <sub>org</sub> accumulation rate (kg m <sup>-2</sup> y <sup>-1</sup> )
100	Cazzola 4	Ap1	7.8	4.67	4.191	18.6	16.7	139.0	1.9	0.05
102		Ap1	7.0	4.58	3.948	20.5	17.7	147.2	2.8	0.08
105		Ap2	7.1	4.19	4.202	7.6	7.6	63.4	0.0	0.00
106	C. Fazio	Ap1	6.4	8.55	7.664	53.4	47.8	398.6	5.5	0.20
107		Ap2	7.5	3.68	2.920	10.8	8.6	71.7	2.2	0.08
108		2Ap	8.0	2.07	1.398	7.6	5.1	42.5	2.5	0.09
109	C. Fazio 2	Ap1	8.0	6.75	6.662	36.0	35.5	296.2	3.3	0.12
110		Ap2	4.6	8.68	8.909	35.7	35.7	297.3	0.1	0.00
111		Ap3/A	6.3	4.83	4.964	4.6	4.6	38.3	0.0	0.00
129	Grotta Rossa	A	6.3	8.76	7.928	31.3	28.4	236.5	3.0	0.07
130	2a1	AC	4.5	9.37	9.027	5.9	5.7	47.3	0.2	0.00
131		C	2.4	10.45	10.242	32.4	31.8	264.8	0.6	0.01
132	Grotta Rossa	2bA	7.4	7.17	6.026	11.1	9.3	77.8	1.8	0.04
133	2a2	AC	7.2	8.37	7.397	30.0	26.5	221.0	3.5	0.08
134		AC	6.7	8.25	7.108	32.6	28.1	233.8	4.5	0.10
135	Grotta Rossa	Ap	9.4	3.47	1.443	14.5	6.0	50.4	8.5	0.19
136	4a1	Bf	8.9	2.16	0.553	8.8	2.3	18.9	6.6	0.15
137	Lauria P1	C	0.7	11.75	11.972	108.4	108.4	903.6	0.0	0.00
138	Lauria P1a	AC	3.3	10.40	10.060	35.6	34.4	287.0	1.1	0.07
139	Lauria P1a	C	1.3	11.25	11.700	114.9	114.9	957.8	0.0	0.00
140	Mazara del	A	9.5	5.51	2.706	13.8	6.8	56.3	7.0	0.14
141	Vallo Ferla	C	3.1	10.95	10.483	148.9	142.6	1188.1	6.3	0.13
142	Mazara del	Ap	6.1	10.91	9.168	46.9	39.4	328.2	7.5	0.17
143	Vallo P4	C	1.3	11.25	11.277	40.1	40.1	334.1	0.0	0.00
144	Mazara del	Ap1	7.8	4.38	2.792	9.9	6.3	52.8	3.6	0.07
145	Vallo P7	Ap2	6.8	3.68	2.894	24.9	19.5	162.8	5.3	0.11
146		C1	6.2	5.13	4.318	15.4	13.0	108.3	2.4	0.05

TABLE A.5: Weathering indices as a function of immobile elements.

Sample ID	Site	Horizon	Ti/Zr	Ti/Nb	Ce/Y	(K+Na)/Ti	WIP
100	Cazzola 4	Ap1	22.17	324.66	5.15	3.28	21.55
102		Ap1	22.62	335.13	5.09	3.32	24.07
105		Ap2	22.46	337.78	5.10	2.67	19.34
106	C. Fazio	Ap1	29.29	404.96	10.74	2.51	18.27
107		Ap2	27.64	425.17	5.86	2.93	29.73
108		2Ap	28.97	456.17	6.60	3.01	30.54
109	C. Fazio 2	Ap1	27.90	432.31	7.97	3.43	16.16
110		Ap2	33.99	425.08	5.94	4.32	11.43
111		Ap3/A	25.89	430.88	6.70	3.06	24.22
129	Grotta Rossa 2a1	A	23.71	458.65	7.89	2.03	10.75
130		AC	21.69	376.20	6.82	1.68	6.42
131		C	34.35	478.08	8.93	1.78	9.13
132	Grotta Rossa 2a2	2bA	25.40	447.94	7.86	2.76	20.11
133		AC	27.74	460.92	6.51	2.72	12.04
134		AC	26.18	445.56	8.89	1.80	12.34
135	Grotta Rossa 4a1	Ap	25.05	370.45	4.66	3.30	33.28
136		Bt	26.82	367.60	4.54	3.28	36.82
137	Lauria P1	C	154.80	255.91	23.79	4.26	0.63
138	Lauria P1a	AC	28.95	506.25	6.18	1.67	3.16
139	Lauria P1a	C	36.63	519.51	3.61	2.30	1.24
140	Mazara del Vallo Ferla	A	19.19	356.45	3.18	2.74	22.56
141		C	40.44	453.43	7.69	1.69	7.13
142	Mazara del Vallo P4	Ap	22.19	487.49	3.89	2.24	6.96
143		C	61.58	279.11	2.33	21.39	11.01
144	Mazara del Vallo P7	Ap1	20.52	350.47	3.79	2.83	23.25
145		Ap2	20.52	349.33	3.41	2.51	21.92
146		C1	21.85	371.41	3.71	2.49	19.24



TABLE A.6: Tau (open system mass-losses).

Sample ID	Site	Horizon	Tau ( $\Sigma$ Cations lost per profile) (kg/m <sup>2</sup> )	Tau ( $\Sigma$ Carbonates lost per profile) (kg/m <sup>2</sup> )	Tau ( $\Sigma$ CaO lost per profile) (kg/m <sup>2</sup> )	Tau ( $\Sigma$ Silicates lost per profile) (kg/m <sup>2</sup> )
100	Cazzola 4	Ap1				
102		Ap1	-1.31	-1.96	0.00	3.48
105		Ap2				
106	C. Fazio	Ap1				
107		Ap2	8.29	299.96	11.90	9.66
108		2Ap				
109	C. Fazio 2	Ap1				
110		Ap2	-16.83	-388.69	-1.20	-2.76
111		Ap3/A				
129	Grotta Rossa	A				
130		2a1	-51.32	-972.27	-38.56	-37.18
131		C				
132	Grotta Rossa	2bA				
133		2a2	-1.78	41.25	-3.09	-1.95
134		AC				
135	Grotta Rossa	Ap	-1.69	33.66	0.06	-0.06
136		4a1				
137		Lauria P1	C	0.00	0.00	0.00
138	Lauria Pia	AC	0.19	-665.47	0.00	0.49
139		C				
140	Mazara del Vallo Ferla	A	-34.75	-947.84	-17.27	-18.32
141		C				
142	Mazara del Vallo P4	Ap	-60.49	-1259.89	-29.24	-43.30
143		C				
144	Mazara del Vallo P7	Ap1	-6.65	-134.64	0.00	-0.63
145		Ap2				
146	CI					

TABLE A.7: Stocks of the oxalate extractables per horizon.

Sample ID	Site	Horizon	Fe stock (ox) (g/m <sup>2</sup> )	Al stock (ox) (g/m <sup>2</sup> )	Mn stock (ox) (g/m <sup>2</sup> )
100	Cazzola 4	Ap1	338.4	240.4	181.4
102		Ap1	334.3	248.2	192.5
105		Ap2	118.6	107.0	75.8
106	C. Fazio	Ap1	153.8	363.3	110.1
107		Ap2	123.3	341.6	77.3
108		2Ap	146.3	441.5	85.8
109	C. Fazio 2	Ap1	90.5	399.8	92.3
110		Ap2	35.5	156.4	58.0
111		Ap3/A	15.2	72.2	16.8
129	Grotta	A	247.7	206.5	76.7
130	Rossa 2a1	AC	25.1	14.2	7.1
131		C	178.5	141.0	54.7
132	Grotta	2bA	64.2	64.2	18.5
133	Rossa 2a2	AC	153.2	145.4	38.4
134		AC	124.3	82.2	27.3
135	Grotta	Ap	517.6	326.8	161.6
136	Rossa 4a1	Bt	1047.6	473.4	242.2
137	Lauria P1	C	52.5	11.9	13.6
138	Lauria P1a	AC	57.0	56.0	30.4
139		C	42.8	17.7	29.6
140	Mazara del Vallo Ferla	A	376.6	197.6	85.5
141		C	266.4	95.7	17.0
142	Mazara del Vallo P4	Ap	141.3	112.8	24.0
143		C	32.0	13.6	133.9
144	Mazara del Vallo P7	Ap1	217.3	216.9	71.1
145		Ap2	667.3	480.1	124.9
146		C1	385.3	279.7	0.0

TABLE A.8: Oxalate-extractable concentrations of *Al*, *Fe*, *Mn* of each horizon with standard deviation.

Sample ID	Site	Horizon	Al (mg/kg)	Fe (mg/kg)	Mn (mg/kg)
100	Cazzola 4	Ap1	850 ± 64.26	604 ± 13.57	456 ± 6.47
102	Cazzola 4	Ap1	747 ± 13.87	555 ± 4.97	430 ± 5.64
105	Cazzola 4	Ap2	599 ± 55.79	540 ± 2.17	383 ± 4.00
106	C. Fazio	Ap1	235 ± 7.38	555 ± 7.87	168 ± 1.80
107	C. Fazio	Ap2	397 ± 11.28	1101 ± 13.14	249 ± 2.07
108	C. Fazio	2Ap	418 ± 18.62	1261 ± 12.65	245 ± 4.34
109	C. Fazio 2	Ap1	169 ± 5.04	745 ± 16.07	172 ± 0.24
110	C. Fazio 2	Ap2	92 ± 4.31	401 ± 1.36	149 ± 1.25
111	C. Fazio 2	Ap3/A	151 ± 5.89	718 ± 52.18	167 ± 4.41
129	Grotta Rossa 2a1	A	645 ± 22.04	538 ± 92.14	200 ± 3.42
130	Grotta Rossa 2a1	AC	509 ± 5.47	288 ± 62.37	143 ± 2.32
131	Grotta Rossa 2a1	C	193 ± 3.29	193 ± 39.20	56 ± 2.65
132	Grotta Rossa 2a2	2bA	738 ± 9.10	487 ± 105.90	162 ± 0.53
133	Grotta Rossa 2a2	AC	456 ± 11.23	433 ± 122.25	114 ± 0.62
134	Grotta Rossa 2a2	AC	523 ± 49.55	413 ± 138.10	160 ± 2.05
135	Grotta Rossa 4a1	Ap	1358 ± 15.98	857 ± 329.64	424 ± 11.63
136	Grotta Rossa 4a1	Bt	1954 ± 9.65	812 ± 316.65	415 ± 2.97
137	Lauria P1	C	59 ± 5.49	13 ± 3.15	15 ± 0.30
138	Lauria P1a	AC	138 ± 8.77	135 ± 2.18	73 ± 0.28
139	Lauria P1a	C	67 ± 1.54	28 ± 1.21	46 ± 0.83
140	Mazara del Vallo Ferla	A	1507 ± 105.80	791 ± 14.88	342 ± 4.98
141	Mazara del Vallo Ferla	C	196 ± 1.84	70 ± 1.95	13 ± 0.08
142	Mazara del Vallo P4	Ap	366 ± 43.52	292 ± 20.51	62 ± 1.43
143	Mazara del Vallo P4	C	69 ± 5.97	29 ± 0.42	288 ± 3.16
144	Mazara del Vallo P7	Ap1	956 ± 58.63	955 ± 16.96	313 ± 8.31
145	Mazara del Vallo P7	Ap2	1246 ± 59.62	897 ± 13.71	233 ± 3.71
146	Mazara del Vallo P7	C	1060 ± 38.50	769 ± 24.11	0 ± 0.02

TABLE A.9: Soil pore analysis (pore diameter  $> 0.03mm$ ) for the sampled horizons.

Sample ID	Site	Horizon	Total pore volume (mm <sup>3</sup> )	Max graph length (mm)	Total porosity (-)	Total surface area pores (mm <sup>2</sup> )	Mean tortuosity (-)	Max graph number (-)	Macro-porosity (-)
100	Cazzola 4	Ap1	3418.28	62542.31	0.04	39072.39	1.12	84.00	0.04
102		Ap1							
105		Ap2							
106	C. Fazio	Ap1	7204.45	85076.76	0.08	67886.22	1.14	137.00	0.085
107		Ap2							
108		2Ap							
109	C. Fazio 2	Ap1	1365.44	9676.99	0.02	8915.82	1.16	65.00	0.016
110		Ap2							
111		Ap3/A							
129	Grotta Rossa 2a1	A	6093.26	82291.60	0.07	67599.84	1.16	154.00	0.072
130		AC							
131		C							
132	Grotta Rossa 2a2	2bA	9735.12	126944.35	0.11	104535.46	1.14	85.00	0.114
133		AC							
134		AC							
135	Grotta Rossa 4a1	Ap	7309.81	79945.09	0.08	68100.67	1.15	144.00	0.084
136		Bt							
137	Lauria P1	C	7236.91	132411.98	0.08	92363.49	1.14	125.00	0.083
138	Lauria P1a	AC	8604.72	153030.24	0.10	104041.03	1.14	180.00	0.099
139		C							
140	Mazara del Vallo Ferla	A	10869.56	222318.51	0.13	130527.88	1.13	112.00	0.13
141		C							
142	Mazara del Vallo P4	Ap							
143		C							
144	Mazara del Vallo P7	Ap1							
145		Ap2							
146		C1							

TABLE A.10: Soil pore analysis (pore diameter > 0.06mm) for the sampled horizons.

Sample ID	Site	Horizon	Total pore volume (mm <sup>3</sup> )	Max graph length (mm)	Total porosity (-) (Macroporosity)	Total surface area pores (mm <sup>2</sup> )	Mean tortuosity (-)	Max graph number (-)
100	Cazzola 4	Ap1	3468.54	46521.00	0.04	34618.46	1.13	39.00
102	Cazzola 4	Ap1						
105	Cazzola 4	Ap2						
106	C. Fazio	Ap1	7279.27	49263.88	0.08	62011.03	1.17	54.00
107	C. Fazio	Ap2						
108	C. Fazio	2Ap	1387.30	4137.12	0.02	7963.77	1.19	21.00
109	C. Fazio 2	Ap1						
110	C. Fazio 2	Ap2						
111	C. Fazio 2	Ap3/A						
129	Grotta R 2a1	A	6174.03	61522.48	0.07	61319.97	1.16	100.00
130	Grotta R 2a1	AC	9784.56	108736.62	0.11	94557.30	1.13	50.00
131	Grotta R 2a1	C	7381.37	65317.68	0.08	62279.85	1.15	89.00
132	Grotta R 2a2	2bA						
133	Grotta R 2a2	AC						
134	Grotta R 2a2	AC						
135	Grotta R 4a1	Ap						
136	Grotta R 4a1	Bt						
137	Lauria P1	C	7267.62	107283.11	0.08	83461.19	1.14	64.00
138	Lauria P1a	AC	8634.22	108043.27	0.10	94211.71	1.15	75.00
139	Lauria P1a	C	11100.56	176475.43	0.13	118565.17	1.12	43.00
140	Mazara del Vallo Ferla	A						
141	Mazara del Vallo Ferla	C						
142	Mazara del Vallo P4	Ap						
143	Mazara del Vallo P4	C						
144	Mazara del Vallo P7	Ap1						
145	Mazara del Vallo P7	Ap2						
146	Mazara del Vallo P7	C1						



TABLE A.12: Correlation of variables Part 2;  $r$  = Pearson's  $r$ ;  $\rho$  = Spearman's rho.

Clay	pH	$\delta^{18}\text{O}_{\text{carb}}$	$\delta^{13}\text{C}_{\text{bulk soil}}$	Soil skeleton	Bulk density	CaCO <sub>3</sub>	Fe concentration	Mn concentration	Al production rate/stock
$r$ : -0.487	X								
X	$\rho$ : 0.677	$r$ : 0.666							
$r$ : -0.388	$\rho$ : 0.495	$r$ : 0.495	$\rho$ : 0.404						
$r$ : -0.441	X			X					
X	$\rho$ : 0.459	X	$r$ : 0.495	$\rho$ : 0.401	X	$r$ : -0.710	$\rho$ : 0.511		
$r$ : -0.487	$\rho$ : -0.730	X	$r$ : 0.631	$\rho$ : -0.589	X	$r$ : -0.505	$\rho$ : 0.511	$\rho$ : 0.463	
$r$ : 0.763	$\rho$ : -0.444	X	$r$ : -0.648	$\rho$ : -0.509	$r$ : -0.417	$\rho$ : -0.582	$\rho$ : 0.624	$\rho$ : 0.549	
$r$ : 0.448	$\rho$ : -0.637	$r$ : -0.447	$r$ : -0.750	X	$\rho$ : -0.509	$\rho$ : -0.610	$\rho$ : 0.875	$\rho$ : 0.872	
X	$\rho$ : -0.784	$\rho$ : -0.416	$\rho$ : -0.799		X	X	$\rho$ : 0.515	$r$ : 0.502	$\rho$ : 0.982
$\rho$ : 0.616	$\rho$ : -0.441	X	$\rho$ : -0.661	$\rho$ : -0.716	X	X	$r$ : -0.681	$r$ : 0.789	$\rho$ : 0.982
X	$\rho$ : -0.567	$r$ : -0.567	$r$ : -0.831	$\rho$ : -0.684	X	X	X	$r$ : 0.789	$\rho$ : 0.723
X	$\rho$ : -0.720	X	$r$ : -0.650	$\rho$ : -0.685	X	$r$ : -0.738	$r$ : 0.789	$r$ : 0.703	$\rho$ : 0.523
X	X	X	$r$ : -0.733	$\rho$ : -0.555	X	$r$ : -0.561	X	X	X
X	X	X	X	X	X	X	X	X	X
$r$ : -0.726	$\rho$ : -0.700	X	$r$ : 0.928	X	X	$r$ : 0.870	$r$ : -0.856	$r$ : -0.701	$\rho$ : -0.833
$r$ : -0.700	$\rho$ : 0.766	X	$r$ : 0.829	X	X	$r$ : 0.821	$r$ : -0.839	X	$\rho$ : -0.700
$r$ : -0.714	X	X	$r$ : 0.921	X	X	$r$ : 0.859	$r$ : -0.845	$r$ : -0.688	$\rho$ : -0.733
$r$ : -0.798	$\rho$ : 0.750	X	$r$ : 0.910	X	X	$r$ : 0.890	$r$ : -0.888	$r$ : -0.687	$\rho$ : -0.866
X	X	X	X	X	X	X	X	X	X
X	X	X	X	X	X	X	X	X	X
$r$ : -0.716	X	X	$r$ : 0.918	X	X	$r$ : 0.859	$r$ : -0.844	$r$ : -0.699	$\rho$ : -0.766

TABLE A.13: Correlation of variables Part 3;  $r$  = Pearson's  $r$ ;  $\rho$  = Spearman's rho.

Fe production rate/stock	Mn production rate/stock	Kaolinite	Mica	Smectite	Chlorite	Total pore volume	Max graph length	Total porosity	Total sur- face area	Mean tortuosity	Max graph number
$\rho$ : 0.658											
$\rho$ : 0.741	X										
$\rho$ : 1.000	X	$r$ : 0.641									
$\rho$ : 0.682	$\rho$ : 0.752	$r$ : 0.755	$r$ : 0.645								
X	X	X	X	X							
$\rho$ : -0.766	$\rho$ : -0.716	X	X	X	X						
$\rho$ : -0.750	X	X	$r$ : -0.912	X	X	$r$ : 0.895					
X	X	X	X	X	X	$r$ : 0.999	$r$ : 0.899				
$\rho$ : -0.833	$\rho$ : -0.733	X	$r$ : -0.890	X	X	$r$ : 0.971	$r$ : 0.962	$r$ : 0.971			
X	X	X	X	X	X	X	X	X	X	X	
X	X	X	X	X	X	X	X	X	X	X	
X	X	X	X	X	X	$r$ : 0.998	$r$ : 0.892	$r$ : 0.998	$r$ : 0.970	X	X





# Bibliography

In: ().

- Aase, J. K. and Siddoway, F. H. (1976). "Influence of Tall Wheatgrass Wind Barriers on Soil Drying". In: *Agronomy Journal* 68 (4), pp. 627–631. DOI: 10.2134/agronj1976.00021962006800040024x.
- Aertsens, J., De Nocker, L., and Gobin, A. (2013). "Valuing the carbon sequestration potential for European agriculture". In: *Land Use Policy* 31 (April 2018), pp. 584–594. DOI: 10.1016/j.landusepol.2012.09.003.
- Aguilera, E., Lassaletta, L., Gattinger, A., and Gimeno, B. S. (2013). "Managing soil carbon for climate change mitigation and adaptation in Mediterranean cropping systems : A meta-analysis". In: *Agriculture , Ecosystems and Environment* 168, pp. 25–36. DOI: 10.1016/j.agee.2013.02.003.
- Ahmad, W., Singh, S., Dijkstra, F., and Dalal, R. (2013). "Inorganic and organic carbon dynamics in a limed acid soil are mediated by plants". In: *Soil Biology and Biochemistry* 57, pp. 549–555. DOI: 10.1016/j.soilbio.2012.10.013.
- Álvaro-Fuentes, J., López, M., Arrue, J., Moret, D., and Paustian, K. (2009). "Tillage and cropping effects on soil organic carbon in Mediterranean semiarid agroecosystems: Testing the Century model". In: *Agriculture, ecosystems & environment* 134 (3-4), pp. 211–217. DOI: 10.1016/j.agee.2009.07.001.
- Amelung, W., Bossio, D., Vries, W. de, Kögel-Knabner, I., Lehmann, J., Amundson, R., Bol, R., Collins, C., Lal, R., Leifeld, J., Minasny, B., Pan, G., Paustian, K., Rumpel, C., Sanderman, J., Groenigen, J. van, Mooney, S., Wesemael, B. van, Wander, M., and Chabbi, A. (2020). "Towards a global-scale soil climate mitigation strategy". In: *Nature Communications* 11 (1), pp. 1–10. DOI: 10.1038/s41467-020-18887-7.
- Amer, A.-M. M., Logsdon, S. D., and Davis, D. (2009). "Prediction of hydraulic conductivity as related to pore size distribution in unsaturated soils". In: *Soil science* 174 (9), pp. 508–515. DOI: 10.1097/SS.0b013e3181b76c29.
- Andrews, M. G. and Taylor, L. L. (2019). "Combating Climate Change Through Enhanced Weathering of Agricultural Soils". In: *Elements* 15 (4), pp. 253–258. DOI: 10.2138/gselements.15.4.253.
- Angst, G., Messinger, J., Greiner, M., Häusler, W., Hertel, D., Kirfel, K., Kögel-Knabner, I., Leuschner, C., Rethemeyer, J., and Mueller, C. W. (2018). "Soil organic carbon stocks in topsoil and subsoil controlled by parent material, carbon input in the rhizosphere, and

- microbial-derived compounds". In: *Soil Biology and Biochemistry* 122 (July 2017), pp. 19–30. DOI: 10.1016/j.soilbio.2018.03.026.
- Arnone, E., Pumo, D., Viola, F., Noto, L. V., and La Loggia, G. (2013). "Rainfall statistics changes in Sicily". In: *Hydrology and Earth System Sciences* 17 (7), pp. 2449–2458. DOI: 10.5194/hess-17-2449-2013.
- Bai, X., Huang, Y., Ren, W., Coyne, M., Jacinthe, P., Tao, B., Hui, D., and Yang, J. (2019). "Responses of soil carbon sequestration to climate-smart agriculture practices: A meta-analysis". In: *Global Change Biology* 25 (8), pp. 2591–2606. DOI: 10.1111/gcb.14658.
- Barbera, V., Poma, I., Gristina, L., Novara, A., and Egli, M. (2012). "Long-term cropping systems and tillage management effects on soil organic carbon stock and steady state level of C sequestration rates in a semiarid environment". In: *Land Degradation and Development* 23 (1), pp. 82–91. DOI: 10.1002/ldr.1055.
- Barbera, V., Raimondi, S., Egli, M., and Plötze, M. (2008). "The influence of weathering processes on labile and stable organic matter in Mediterranean volcanic soils". In: *Geoderma* 143 (1-2), pp. 191–205. DOI: 10.1016/j.geoderma.2007.11.002.
- Baskaran, S. (2010). "Structure and Regulation of Yeast Glycogen Synthase". PhD thesis. Indiana University.
- Berling, D. J., Leake, J. R., Long, S. P., Scholes, J. D., Ton, J., Nelson, P. N., Bird, M., Kantzas, E., Taylor, L. L., Sarkar, B., Kelland, M., DeLucia, E., Kantola, I., Müller, C., Rau, G., and Hansen, J. (2018). "Farming with crops and rocks to address global climate, food and soil security perspective". In: *Nature Plants* 4 (3), pp. 138–147. DOI: 10.1038/s41477-018-0108-y.
- Blume, H.-P., Brümmer, G. W., Horn, R., Kandeler, E., Kögel-Knabner, I., Kretschmar, R., Stahr, K., and Wilke, B.-M. (2010). *Lehrbuch der Bodenkunde*. 16th ed. Heidelberg Germany: Spektrum Akademischer Verlag.
- Boardman, B., Hurst, A., and Fawcett, T. (2002). *Carbon UK - ECI RESEARCH REPORT 25*. Tech. rep. Oxford UK: University of Oxford, p. 64. DOI: 10.13140/RG.2.1.3985.3685.
- Bradford, M. A., Wieder, W. R., Bonan, G. B., Fierer, N., Raymond, P. A., and Crowther, T. W. (2016). "Managing uncertainty in soil carbon feedbacks to climate change". In: *Nature Climate Change* 6 (8), pp. 751–758. DOI: 10.1038/nclimate3071.
- Brown, K. and Wherrett, A. (2020). *Bulk Density – Measurement*. <http://www.soilquality.org.au/factsheets/bulk-density-measurement>, visited 2020-04-01.
- Carter, M. and Gregorich, E. (2006). *Soil Sampling and Methods of Analysis*. Vol. 2, pp. 1–1224. DOI: 10.2134/jeq2008.0018br.
- Caruso, A., Pierre, C., Blanc-Valleron, M.-M., and Rouchy, J. (2015). "Carbonate deposition and diagenesis in evaporitic environments: The evaporative and sulphur-bearing limestones during the settlement of the Messinian Salinity Crisis in Sicily and Calabria". In: *Palaeogeography, Palaeoclimatology, Palaeoecology* 429, pp. 136–162. DOI: 10.1016/j.palaeo.2015.03.035.

- Chadwick, O. A., Brimhall, G. H., and Hendricks, D. M. (1990). "From a black to a gray box — a mass balance interpretation of pedogenesis". In: *Geomorphology* 3 (3). Proceedings of the 21st Annual Binghamton Symposium in Geomorphology, pp. 369–390. DOI: 10.1016/0169-555X(90)90012-F.
- Chen, S., Arrouays, D., Angers, D. A., Martin, M. P., and Walter, C. (2019). "Soil carbon stocks under different land uses and the applicability of the soil carbon saturation concept". In: *Soil and Tillage Research* 188 (September), pp. 53–58. DOI: 10.1016/j.still.2018.11.001.
- Chenu, C., Angers, D. A., Barré, P., Derrien, D., Arrouays, D., and Balesdent, J. (2019). "Increasing organic stocks in agricultural soils: Knowledge gaps and potential innovations". In: *Soil and Tillage Research* 188 (April), pp. 41–52. DOI: 10.1016/j.still.2018.04.011.
- Chivenge, P., Murwira, H., Giller, K., Mapfumo, P., and Six, J. (2007). "Long-term impact of reduced tillage and residue management on soil carbon stabilization: Implications for conservation agriculture on contrasting soils". In: *Soil and Tillage Research* 94 (2), pp. 328–337. DOI: 10.1016/j.still.2006.08.006.
- Connors, V. J., Cummings, J. P., and Madden, T. (2020). "Strategic plan." In: *Journal of the American Optometric Association* 70 (7), pp. 417–426. DOI: 10.29085/9781783300792.002.
- Cortizas, A. M., Gayoso, E. G.-R., Muñoz, J. N., Pombal, X. P., Buurman, P., and Terribile, F. (2003). "Distribution of some selected major and trace elements in four Italian soils developed from the deposits of the Gauro and Vico volcanoes". In: *Geoderma* 117 (3-4), pp. 215–224. DOI: 10.1016/S0016-7061(03)00124-1.
- Cotrufo, M. F., Ranalli, M. G., Haddix, M. L., Six, J., and Lugato, E. (2019). "Soil carbon storage informed by particulate and mineral-associated organic matter". In: *Nature Geoscience* 12 (12), pp. 989–994. DOI: 10.1038/s41561-019-0484-6.
- Crowther, T. W., Todd-Brown, K. E., Rowe, C. W., Wieder, W. R., Carey, J. C., MacHmuller, M. B., Snoek, B. L., Fang, S., Zhou, G., Allison, S. D., Blair, J. M., Bridgham, S. D., Burton, A. J., Carrillo, Y., Reich, P. B., Clark, J. S., Classen, A. T., Dijkstra, F. A., Elberling, B., Emmett, B. A., Estiarte, M., Frey, S. D., Guo, J., Harte, J., Jiang, L., Johnson, B. R., Kroël-Dulay, G., Larsen, K. S., Laudon, H., Lavalley, J. M., Luo, Y., Lupascu, M., Ma, L. N., Marhan, S., Michelsen, A., Mohan, J., Niu, S., Pendall, E., Peñuelas, J., Pfeifer-Meister, L., Poll, C., Reinsch, S., Reynolds, L. L., Schmidt, I. K., Sistla, S., Sokol, N. W., Templer, P. H., Treseder, K. K., Welker, J. M., and Bradford, M. A. (2016). "Quantifying global soil carbon losses in response to warming". In: *Nature* 540 (7631), pp. 104–108. DOI: 10.1038/nature20150.
- Dahlgren, R., Boettinger, J., Huntington, G., and Amundson, R. (1997). "Soil development along an elevational transect in the western Sierra Nevada, California". In: *Geoderma* 78 (3), pp. 207–236. DOI: 10.1016/S0016-7061(97)00034-7.
- Dahms, D., Favilli, F., Krebs, R., and Egli, M. (2012). "Soil weathering and accumulation rates of oxalate-extractable phases derived from alpine chronosequences of up to 1Ma in age". In: *Geomorphology* 151-152, pp. 99–113. DOI: 10.1016/j.geomorph.2012.01.021.

- Di Bella, M., Italiano, F., Romano, D., Quartieri, S., Pino, P., Tripodo, A., and Sabatino, G. (2020). "Massive dolomites in the Messinian evaporitic sequence (Sicily, Italy): multi-analytical characterization and implications for the dolomitization processes". In: *Carbonates and Evaporites* 35 (1), pp. 1–13. DOI: 10.1007/s13146-020-00559-8.
- Dietrich, F., Diaz, N., Deschamps, P., Ngounou Ngatcha, B., Sebag, D., and Verrecchia, E. (2017). "Origin of calcium in pedogenic carbonate nodules from silicate watersheds in the Far North Region of Cameroon: Respective contribution of in situ weathering source and dust input". In: *Chemical Geology* 460 (March), pp. 54–69. DOI: 10.1016/j.chemgeo.2017.04.015.
- Egli, M., Brandová, D., Cherubini, P., and Ivy Ochs, S. (2020a). *Geochronologie I (GEO 351.2) Mosaiksteine der Geochronologie: Methoden und Anwendungsbeispiele*.
- Egli, M. and Fitze, P. (2000). "Formulation of pedologic mass balance based on immobile elements: A revision". In: *Soil Science* 165 (5), pp. 437–443. DOI: 10.1097/00010694-200005000-00008.
- Egli, M., Fitze, P., and Mirabella, A. (2001a). "Weathering and evolution of soils formed on granitic, glacial deposits: Results from chronosequences of Swiss alpine environments". In: *CATENA* 45, pp. 19–47. DOI: 10.1016/S0341-8162(01)00138-2.
- Egli, M., Mavris, C., Mirabella, A., and Giaccari, D. (2010). "Soil organic matter formation along a chronosequence in the Morteratsch proglacial area (Upper Engadine, Switzerland)". In: *Catena* 82 (2), pp. 61–69. DOI: 10.1016/j.catena.2010.05.001.
- Egli, M., Favilli, F., Krebs, R., Pichler, B., and Dahms, D. (2012). "Soil organic carbon and nitrogen accumulation rates in cold and alpine environments over 1 Ma". In: *Geoderma* 183, pp. 109–123. DOI: 10.1016/j.geoderma.2012.03.017.
- Egli, M., Fitze, P., and Mirabella, A. (2001b). "Weathering and evolution of soils formed on granitic, glacial deposits: results from chronosequences of Swiss alpine environments". In: *Catena* 45 (1), pp. 19–47. DOI: 10.1016/S0341-8162(01)00138-2.
- Egli, M., Plötze, M., Tikhomirov, D., Kraut, T., Wiesenberg, G. L., Lauria, G., and Raimondi, S. (2020b). "Soil development on sediments and evaporites of the Messinian crisis". In: *Catena* 187, p. 104368. DOI: 10.1016/j.catena.2019.104368.
- Elliott, E. T. (1986). "Aggregate Structure and Carbon, Nitrogen, and Phosphorus in Native and Cultivated Soils". In: *Soil Science Society of America Journal* 50 (3), pp. 627–633. DOI: 10.2136/sssaj1986.03615995005000030017x.
- Elmer, M., Gerwin, W., Schaaf, W., Zaplata, M. K., Hohberg, K., Nenov, R., Bens, O., and Hüttel, R. F. (2013). "Dynamics of initial ecosystem development at the artificial catchment Chicken Creek, Lusatia, Germany". In: *Environmental Earth Sciences* 69 (2), pp. 491–505. DOI: 10.1007/s12665-013-2330-2.
- Fantappiè, M., Priori, S., and Costantini, E. A. (2015). "Soil erosion risk, Sicilian Region (1:250,000 scale)". In: *Journal of Maps* 11 (2), pp. 323–341. DOI: 10.1080/17445647.2014.956349.

- Fedo, C. M., Wayne Nesbitt, H., and Young, G. M. (1995). "Unraveling the effects of potassium metasomatism in sedimentary rocks and paleosols, with implications for paleoweathering conditions and provenance". In: *Geology* 23 (10), pp. 921–924. DOI: 10.1130/0091-7613(1995)023<0921:UTEOPM>2.3.CO;2.
- Fink, J. R., Inda, A., Tiecher, T., and Barrón, V. (2016). "Iron oxides and organic matter on soil phosphorus availability". In: *Ciencia E Agrotecnologia* 40, pp. 369–379. DOI: 10.1590/1413-70542016404023016.
- Fortner, S. K., Lyons, W. B., Carey, A. E., Shipitalo, M. J., Welch, S. A., and Welch, K. A. (2012). "Silicate weathering and CO<sub>2</sub> consumption within agricultural landscapes, the Ohio-Tennessee River Basin, USA". In: *Biogeosciences* 9 (3), pp. 941–955. DOI: 10.5194/bg-9-941-2012.
- Francaviglia, R., Di Bene, C., Farina, R., Salvati, L., and Vicente-Vicente, J. L. (2019). "Assessing "4 per 1000" soil organic carbon storage rates under Mediterranean climate: a comprehensive data analysis". In: *Mitigation and Adaptation Strategies for Global Change* 24 (5), pp. 795–818. DOI: 10.1007/s11027-018-9832-x.
- Gaillardet, J., Calmels, D., Romero-Mujalli, G., Zakharova, E., and Hartmann, J. (2019). "Global climate control on carbonate weathering intensity". In: *Chemical Geology* 527 (May), p. 118762. DOI: 10.1016/j.chemgeo.2018.05.009.
- Garland, G. M., Suddick, E., Burger, M., Horwath, W., and Six, J. (2014). "Direct N<sub>2</sub>O emissions from a Mediterranean vineyard: Event-related baseline measurements". In: *Agriculture, Ecosystems & Environment* 195, pp. 44–52. DOI: 10.1016/j.agee.2014.05.018.
- Gerwin, W., Schaaf, W., Biemelt, D., Winter, S., Fischer, A., Veste, M., and Hüttl, R. F. (2011). "Overview and first results of ecological monitoring at the artificial watershed Chicken Creek (Germany)". In: *Physics and Chemistry of the Earth* 36 (1-4), pp. 61–73. DOI: 10.1016/j.pce.2010.11.003.
- Gerzabek, M. H., Haberhauer, G., and Kirchmann, H. (2001). "Soil Organic Matter Pools and Carbon-13 Natural Abundances in Particle-Size Fractions of a Long-Term Agricultural Field Experiment Receiving Organic Amendments". In: *Soil Science Society of America Journal* 65 (2), pp. 352–358. DOI: 10.2136/sssaj2001.652352x.
- Gessesse, T. A. and Khamzina, A. (June 2018). "How reliable is the Walkley-Black method for analyzing carbon-poor, semi-arid soils in Ethiopia?" English. In: *Journal of Arid Environments* 153, pp. 98–101. DOI: 10.1016/j.jaridenv.2018.01.008.
- Global Carbon Project (2018). "Supplemental data of Global Carbon Budget 2018 (Version 1.0) [Data set]". In: *Earth System Science Data* 10 (4), pp. 2141–2194. DOI: 10.18160/gcp-2018.
- Gocke, M., Pustovoytov, K., Kühn, P., Wiesenberg, G., Löscher, M., and Kuzyakov, Y. (2011). "Carbonate rhizoliths in loess and their implications for paleoenvironmental reconstruction revealed by isotopic composition:  $\delta^{13}\text{C}$ ,  $^{14}\text{C}$ ". In: *Chemical Geology* 283 (3), pp. 251–260. DOI: 10.1016/j.chemgeo.2011.01.022.

- Gocke, M., Pustovoytov, K., and Kuzyakov, Y. (2012). "Pedogenic carbonate formation: Recrystallization versus migration Process rates and periods assessed by  $^{14}\text{C}$  labeling". In: *Global Biogeochemical Cycles* 26 (1), pp. 1–12. DOI: 10.1029/2010GB003871.
- Hamilton, S. K., Kurzman, A. L., Arango, C., Jin, L., and Robertson, G. P. (2007). "Evidence for carbon sequestration by agricultural liming". In: *Global Biogeochemical Cycles* 21 (2), pp. 1–13. DOI: 10.1029/2006GB002738.
- Harden, J. W. (1982). "A quantitative index of soil development from field descriptions: Examples from a chronosequence in central California". In: *Geoderma* 28 (1), pp. 1–28. DOI: 10.1016/0016-7061(82)90037-4.
- Harrington, C. D. and Whitney, J. W. (1987). "Scanning electron microscope method for rock-varnish dating". In: *Geology* 15 (10), pp. 967–970. DOI: 10.1130/0091-7613(1987)15<967:SEMMFR>2.0.CO;2.
- Hartmann, J., West, A. J., Renforth, P., Köhler, P., De La Rocha, C. L., Wolf-Gladrow, D. A., Dürr, H. H., and Scheffran, J. (2013). "Enhanced chemical weathering as a geoengineering strategy to reduce atmospheric carbon dioxide, supply nutrients, and mitigate ocean acidification". In: *Reviews of Geophysics* 51 (2), pp. 113–149. DOI: 10.1002/rog.20004.
- Hassink, J. (1992). "Effects of soil texture and structure on carbon and nitrogen mineralization in grassland soils". In: *Biology and Fertility of Soils* 14 (2), pp. 126–134. DOI: 10.1007/BF00336262.
- Hicks Pries, C., Castanha, C., Porras, R., Phillips, C., and Torn, M. S. (2018). "Response to Comment on "The whole-soil carbon flux in response to warming"". In: *Science* 359 (6378), pp. 1420–1423. DOI: 10.1126/science.aao0457.
- Hilley, G. and Porder, S. (2008). "A framework for predicting global silicate weathering and  $\text{CO}_2$  drawdown rates over geologic time-scales". In: *Proceedings of the National Academy of Sciences* 105 (44), pp. 16855–16859. DOI: 10.1073/pnas.0801462105.
- Hirmas, D., Gimenez, D., Nemes, A., Kerry, R., Brunsell, N., and Wilson, C. (2018). "Climate-induced changes in continental-scale soil macroporosity may intensify water cycle". In: *Nature* 561 (7721), pp. 100–103. DOI: 10.1038/s41586-018-0463-x.
- Hobley, E. U., Baldock, J., and Wilson, B. (2016). "Environmental and human influences on organic carbon fractions down the soil profile". In: *Agriculture, Ecosystems and Environment* 223, pp. 152–166. DOI: 10.1016/j.agee.2016.03.004.
- Hoogsteen, M. J., Lantinga, E. A., Bakker, E. J., Groot, J. C., and Tiftonell, P. A. (2015). "Estimating soil organic carbon through loss on ignition: Effects of ignition conditions and structural water loss". In: *European Journal of Soil Science* 66 (2), pp. 320–328. DOI: 10.1111/ejss.12224.
- Hoogsteen, M. J., Lantinga, E. A., Bakker, E. J., and Tiftonell, P. A. (2018). "An Evaluation of the Loss-on-Ignition Method for Determining the Soil Organic Matter Content of Calcareous Soils". In: *Communications in Soil Science and Plant Analysis* 49 (13), pp. 1541–1552. DOI: 10.1080/00103624.2018.1474475.

- Jackson, R. B., Lajtha, K., Crow, S. E., Hugelius, G., Kramer, M. G., and Piñeiro, G. (2017). "The Ecology of Soil Carbon: Pools, Vulnerabilities, and Biotic and Abiotic Controls". In: *Annual Review of Ecology, Evolution, and Systematics* 48 (1), pp. 419–445. DOI: 10.1146/annurev-ecolsys-112414-054234.
- Jarvis, N. (2007). "A review of non-equilibrium water flow and solute transport in soil macropores: Principles, controlling factors and consequences for water quality". In: *European Journal of Soil Science* 58 (3), pp. 523–546. DOI: 10.1111/j.1365-2389.2007.00915.x.
- Jenny, H. (1941). *Factors of soil formation; a sytem of quantitative pedology*. Tech. rep.
- Jones, D., Dennis, P., Owen, A., and Van Hees, P. (2003). "Organic acid behavior in soils—misconceptions and knowledge gaps". In: *Plant and soil* 248 (1-2), pp. 31–41. DOI: 10.1023/A:1022304332313.
- Köhler, P., Hartmann, J., and Wolf-Gladrow, D. (2010). "Geoengineering potential of artificially enhanced silicate weathering of olivine". In: *Proceedings of the National Academy of Sciences* 107 (47), pp. 20228–20233. DOI: 10.1073/pnas.1000545107.
- Laban, P., Metternicht, G., and Davies, J. (2018). *Soil biodiversity and soil organic carbon: keeping drylands alive*. DOI: 10.2305/iucn.ch.2018.03.en.
- Ladd, J., Foster, R., Nannipieri, P., and Oades, J. (1996). "Soil structure and biological activity". In: *Soil biochemistry* 9, pp. 23–78.
- Lal, R. (2018). "Digging deeper: A holistic perspective of factors affecting soil organic carbon sequestration in agroecosystems". In: *Global Change Biology* 24 (8), pp. 3285–3301. DOI: 10.1111/gcb.14054.
- Larsbo, M., Koestel, J., and Jarvis, N. (2014). "Relations between macropore network characteristics and the degree of preferential solute transport". In: *Hydrology and Earth System Sciences* 18 (12), pp. 5255–5269. DOI: 10.5194/hess-18-5255-2014.
- Liu, Z., Dreybrodt, W., and Liu, H. (2011). "Atmospheric CO<sub>2</sub> sink: Silicate weathering or carbonate weathering?" In: *Applied Geochemistry* 26, pp. 292–294. DOI: 10.1016/j.apgeochem.2011.03.085.
- Lombardo, V. and Raimondi, S. (1991). "Valore agronomico di substrati culturali ottenuti dalla trasformazione delle «sciare»". In: *L'Informatore Agrario* 47 (26), pp. 53–59.
- López-Bellido, R. J., Fontán, J. M., López-Bellido, F. J., and López-Bellido, L. (2010). "Carbon sequestration by tillage, rotation, and nitrogen fertilization in a mediterranean vertisol". In: *Agronomy Journal* 102 (1), pp. 310–318. DOI: 10.2134/agronj2009.0165.
- Luo, Z., Wang, E., Sun, O. J., Smith, C. J., and Probert, M. E. (2011). "Modeling long-term soil carbon dynamics and sequestration potential in semi-arid agro-ecosystems". In: *Agricultural and Forest Meteorology* 151 (12), pp. 1529–1544. DOI: 10.1016/j.agrformet.2011.06.011.
- Luo, Z., Wang, E., and Sun, O. J. (2010). "Soil carbon change and its responses to agricultural practices in Australian agro-ecosystems: A review and synthesis". In: *Geoderma* 155 (3-4), pp. 211–223. DOI: 10.1016/j.geoderma.2009.12.012.



- Manley, D. (2014). "Carbon in dryland soils". In: *Les dossiers thématiques du CSFD Issue 10*. 10. French Scientific Committee on Desertification.
- Martín-Martín, J., Travé, A., Gomez-Rivas, E., Salas, R., Sizun, J.-P., Vergés, J., Corbella, M., Stafford, S., and Alfonso, P. (2015). "Fault-controlled and stratabound dolostones in the Late Aptian–earliest Albian Benassal Formation (Maestrat Basin, E Spain): Petrology and geochemistry constrains". In: *Marine and Petroleum Geology* 65, pp. 83–102. DOI: 10.1016/j.marpetgeo.2015.03.019.
- Maurici, G. (1983). "I Suoli irrigati con le acque reflue del Comune di Corleone", pp. 1–128.
- Mavris, C., Plötze, M., Mirabella, A., Giaccai, D., Valboa, G., and Egli, M. (2011). "Clay mineral evolution along a soil chronosequence in an Alpine proglacial area". In: *Geoderma* 165 (1), pp. 106–117. DOI: 10.1016/j.geoderma.2011.07.010.
- McNally, S., Beare, M., Curtin, D., Meenken, E., Kelliher, F., Calvelo Pereira, R., Shen, Q., and Baldock, J. (2017). "Soil carbon sequestration potential of permanent pasture and continuous cropping soils in New Zealand". In: *Global Change Biology* 23 (11), pp. 4544–4555. DOI: 10.1111/gcb.13720.
- Minasny, B., An, Malone, B. P., McBratney, A. B., Angers, D. A., Arrouays, D., Chambers, A., Chaplot, V., Chen, Z. S., Cheng, K., Das, B. S., Field, D. J., Gimona, A., Hedley, C. B., Hong, S. Y., Mandal, B., Marchant, B. P., Martin, M., McConkey, B. G., Mulder, V. L., O'Rourke, S., Forges, A. C. Richer-de, Odeh, I., Padarian, J., Paustian, K., Pan, G., Poggio, L., Savin, I., Stolbovoy, V., Stockmann, U., Sulaeman, Y., Tsui, C. C., Vågen, T. G., Wesemael, B. van, and Winowiecki, L. (2017). "Soil carbon 4 per mille". In: *Geoderma* 292, pp. 59–86. DOI: 10.1016/j.geoderma.2017.01.002.
- Mooney, S. J. (2002). "Three-dimensional visualization and quantification of soil macroporosity and water flow patterns using computed tomography". In: *Soil Use and Management* 18 (2), pp. 142–151. DOI: 10.1111/j.1475-2743.2002.tb00232.x.
- Muhs, D. and Benedict, J. (2006). "Eolian additions to late Quaternary alpine soils, Indian Peaks Wilderness Area, Colorado Front Range". English. In: *Arctic, Antarctic, and Alpine Research* 38 (1), pp. 120–130. DOI: 10.1657/1523-0430(2006)038[0120:EATLQA]2.0.CO;2.
- Munoz-Rojas, M., Jordan, A., Zavala, L. M., De La Rosa, D., Abd-Elmabod, S. K., and Anaya-Romero, M. (2012). "Organic carbon stocks in Mediterranean soil types under different land uses (Southern Spain)". In: *Solid Earth* 3 (2), pp. 375–386. DOI: 10.5194/se-3-375-2012.
- Musso, A., Lamorski, K., Cezary, S., Geitner, C., Hunt, A., Greinwald, K., and Egli, M. (2019). "Evolution of soil pores and their characteristics in a siliceous and calcareous proglacial area". In: *Catena* 182 (November 2018). DOI: 10.1016/j.catena.2019.104154.
- NA (2020). *Sicily overview map*. (url: [https://d-maps.com/carte.php?num\\_car=8295&lang=de](https://d-maps.com/carte.php?num_car=8295&lang=de)).

- Nemes, A., Rawls, W. J., and Pachepsky, Y. A. (2005). "Influence of organic matter on the estimation of saturated hydraulic conductivity". In: *Soil Science Society of America Journal* 69 (4), pp. 1330–1337. DOI: 10.2136/sssaj2004.0055.
- Nesbitt, H. and Young, G. M. (1989). "Formation and diagenesis of weathering profiles". In: *The Journal of Geology* 97 (2), pp. 129–147.
- Novara, A., Minacapilli, M., Santoro, A., Rodrigo-Comino, J., Carrubba, A., Sarno, M., Venezia, G., and Gristina, L. (2019). "Real cover crops contribution to soil organic carbon sequestration in sloping vineyard". In: *Science of the Total Environment* 652, pp. 300–306. DOI: 10.1016/j.scitotenv.2018.10.247.
- Oehlert, A. M. and Swart, P. K. (2014). "Interpreting carbonate and organic carbon isotope covariance in the sedimentary record". In: *Nature Communications* 5 (1), pp. 1–7. DOI: 10.1038/ncomms5672.
- Omdi, F., Daoudi, L., and Fagel, N. (2018). "Origin and distribution of clay minerals of soils in semi-arid zones: example of Ksob watershed (Western High Atlas, Morocco)". In: *Applied Clay Science* 163, pp. 81–91. DOI: 10.1016/j.clay.2018.07.013.
- Osunbitan, J., Oyedele, D., and Adekalu, K. (2005). "Tillage effects on bulk density, hydraulic conductivity and strength of a loamy sand soil in southwestern Nigeria". In: *Soil and Tillage Research* 82 (1), pp. 57–64. DOI: 10.1016/j.still.2004.05.007.
- Paris Agreement (2015). *Paris Agreement*.
- Parker, A. (1970). "An index of weathering for silicate rocks". In: *Geological Magazine* 107 (6), pp. 501–504. DOI: 10.1017/S0016756800058581.
- Porder, S. (2019). "How Plants Enhance Weathering and How Weathering is Important to Plants". In: *Elements* 15 (4), pp. 241–246. DOI: 10.2138/gselements.15.4.241.
- Raimondi, S. (2019). "Trasformazione delle sciare di c.da ferla comune di mazara del vallo (TP)". unpublished. Palermo.
- Raimondi, S., Lauria, G., and Egli, M. (2020). "Ammendamento della massa terrosa dei versuoli premessa indispensabile per una frutticoltura sostenibile in sicilia". unpublished.
- Ramaiah, N. (2014). "Role of Heterotrophic Bacteria in Marine Ecological Processes". In: *Marine Microbiology: Facets and Opportunities*. April, pp. 27–38.
- Rasmussen, C., Heckman, K., Wieder, W. R., Keiluweit, M., Lawrence, C. R., Berhe, A. A., Blankinship, J. C., Crow, S. E., Druhan, J. L., Hicks Pries, C. E., Marin-Spiotta, E., Plante, A. F., Schädel, C., Schimel, J. P., Sierra, C. A., Thompson, A., and Wagai, R. (2018). "Beyond clay: towards an improved set of variables for predicting soil organic matter content". In: *Biogeochemistry* 137 (3), pp. 297–306. DOI: 10.1007/s10533-018-0424-3.
- Renforth, P. and Henderson, G. (2017). "Assessing ocean alkalinity for carbon sequestration". In: *Reviews of Geophysics* 55 (3), pp. 636–674. DOI: 10.1002/2016RG000533.
- Riar, A. and Coventry, D. (2013). "Chapter 4 - Nitrogen Use as a Component of Sustainable Crop Systems". In: *Agricultural Sustainability*. Ed. by G. S. Bhullar and N. K. Bhullar. San Diego: Academic Press, pp. 63–76. DOI: 10.1016/B978-0-12-404560-6.00004-6.

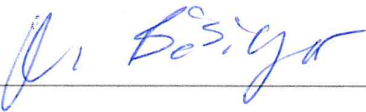
- Ridler, T. and Calvard, S. (1978). "Picture Thresholding Using an Iterative Selection Method". In: *IEEE Transactions on Systems, Man and Cybernetics* smc-8 (8), pp. 630–632. DOI: 10.1109/TSMC.1978.4310039.
- Romero-Mujalli, G., Hartmann, J., and Börker, J. (2019). "Temperature and CO<sub>2</sub> dependency of global carbonate weathering fluxes – Implications for future carbonate weathering research". In: *Chemical Geology* 527 (July), p. 118874. DOI: 10.1016/j.chemgeo.2018.08.010.
- Sanz-Cobena, A., Lassaletta, L., Aguilera, E., Prado, A. del, Garnier, J., Billen, G., Iglesias, A., Sánchez, B., Guardia, G., Abalos, D., Plaza-Bonilla, D., Puigdueta-Bartolomé, I., Moral, R., Galán, E., Arriaga, H., Merino, P., Infante-Amate, J., Mejjide, A., Pardo, G., Álvaro-Fuentes, J., Gilsanz, C., Báez, D., Doltra, J., González-Ubierna, S., Cayuela, M. L., Menéndez, S., Díaz-Pinés, E., Le-Noë, J., Quemada, M., Estellés, F., Calvet, S., Grinsven, H. J. van, Westhoek, H., Sanz, M. J., Gimeno, B. S., Vallejo, A., and Smith, P. (2017). "Strategies for greenhouse gas emissions mitigation in Mediterranean agriculture: A review". In: *Agriculture, Ecosystems and Environment* 238, pp. 5–24. DOI: 10.1016/j.agee.2016.09.038.
- Scalenghe, R., Territo, C., Petit, S., Terribile, F., and Righi, D. (2016). "The role of pedogenic overprinting in the obliteration of parent material in some polygenetic landscapes of Sicily (Italy)". In: *Geoderma Regional* 7 (1), pp. 49–58. DOI: 10.1016/j.geodrs.2016.01.003.
- Schaaf, W., Bens, O., Fischer, A., Gerke, H. H., Gerwin, W., Grünewald, U., Holländer, H. M., Kögel-Knabner, I., Mutz, M., Schloter, M., Schulin, R., Veste, M., Winter, S., and Hüttl, R. F. (2011). "Patterns and processes of initial terrestrial-ecosystem development". In: *Journal of Plant Nutrition and Soil Science* 174 (2), pp. 229–239. DOI: 10.1002/jpln.201000158.
- Shao, J., Yang, S., and Li, C. (2012). "Chemical indices (CIA and WIP) as proxies for integrated chemical weathering in China: Inferences from analysis of fluvial sediments". In: *Sedimentary Geology* 265-266, pp. 110–120. DOI: 10.1016/j.sedgeo.2012.03.020.
- Singh, M., Sarkar, B., Sarkar, S., Churchman, J., Bolan, N., Mandal, S., Menon, M., Purakayastha, T. J., and Beerling, D. J. (2018). "Stabilization of Soil Organic Carbon as Influenced by Clay Mineralogy". In: *Advances in Agronomy*. 1st ed. Vol. 148. Elsevier Inc., pp. 33–84. DOI: 10.1016/bs.agron.2017.11.001.
- Sissoko, A. and Kpombrekou-A, K. (2010). "Carbon decomposition in broiler litter-amended soils". In: *Soil Biology and Biochemistry* 42 (4), pp. 543–550. DOI: 10.1016/j.soilbio.2009.10.007.
- Soussana, J.-F., Soussana, J.-F., Loiseau, P., Vuichard, N., Ceschia, E., Balesdent, J., Chevallier, T., and Arrouays, D. (2004). "Carbon cycling and sequestration opportunities in temperate grasslands". In: *Soil Use and Management* 20 (2), pp. 219–230. DOI: 10.1079/sum2003234.

- Sposito, G., Skipper, N. T., Sutton, R., Park, S.-h., Soper, A. K., and Greathouse, J. A. (1999). "Surface geochemistry of the clay minerals". In: *Proceedings of the National Academy of Sciences* 96 (7), pp. 3358–3364. DOI: 10.1073/pnas.96.7.3358.
- Streifer, J., Amann, T., Bauer, N., Kriegler, E., and Hartmann, J. (2018). "Potential and costs of carbon dioxide removal by enhanced weathering of rocks". In: *Environmental Research Letters* 13 (3). DOI: 10.1088/1748-9326/aaa9c4.
- Tabor, N. J., Myers, T. S., Gulbranson, E., Rasmussen, C., Sheldon, N. D., Driese, S., and Nordt, L. (2013). "Carbon stable isotope composition of modern calcareous soil profiles in California: implications for CO<sub>2</sub> reconstructions from calcareous paleosols". In: *New Frontiers in Paleopedology and Terrestrial Paleoclimatology*. Vol. 104. SEPM (Society for Sedimentary Geology), pp. 17–34. DOI: 10.2110/sepm.104.07.
- Taylor, L. L., Beerling, D. J., Quegan, S., and Banwart, S. A. (2017). "Simulating carbon capture by enhanced weathering with croplands: An overview of key processes highlighting areas of future model development". In: *Biology Letters* 13 (4). DOI: 10.1098/rsbl.2016.0868.
- Trumpy, E., Donato, A., Gianelli, G., Gola, G., Minissale, A., Montanari, D., Santilano, A., and Manzella, A. (2015). "Geothermics Data integration and favourability maps for exploring geothermal systems in Sicily, southern Italy". In: *Geothermics* 56, pp. 1–16. DOI: 10.1016/j.geothermics.2015.03.004.
- United Nations Framework Convention on Climate Change (2015). *4 per 1000 initiative*.
- USDA (1987). *Soil Mechanics Level I Module 3 - USDA Textural Soil Classification*. book.
- Van Straaten, P. (2007). *Agrogeology : The use of rocks for crops*. Ontario: Enviroquest Ltd., p. 426.
- Velbel, M. (1988). "Weathering and soil-forming processes". In: *Forest hydrology and ecology at Coweeta*. Springer, pp. 93–102.
- Vervoort, R. W. and Cattle, S. R. (2003). "Linking hydraulic conductivity and tortuosity parameters to pore space geometry and pore-size distribution". In: *Journal of Hydrology* 272 (1-4), pp. 36–49. DOI: 10.1016/S0022-1694(02)00253-6.
- Vicente-Vicente, J. L., García-Ruiz, R., Francaviglia, R., Aguilera, E., and Smith, P. (2016). "Soil carbon sequestration rates under Mediterranean woody crops using recommended management practices: A meta-analysis". In: *Agriculture, Ecosystems and Environment* 235, pp. 204–214. DOI: 10.1016/j.agee.2016.10.024.
- Viola, F., Liuzzo, L., Noto, L. V., Lo Conti, F., and La Loggia, G. (2014). "Spatial distribution of temperature trends in Sicily". In: *International Journal of Climatology* 34 (1), pp. 1–17. DOI: 10.1002/joc.3657.
- Weaver, C. E. and Pollard, L. D. (1973). "Chapter 6 Chlorite". In: *The Chemistry of Clay Minerals*. Vol. 15. Developments in Sedimentology. Elsevier, pp. 87–98. DOI: 10.1016/S0070-4571(09)70009-3.
- Weil, R. and Brady, N. (2017). *The Nature and Properties of Soils*. 15th ed.

- West, T. O. and Six, J. (2007). "Considering the influence of sequestration duration and carbon saturation on estimates of soil carbon capacity". In: *Climatic Change* 80 (1-2), pp. 25–41. DOI: 10.1007/s10584-006-9173-8.
- White, A. F. and Brantley, S. L. (2003). "The effect of time on the weathering of silicate minerals: Why do weathering rates differ in the laboratory and field?" In: *Chemical Geology* 202 (3-4), pp. 479–506. DOI: 10.1016/j.chemgeo.2003.03.001.
- Wiesmeier, M., Urbanski, L., Hobbey, E., Lang, B., Lützow, M. V., Marin-spiotta, E., Wesemael, B. V., Rabot, E., Ließ, M., Garcia-franco, N., Wollschläger, U., Vogel, H.-J., and Kögel-knabner, I. (2019). "Geoderma Soil organic carbon storage as a key function of soils - A review of drivers and indicators at various scales". In: *Geoderma* 333 (July 2018), pp. 149–162. DOI: 10.1016/j.geoderma.2018.07.026.
- WRB (2015). *World reference base for soil resources 2014 International soil classification system*. Report.
- Yang, S., Jung, H.-S., and Li, C. (2004). "Two unique weathering regimes in the Changjiang and Huanghe drainage basins: geochemical evidence from river sediments". In: *Sedimentary Geology* 164 (1-2), pp. 19–34. DOI: 10.1016/j.sedgeo.2003.08.001.
- Zamanian, K., Pustovoytov, K., and Kuzyakov, Y. (2016). "Pedogenic carbonates: Forms and formation processes". In: *Earth-Science Reviews* 157, pp. 1–17. DOI: 10.1016/j.earscirev.2016.03.003.
- Zhao, H., Zhang, H., Shar, A., Liu, J., Chen, Y., Chu, S., and Tian, X. (2018). "Enhancing organic and inorganic carbon sequestration in calcareous soil by the combination of wheat straw and wood ash and/or lime". In: *PLoS ONE* 13 (10), pp. 1–16. DOI: 10.1371/journal.pone.0205361.

## Declaration of Authorship

Personal declaration: I hereby declare that the submitted thesis is the result of my own, independent work. All external sources are explicitly acknowledged in the thesis.

Signed:   
\_\_\_\_\_

Date: 26.01.2021  
\_\_\_\_\_